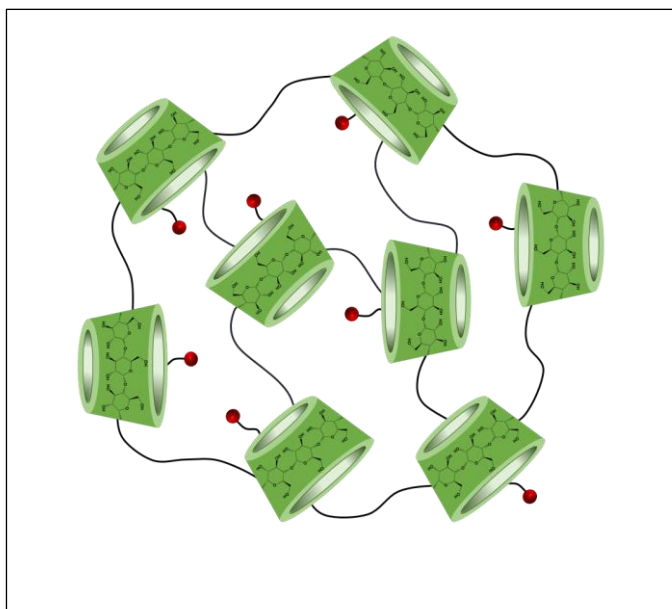




Università degli Studi di Torino

PhD Programme in Chemical and Materials Sciences XXXII Cycle

**Synthesis and Characterization of Hyper
Cross-Linked Polymers and Their
Applications in Drug Delivery**



Nilesh Kumar Dhakar

Supervisor:
Prof. Francesco Trotta



Università degli Studi di Torino

PhD Programme in Chemical and Materials Sciences XXX cycle

Synthesis and Characterization of Hyper Cross-Linked Polymers and Their Applications in Drug Delivery

Candidate: **Nilesh Kumar Dhakar**

Supervisor: Prof. **Francesco Trotta**

Jury Members: Prof. **Michele Laus**
Università Piemonte Orientale
Dipartimento DISIT

Prof. **Antonino Mazzaglia**
CNR Messina
Istituto Studio Materiali Nanostrutturati (ISMN)

Prof. **Roberta Cavalli**
Università di Torino
Dipartimento di Scienza e Tecnologia del
Farmaco

Head of the Doctoral School: Prof. Massimo Maffei

PhD Programme Coordinator: Prof. Mario Chiesa

Prof. Bartolomeo Civalleri

Torino, 2020

Abstract

Abstract

Cyclodextrins are a family of cyclic oligosaccharides and are considered as drug carriers due to their structure and properties. Moreover, cyclodextrin can be crosslinked with various crosslinking agents in order to develop hyper crosslinked polymers also called the nanosponges (NSs). The properties of the prepared NSs are highly dependent on the nature and concentration of the crosslinker. The synthesis, characterization, and application of the NSs in different fields are reported in the literature.

In the present thesis, we developed different types of NSs and their application in the drug delivery has been evaluated. Mainly, carbonate, ester-based, and glutathione-responsive NSs were prepared by 1-1'-carbonyldiimidazole, pyromellitic dianhydride, and 2-hydroxyethyl disulfide, respectively. The effect of these prepared NSs on the physicochemical properties of different drug molecules such as Kynurenic acid, resveratrol, oxyresveratrol, and curcumin was studied. The post-synthetic modification of the ester-based NSs with biotin was also performed. Depending on the applications and properties of the NSs five different projects have been carried out.

Kynurenic acid (KYNA) demonstrates several pharmacological activities such as antioxidant, neuroprotective and free radical scavenging properties. However, the therapeutic activity of KYNA is affected by its low aqueous solubility. We developed KYNA loaded cyclodextrin nanosponges to improve the solubility and therapeutic activity of kynurenic acid. Several characterization techniques were

Abstract

used to determine the formation of the inclusion complex of kynurenic acid with NSs.

The solubility profile of KYNA alone and in the presence of nanosponges clearly indicated the increase in the aqueous solubility compared to native cyclodextrin. The developed KYNA loaded NSs showed good stability during storage. Several methods were used to determine the antioxidant activity of KYNA alone and compared with kynurenic acid loaded nanosponges which confirmed that the better antioxidant activity was observed compared to free kynurenic acid. The cytotoxicity study confirmed that the prepared NSs are non-toxic and KYNA loaded NSs do not promote cell death due to protective nature of the KYNA.

Resveratrol (RES) and Oxyresveratrol (OXY) can be obtained from a variety of natural sources. Both are considered as effective molecules against different disease conditions due to their antioxidant, anti-inflammatory, and anti-tumor activity. However, their therapeutic activity is limited due to low solubility, photosensitivity, and aqueous instability. We developed RES and OXY loaded NSs in order to improve their solubility and stability. Drug loaded NSs showed significant improvement in the stability of drug molecules after UV-exposure. Antioxidant study of RES and OXY loaded NSs further showed high activity compared to respective drugs alone. We also demonstrated the anticancer activity of RES and OXY loaded NSs against DU-145 prostate cancer cell lines which confirmed that high solubility and stability of drug molecules affect the overall performance of drug molecules in the drug delivery in terms of high anticancer activity.

Abstract

In the next work, we determined the encapsulation constant of different nanosponges prepared from 1-1'-carbonyldiimidazole using a novel method. This work was carried out in collaboration with Prof. José Manuel López-Nicolás, with the help of Adrián Matencio at Department of Biochemistry and Molecular Biology-A. Faculty of Biology. University of Murcia. Murcia, Spain. The prepared NSs were used to encapsulate oxyresveratrol. The encapsulation of the OXY was confirmed with several methods. OXY is an unstable drug molecule so we determined the stability of OXY in simulated biological fluids. Moreover, the anticancer activity of OXY loaded NSs against HCT116 and HT29 cell lines was also studied.

We demonstrated the application of the stimuli-responsive cyclodextrin NSs for the selective targeting of the RES. This work was carried out in collaboration with Prof. Ciro Isidoro, with the help of Alessandra Ferraresi at the Laboratory of Molecular Pathology, Department of Health Sciences, Università del Piemonte Orientale "A. Avogadro", Novara, Italy. Selective drug delivery can be achieved to release the drug at a target site in a response to the cellular microenvironment (i.e. glutathione) of the cancer cells without affecting the physiology of the normal cells. We performed cell internalization studies to confirm the preferential uptake of the nanocarrier to the cancer cells. Moreover, cytotoxicity studies were also performed which confirmed that the cancerous cells are highly affected while normal cells remain unaffected.

Another targeting approach is the development of the nanocarrier with targeting moieties attached to the surface of nanocarriers in order to improve the drug delivery to a specific site. We developed

Abstract

the biotin-functionalized NSs (Bio-NSs) and the presence of biotin on nanocarrier was also determined. Bio-NSs were used to perform the encapsulation of curcumin (CUR). CUR is a phytopolyphenol with different pharmacological properties. However, CUR is practically insoluble at acidic and neutral pH which subsequently affects the bioavailability. We demonstrated that the CUR solubilization was enhanced significantly with NSs. Moreover, the formation of the inclusion complex was also confirmed. The in-vitro release profile of CUR was also performed to confirm that solubilization of the CUR leads to a better drug release profile compared to CUR alone.

Acknowledgements

Acknowledgements

I take this opportunity to thank each and every person who has helped me throughout my research work.

I would like to convey my sincere gratitude to my supervisor, Prof. Francesco Trotta for his precious guidance without which this work would not have been possible. He gave me the support, direction, encouragement and valuable suggestions that will be helpful for my future professional life. I will always cherish the experience that I have gained under his supervision throughout my life.

I would also like to thank the jury members for giving their time to evaluate my work.

I want to thank Prof. Roberta Cavalli and Prof. Chiara Dianzani (Department of Pharmaceutical Sciences and Technology) and their research groups for their help and co-operation to perform biological studies.

I would like to express my gratitude to Prof. Ciro Isidoro and Prof. José Manuel López-Nicolás for collaborating with us on different projects reported in this thesis.

I would like to thank the University of Turin, Italy for providing the Doctoral Research Fellowship.

I am immensely grateful to all my lab mates, who supported and helped me throughout my Ph.D. period. Apart from fun, I have learned a lot from all of them and I am extremely grateful to Giorgia, Anastasia, Claudio, Maria, Alberto, Shohreh, Asma, and Gjylje. They have been very helpful and co-operative

Acknowledgements

throughout. I will cherish these memories throughout my life.

I gratefully acknowledge Sushil and Fabrizio for helping me with my work and their immense support.

Most of all, I would like to thank my loving and caring mother, sister and my brother who have constantly supported me in all my decisions. Their unconditional love and support are the pillars of my life. All words combined in this world will not be enough for everything that they have done for me. I would like to acknowledge my late father, whose blessings are always with me. Finally to my close friend Amrita who was always very supportive.

Above all, I would like to thank ALMIGHTY GOD for all that he has given me, my parents, a good home, a healthy mind and body.

Table of Contents

| | |
|--|-------|
| Abstract | I |
| Acknowledgements | V |
| Table of Contents | VII |
| List of Figures | XV |
| List of Tables..... | XIX |
| List of abbreviations..... | XXI |
| List of Publications | XXIII |
| 1. Introduction | 1 |
| 1.1 Pharmaceutical Nanotechnology..... | 1 |
| 1.2 Cyclodextrins..... | 2 |
| 1.3 Safety and Regulatory Status of CDs | 5 |
| 1.4 Cyclodextrin-based Nanosponges | 5 |
| 1.4.1 Classification of CDNSs..... | 6 |
| 1.4.1.1 Cyclodextrin-based Carbamate Nanosponges | 6 |
| 1.4.1.2 Cyclodextrin-based Carbonate Nanosponges | 7 |
| 1.4.1.3 Cyclodextrin-based Ester Nanosponges..... | 8 |
| 1.4.1.4 Cyclodextrin-based Ether Nanosponges | 9 |
| 1.4.1.5 Functionalized Nanosponges..... | 10 |
| 1.4.1.6 Cyclodextrin-calixarene Nanosponge | 11 |
| 1.4.1.7 Stimuli-responsive Nanosponges | 11 |
| 1.4.1.8 Molecularly Imprinted Nanosponges | 12 |
| 1.4.2 Method for the Preparation of the NSs..... | 13 |
| 1.4.2.1 Solvent-based Method..... | 13 |
| 1.4.2.2 Melt/Fusion Method | 13 |
| 1.4.2.3 Ultrasound-assisted Synthesis | 14 |

| | | |
|----------|--|----|
| 1.4.2.4 | Microwave-assisted Synthesis..... | 14 |
| 1.4.3 | Factors Affecting Nanosponges Formation | 14 |
| 1.4.3.1 | Types of Crosslinker and Polymer | 14 |
| 1.4.3.2 | Degree of Substitution..... | 15 |
| 1.4.3.3 | Complexation Temperature..... | 15 |
| 1.4.4 | Characterization of Nanosponges..... | 16 |
| 1.4.4.1 | Morphological Evaluation | 16 |
| 1.4.4.2 | Polydispersity and Zeta Potential Determination.... | 16 |
| 1.4.4.3 | Drug Loading and Entrapment Efficiency..... | 17 |
| 1.4.4.4 | Porosity and Surface Area..... | 17 |
| 1.4.4.5 | Swelling and Water Uptake Studies..... | 17 |
| 1.4.4.6 | In-vitro Release Studies..... | 18 |
| 1.4.4.7 | Fourier Transform Infrared Spectroscopy and Raman Spectroscopy (FTIR)..... | 18 |
| 1.4.4.8 | Thermal Analysis..... | 19 |
| 1.4.4.9 | Crystalline and Amorphous Nature of the NSs..... | 19 |
| 1.4.4.10 | In-vitro Stability Studies..... | 20 |
| 1.5 | Applications of the Nanosponges | 20 |
| 1.5.1 | Solubilization of Poorly Water-soluble Drug Molecules . | 20 |
| 1.5.2 | Modulation of Drug Release Profile | 21 |
| 1.5.3 | Nanosponges as a Drug Delivery Carrier | 22 |
| 1.5.4 | Protein Delivery | 23 |
| 1.5.5 | Protection from Degradation | 23 |
| 1.5.6 | Gas Delivery | 24 |
| 1.5.7 | Water Purification | 24 |
| 1.6 | Literature Survey | 25 |
| 1.6.1 | Literature Related to Nanosponges | 25 |
| 1.6.2 | Literature Related to the Selected Drug Molecules..... | 33 |

| | |
|--|----|
| 1.6.2.1 Profile of Kynurenic Acid..... | 33 |
| 1.6.2.1.1 Metabolic Pathway of KYNA | 35 |
| 1.6.2.1.2 Analytical Methods for the Determination of KYNA | 37 |
| 1.6.2.2 Profile of Resveratrol..... | 38 |
| 1.6.2.2.1 Pharmacokinetics of Resveratrol..... | 40 |
| 1.6.2.2.2 Analytical Methods for the Determination of RES | 41 |
| 1.6.2.3 Profile of Oxyresveratrol..... | 42 |
| 1.6.2.3.1 Pharmacokinetics of Oxyresveratrol..... | 45 |
| 1.6.2.3.2 Analytical Methods for the Determination of OXY | 46 |
| 1.6.2.4 Profile of Curcumin | 47 |
| 1.6.2.4.1 Pharmacokinetics of Curcumin | 49 |
| 1.6.2.4.2 Analytical Methods for the Determination of CUR | 49 |
| 2. Aims | 53 |
| 3. Material and Methods..... | 59 |
| 3.1 Chemicals | 59 |
| 3.2 Characterization Techniques | 60 |
| 3.2.1 Determination of Particle Size, Polydispersity Index, and Zeta Potential | 60 |
| 3.2.2 Differential Scanning Calorimetry (DSC)..... | 60 |
| 3.2.3 Thermogravimetric analysis (TGA)..... | 60 |
| 3.2.4 Fourier Transform Infrared Spectroscopy (FTIR)..... | 61 |
| 3.2.5 X-ray Powder Diffraction Studies (PXRD)..... | 61 |
| 3.2.6 Morphology Evaluation | 61 |
| 3.2.7 BET Analysis..... | 62 |
| 3.3 Kynurenic Acid (KYNA) Loaded Cyclodextrin Nanosponges..... | 63 |

| | | |
|--------|--|----|
| 3.3.1 | Synthesis of β -cyclodextrin Nanosponges (β -CDNSs) ... | 63 |
| 3.3.2 | Swelling Degree of Nanosponges..... | 64 |
| 3.3.3 | Determination of Percentage Crosslinking..... | 64 |
| 3.3.4 | Solubilization of the KYNA | 65 |
| 3.3.5 | Preparation of KYNA Loaded Nanosponges..... | 65 |
| 3.3.6 | Quantitative Determination of KYNA | 66 |
| 3.3.7 | KYNA Loading within the NSs | 66 |
| 3.3.8 | Characterization of the KYNA Loaded NSs | 66 |
| 3.3.9 | In-vitro Drug Release Profile of KYNA | 67 |
| 3.3.10 | Evaluation of Antioxidant Activity | 68 |
| 3.3.11 | Cell Viability Studies | 70 |
| 3.3.12 | Stability Studies | 70 |
| 3.4 | Resveratrol (RES) and Oxyresveratrol (OXY) Containing Cyclodextrin Nanosponges..... | 71 |
| 3.4.1 | Synthesis of Carbonate-based Nanosponges..... | 71 |
| 3.4.2 | Solubilization of RES and OXY | 71 |
| 3.4.3 | Preparation of RES and OXY Loaded Nanosponge | 71 |
| 3.4.4 | Quantitative Determination of RES and OXY by HPLC .. | 72 |
| 3.4.5 | Determination of RES or OXY Loading..... | 72 |
| 3.4.6 | Characterization of Drug Loaded NSs | 72 |
| 3.4.7 | In-Vitro Drug Release Profile..... | 73 |
| 3.4.8 | Photodegradation Study | 74 |
| 3.4.9 | Antioxidant Activity of RES and OXY | 74 |
| 3.4.10 | Cytotoxicity Studies | 74 |
| 3.5 | Determination of Complexation Constant and Activity Against Colon Cancer by OXY Loaded NSs | 76 |
| 3.5.1 | Synthesis of NSs of Different Cyclodextrins..... | 76 |
| 3.5.2 | Determination of Apparent Encapsulation Constant | 76 |

| | |
|--|----|
| 3.5.3 Drug Loading and Encapsulation Efficiency..... | 78 |
| 3.5.4 Characterization of OXY Loaded NSs..... | 79 |
| 3.5.5 In-vitro Drug Release Profile..... | 79 |
| 3.5.6 In-vitro Digestion Studies..... | 80 |
| 3.5.7. In-vitro Cell Cytotoxicity Studies..... | 80 |
| 3.6 Stimuli-responsive Cyclodextrin Nanosponges for Resveratrol | 82 |
| 3.6.1 Synthesis of Glutathione-responsive Cyclodextrin Nanosponges..... | 82 |
| 3.6.2 Elemental Analysis..... | 82 |
| 3.6.3 Preparation of Drug Loaded and Fluorescent NSs..... | 83 |
| 3.6.4 Quantitative Determination and Drug Loading..... | 84 |
| 3.6.5 Characterization of Drug loaded NSs..... | 84 |
| 3.6.6 In-Vitro Drug Release Profile of RES-GSHNSs..... | 84 |
| 3.6.7 In-Vitro Biological Assays..... | 85 |
| 3.6.7.1 Cell Internalization Study..... | 85 |
| 3.6.7.2 Cell Viability Study..... | 85 |
| 3.6.7.3 Propidium Iodide Staining..... | 86 |
| 3.7 Synthesis of Biotin-functionalized Ester-based NSs and Encapsulation of Curcumin..... | 87 |
| 3.7.1 Synthesis of Ester-based NSs..... | 87 |
| 3.7.2 Biotin-Functionalization of the NSs (Bio-NSs)..... | 87 |
| 3.7.3 Elemental Analysis of Bio-NSs..... | 88 |
| 3.7.4 Determination of the Biotin Concentration by HABA-Avidin Assay..... | 88 |
| 3.7.5 Quantitative Determination of the CUR..... | 89 |
| 3.7.6 Solubilization of Curcumin (CUR)..... | 89 |
| 3.7.7 CUR Loading with Bio-NSs..... | 89 |

| | |
|--|-----|
| 3.7.8 Characterization of the BIO-NSs and CUR Loaded Bio-NSs | 90 |
| 3.7.9 In-vitro Release Profile of CUR Loaded Bio-NSs..... | 90 |
| 4. Results and Discussion..... | 93 |
| 4.1 Kynurenic Acid Loaded Nanosponges for Controlled Drug Delivery | 93 |
| 4.1.1 Physicochemical Characterization of NSs and KYNA Loaded NSs..... | 93 |
| 4.1.2 Release Profile of KYNA | 102 |
| 4.1.3 Antioxidant Activity of KYNA Loaded NSs..... | 103 |
| 4.1.4 In-vitro Cell Viability of KYNA Loaded NSs | 108 |
| 4.1.5 Storage Stability of KYNA Loaded NSs..... | 110 |
| 4.2 Comparative Evaluation of the Anticancer Activity of RES and OXY..... | 112 |
| 4.2.1 Physicochemical Characterization of RES and OXY Loaded NSs | 112 |
| 4.2.2 Release Profile of RES and OXY Loaded NSs | 117 |
| 4.2.3 Photodegradation Study | 120 |
| 4.2.4 DPPH Assay of RES and OXY Loaded NSs..... | 121 |
| 4.2.5 Anticancer Activity of RES and OXY Loaded NSs..... | 122 |
| 4.3 Determination of Encapsulation Constant of the NSs and Activity Against Colon Cancer by OXY Loaded NSs | 125 |
| 4.3.1 Encapsulation Constant of the NSs | 125 |
| 4.3.2 Physicochemical Characterization of the OXY Loaded NSs | 127 |
| 4.3.3 In-vitro Drug Release Profile | 129 |
| 4.3.4 In-vitro Digestion Study of OXY | 130 |
| 4.3.5 Activity of OXY Against Colon Cancer | 132 |
| 4.4 Stimuli-responsive Drug Delivery System of Resveratrol... | 134 |

| | |
|--|-----|
| 4.4.1 Physiochemical Characterization of the GSHNSs and RES-GSHNSs..... | 134 |
| 4.4.2 Release Profile of RES from GSHNSs..... | 140 |
| 4.4.3 Biological Studies..... | 141 |
| 4.4.3.1 Cell Internalization, Cell Viability and Necrosis Study | 141 |
| 4.4.3.2 Effect of GSH depletion on Cell Internalization, Cell Viability and Necrosis Study | 150 |
| 4.5 Biotin-modified Nanosponges for Active Targeting of the Therapeutics | 157 |
| 4.5.1 Characterization of the Biotin-modified Nanosponges | 157 |
| 4.5.2 Release Profile of Curcumin from Bio-NSs. | 163 |
| 5. Conclusion | 167 |
| References..... | 173 |

List of Figures

| | |
|---|-----|
| Figure 1. 1 Structure of β -Cyclodextrin | 2 |
| Figure 1. 2 Inclusion complex of drug-CD. | 4 |
| | |
| Figure 4. 1 Schematic representation of CDI-based cyclodextrin nanosponges..... | 93 |
| Figure 4. 2 FTIR spectra of (i) calibration standards and (ii) nanosponges..... | 94 |
| Figure 4. 3 (i) The percentage crosslinking at different molar ratio (n=3). (ii) Theoretical vs. actual crosslinker concentration (n=3). | 95 |
| Figure 4. 4 Solubilization of KYNA with different NSs..... | 96 |
| Figure 4. 5 Particle size distribution of blank NSs (A) and KYNA loaded NSs (B). | 97 |
| Figure 4. 6 DSC thermogram of the different samples..... | 98 |
| Figure 4. 7 FTIR spectra of the different samples. | 99 |
| Figure 4. 8 PXRD pattern of the different samples. | 100 |
| Figure 4. 9 FE-SEM images of (A) Blank and (B) KYNA-loaded NSs | 101 |
| Figure 4. 10 N ₂ absorption-desorption (A) and porosity curve of β -CDNS2 (B). | 101 |
| Figure 4. 11 N ₂ absorption-desorption (A) and porosity curve of KYNA loaded NSs (B). | 102 |
| Figure 4. 12 In-vitro release kinetics of KYNA..... | 103 |
| Figure 4. 13 A schematic of the formation of TBA-MDA Adduct. | 104 |
| Figure 4. 14 The inhibition of lipid peroxidation by KYNA loaded NS in the absence of oxidizing agent (left) and in the presence of the oxidizing agent (right). *** P < 0.0001. | 105 |
| Figure 4. 15 A schematic of DPPH inhibition by KYNA. | 106 |
| Figure 4. 16 The Percentage DPPH inhibition of KYNA, KYNA loaded NS and L-ascorbic acid. | 106 |
| Figure 4. 17 A schematic of H ₂ O ₂ inhibition by KYNA..... | 107 |
| Figure 4. 18 The H ₂ O ₂ scavenging activity of KYNA, KYNA loaded NS and L-ascorbic acid. | 108 |
| Figure 4. 19 Cytotoxicity of the blank NSs. | 109 |

| | |
|---|-----|
| Figure 4. 20 Cytotoxicity of the KYNA loaded NSs. | 110 |
| Figure 4. 21 The in-vitro stability study of blank NS and KYNA loaded NS to determine particles size (A) and zeta potential (B). All the values present in terms of mean \pm SD (n = 3). | 111 |
| Figure 4. 22 Solubilization of the RES and OXY within the NSs. ** p < 0.001; RES vs. RES-NS and *** p < 0.0001; OXY vs. OXY-NS. | 112 |
| Figure 4. 23 Particle size distribution of RES-NS (A) and OXY-NS (B). | 114 |
| Figure 4. 24 FTIR spectra of RES, OXY, PM-RES, PM-OXY, RES-NS, OXY-NS and blank NS..... | 115 |
| Figure 4. 25 DSC thermograms of RES, OXY, PM-RES, PM-OXY, RES-NS, OXY-NS and blank NS..... | 115 |
| Figure 4. 26 PXRD pattern of RES, OXY, RES-NS, OXY-NS and blank NS. | 116 |
| Figure 4. 27 TEM images of (a) RES-NS and (b) OXY-NS. | 117 |
| Figure 4. 28 The release profile of (a) RES vs. RES-NS and (b) OXY vs. OXY-NS..... | 118 |
| Figure 4. 29 Photodegradation study of (a) RES vs. RES-NS and (b) OXY vs. OXY-NS..... | 120 |
| Figure 4. 30 DPPH inhibition activity of (a) RES vs. RES-NS and (b) OXY vs. OXY-NS. ** p < 0.01 and *** p < 0.001. | 122 |
| Figure 4. 31 Cell cytotoxicity study of (A) Blank NS, (B) RES vs. RES-NS, and (C) OXY vs. OXY-NS after 96 hours. *p<0.05..... | 124 |
| Figure 4. 32 Effect of increasing OXY concentration on absorbance at 48 h with 1% of β -CDI 1:4 in water at 25 $^{\circ}$ C. Insert. Benesi-Hildebrand plot of OXY complexed to β -CD-CDI 1:4. The β -CDI 1:8 nanosponge showed the highest K_{Fapp} , perhaps due to its higher number of CDs per gram. | 126 |
| Figure 4. 33 FTIR spectra of OXY, β -CDI 1:4 and OXY-loaded β -CDI 1:4. Legend: (—) OXY, (···) β -CDI 1:4 and (·—·) OXY loaded β -CDI 1:4..... | 127 |
| Figure 4. 34 DSC thermogram of OXY, β -CDI 1:4 and OXY-loaded β -CDI 1:4. Legend: (—) OXY, (···) β -CDI 1:4 and (·—·) OXY loaded β -CDI 1:4..... | 128 |

| | |
|---|-----|
| Figure 4. 35 TGA curves of OXY, β -CDI 1:4 and OXY-loaded β -CDI 1:4. Legend: (—) OXY, (···) β -CDI 1:4 and (·—·—·) OXY loaded β -CDI 1:4..... | 129 |
| Figure 4. 36 In-vitro release profile of OXY or complex at pH 7.4 and 5.5 at 37 °C. Legend: (Δ) OXY loaded β -CDI 1:4 at pH 7.4 and (\blacktriangle) OXY loaded β -CDI 1:4 at pH 5.5. | 130 |
| Figure 4. 37 Relative abundance of OXY after stomach and intestine digestion without (black) and with (gray) CD-NS. The data are normalized using initial OXY abundance..... | 131 |
| Figure 4. 38 Cytotoxicity of OXY, OXY-NS, and NS alone on HT29 cell lines. ** $p < 0.01$; OXY vs. OXY-NS..... | 133 |
| Figure 4. 39 Cytotoxicity of OXY, OXY-NS, and NS alone on HCT116 cell lines. ** $p < 0.01$; OXY vs. OXY-NS..... | 133 |
| Figure 4. 40 Structure of the GSHNSs..... | 134 |
| Figure 4. 41 Solubilization of the RES with GSHNSs. (** $p < 0.0001$). | 135 |
| Figure 4. 42 Particle size distribution of GSHNSs (A), RES loaded GSHNS (B), and Fluorescent GSHNSs (C)..... | 137 |
| Figure 4. 43 FTIR spectra of RES, PM-RES, RES-GSHNS, and GSHNS. | 138 |
| Figure 4. 44 DSC thermograms of RES, PM-RES, RES-GSHNS, and GSHNS..... | 139 |
| Figure 4. 45 PXRD pattern of RES, RES-GSHNS, and GSHNS..... | 139 |
| Figure 4. 46 Morphology of the RES-GSHNSs (A) TEM and (B) FE-SEM..... | 140 |
| Figure 4. 47 Release profile of the RES and RES-GSHNSs..... | 141 |
| Figure 4. 48 Internalization of C-6 loaded GSHNSs in (A) Normal fibroblast cells, (B) MCF 10A cells (C) OVCAR3 cells, and (D) MDAMB231 cell lines..... | 143 |
| Figure 4. 49 Cell viability of different cell lines at increasing concentration of the RES loaded GSHNSs after 24 hours (A), and 48 hours (B). | 146 |
| Figure 4. 50 Determination of the necrotic cells after treatment with RES loaded GSHNSs at 24 hours (A), and 48 hours (B). | 149 |
| Figure 4. 51 Comparison between internalization rate in (A) OVCAR3 and (B) MDAMB231 cancer cells exposed to C-6-GSH-NSs | |

with/without BSO pre-treatment. **** p< 0.0001; ***p < 0.001; **p < 0.01; *p < 0.05. 152

Figure 4. 52 Comparison of the mitochondrial vitality in OVCAR3 and MDAMB231 cells exposed to RES-GSH-NSs for 24h and 48h with/without BSO pre-treatment. **** p< 0.0001; ***p < 0.001; **p < 0.01; *p < 0.05. 154

Figure 4. 53 Comparison of necrotic cell mortality in (A) OVCAR3 and (B) MDAMB231 cells exposed to RES-GSH-NSs for 24h and 48h with/without BSO pre-treatment. **** p< 0.0001; ***p < 0.001. 156

Figure 4. 54 A schematic of the biotinylated NSs..... 157

Figure 4. 55 UV-Vis absorbance of the HABA/avidin complex and Bio-NSs..... 159

Figure 4. 56 Solubilization of the CUR alone, with β -CD, and Bio-NSs..... 159

Figure 4. 57 FTIR spectra of biotinylated NSs. 160

Figure 4. 58 FTIR spectra of CUR, PM and CUR-Bio-NS..... 161

Figure 4. 59 DSC thermograms of biotinylated NSs. 162

Figure 4. 60 DSC thermograms of CUR, PM and CUR-Bio-NS..... 163

Figure 4. 61 Release profile of the CUR and CUR-Bio-NS. 163

List of Tables

| | |
|---|-----|
| Table 1. 1 Properties of cyclodextrins in Pharmacopoeia | 3 |
| Table 1. 2 Nanosponges for the several pharmaceutical applications. | 25 |
| Table 1. 3 Properties of Kynurenic Acid..... | 34 |
| Table 1. 4 Analytical methods of KYNA | 37 |
| Table 1. 5 Properties of resveratrol | 39 |
| Table 1. 6 Analytical methods of RES | 41 |
| Table 1. 7 Properties of oxyresveratrol | 44 |
| Table 1. 8 Analytical methods of OXY | 46 |
| Table 1. 9 Properties of curcumin..... | 48 |
| Table 1. 10 Analytical methods of CUR | 49 |
| | |
| Table 3. 1 Quantities of chemical for the synthesis of nanosponges. | 63 |
| | |
| Table 4. 1 The percentage cross-linking determination..... | 95 |
| Table 4. 2 Physicochemical properties of Blank NSs and KYNA loaded NSs. | 97 |
| Table 4. 3 Physicochemical properties of RES-NS and OXY-NSs. | 113 |
| Table 4. 4 Release kinetic models for RES-NS and OXY-NSs. | 119 |
| Table 4. 5 Apparent K_{Fapp} (M^{-1}), SD (+/-) values and correlation coefficients for OXY/CD complexes at 25 °C in water. | 126 |
| Table 4. 6 Physicochemical properties of GSHNSs and RES-GSHNSs. | 136 |
| Table 4. 7 Elemental analysis of the NSs and Bio-NSs. | 158 |

List of abbreviations

| | |
|--------|---|
| BIO-NS | Biotin-functionalized cyclodextrin nanosponges |
| BET | Brunauer-Emmett-Teller |
| CUR | Curcumin |
| CD | Cyclodextrin |
| CDNSs | Cyclodextrin nanosponges |
| DPC | Diphenyl carbonate |
| DL | Drug loading |
| DLS | Dynamic light scattering |
| EE | Entrapment efficiency |
| EU | European union |
| FE-SEM | Field emission scanning electron microscopy |
| FTIR | Fourier transform infrared spectroscopy |
| GSH | Glutathione |
| GSHNSs | Glutathione-responsive cyclodextrin nanosponges |
| HPLC | High-performance liquid chromatography |
| S_0 | Intrinsic solubility |
| KYNA | Kynurenic acid |
| CDI | N-N'-carbonyldiimidazole |
| OXY | Oxyresveratrol |

List of abbreviations (Contd.)

| | |
|------|----------------------------------|
| PM | Physical mixture |
| PXRD | Powder X-Ray Diffraction |
| PMDA | Pyromellitic dianhydride |
| RES | Resveratrol |
| SEM | Scanning electron microscopy |
| TGA | Thermogravimetric analysis |
| TEM | Transmission electron microscopy |

List of Publications

This segment contains the list of publications obtained during the Ph.D. period.

1. Adrián Matencio, Nilesh Kumar Dhakar, Federica Bessone, Giorgia Musso, Roberta Cavalli, Chiara Dianzani, Francisco García-Carmona, José Manuel López-Nicolás, and Francesco Trotta. Study of oxyresveratrol complexes with insoluble cyclodextrin based nanosponges: developing a novel way to obtain their complexation constants and application in an anticancer study, *Carbohydrate Polymers*, Volume 231, 2020, 115763.
2. Nilesh Kumar Dhakar, Adrián Matencio, Fabrizio Caldera, Monica Argenziano, Roberta Cavalli, Chiara Dianzani, Marco Zanetti, José Manuel López-Nicolás, and Francesco Trotta., Comparative Evaluation of Solubility, Cytotoxicity and Photostability Studies of Resveratrol and Oxyresveratrol Loaded Nanosponges, *Pharmaceutics* 2019, 11(10), 545.
3. Alberto Rubin Pedrazzo, Alessandra Smarra, Fabrizio Caldera, Giorgia Musso, Nilesh Kumar Dhakar, Claudio Cecone, Asma Hamedi, Ilaria Corsi, and Francesco Trotta., Eco-Friendly β -cyclodextrin and Linecaps Polymers for the Removal of Heavy Metals. *Polymers* 2019, 11, 1658. (Remark: This publication is not related to Ph.D. thesis).
4. Nilesh Kumar Dhakar, Fabrizio Caldera, Federica Bessone, Claudio Cecone, Alberto Rubin Pedrazzo, Roberta Cavalli, Chiara Dianzani, Francesco Trotta., Evaluation of solubility enhancement, antioxidant activity, and cytotoxicity studies of kynurenic acid loaded cyclodextrin nanosponge. *Carbohydrate Polymers*, Volume 224, 2019, 115168, doi: 10.1016/j.carbpol.2019.115168.
5. Nilesh Kumar Dhakar (2019), Metal and Metal Oxide Nanosponges: Synthesis and Applications in Francesco Trotta and Andrea Mele (Eds.) *Nanosponges: Synthesis and Applications* (1st Ed., pp. 143-171),

Published by Wiley-VCH Verlag GmbH & Co. KGaA. (Remark: This publication is not related to Ph.D. thesis).

6. Saveria Femminò, Claudia Penna, Federica Bessone, Fabrizio Caldera, Nilesh Dhakar, Daniele Cau, Pasquale Pagliaro, Roberta Cavalli, Francesco Trotta., α -Cyclodextrin, and α -Cyclodextrin Polymers as Oxygen Nanocarriers to Limit Hypoxia/Reoxygenation Injury: Implications from an In Vitro Model. *Polymers* 2018, 10, 211, doi: 10.3390/polym10020211. (Remark: This publication is not related to Ph.D. thesis).

Conferences

1. N. K. Dhakar, F. Caldera, F. Trotta, A. Ferraresi, M. Palminteri, C. Isidoro, Stimuli-Responsive Cyclodextrin Nanosponge for the Delivery of Resveratrol, 6th European Conference on cyclodextrins, University of Santiago de Compostela, October 2-4, 2019 in Santiago, Spain.
2. Attended 4th International Summer School on cyclodextrins organized by Italian Association of Chemistry and Technology of Cyclodextrins held during June 10-12, 2019 in Milan, Italy.
3. N. K. Dhakar, F. Caldera, F. Bessone, R. Cavalli, F. Trotta, Kynurenic Acid Loaded Cyclodextrin Nanosponge: Improved Solubilization and Antioxidant Property, 14th Annual Meet on Euro Ethnopharmacology, Amsterdam, Netherlands, April 25-26, 2019,
4. A. Rubin, N. K. Dhakar, M. Tannous, F. Trotta, Dextrin-based nanosponges as an innovative tool for anticancer drug delivery. International workshop No Cancer (UNIPO), Novara, Italy, 29-30 October 2017.

Chapter 1

Introduction

Introduction

1. Introduction

1.1 Pharmaceutical Nanotechnology

The term nanotechnology was discovered in the 19th century which is broadly defined as the synthesis of the particles with a dimension of less than 100 nm [1]. Nanoparticles (NPs) are considered as the most promising nanomaterials which exhibit all the three dimensions in the nanometer range. Because of their size, NPs can easily enter the cells leading to their intracellular accumulation to facilitate the release of entrapped active molecules. The development of nanomedicine involves the synthesis of an NPs based drug delivery system to improve the solubility of drug, sustained release profile, better biodistribution and intracellular accumulation of the active substances encapsulated within the nanomaterials [2].

A large number of active drug molecules exhibit poor aqueous solubility which further makes it difficult to deliver these drug molecules. Moreover, some of them are physiologically unstable molecules and thus exhibit degradation in aqueous systems or in different physiological pH. NPs based drug delivery systems gained tremendous interest because of the possibility to entrap active molecules and to alter their physicochemical properties. The shape, size, and surface of NPs can be tuned to impart the desired properties to the nanocarrier to facilitate their transport across the biological membranes [3,4]. Recently, researchers have generated interest in the development of the mesoporous or nanoporous nanomedicines because of their ability to overcome challenges related to drug molecules [5,6].

Introduction

1.2 Cyclodextrins

Cyclodextrins (CDs) are cyclic oligosaccharides with truncated cone-shaped structures with hydrophobic inner cavity and hydrophilic outer surface [7,8]. CDs are composed of α -D-glucopyranose units formed by α -1-4-linked glucose units. Most commonly used cyclodextrins are α , β , and γ -CD, which composed of 6, 7, and 8 α -D-glucopyranose units, respectively [9]. The arrangement of α -D-glucopyranose units provides chair conformation of the CDs, in which primary hydroxyl groups are located at the narrow edge and secondary hydroxyl groups are located at wider edge of the CDs. The presence of these hydroxyl groups imparts hydrophilicity to the CDs. The central cavity of CD is lined by skeletal carbons and ethereal oxygen, responsible for the lipophilicity of the CDs [10].

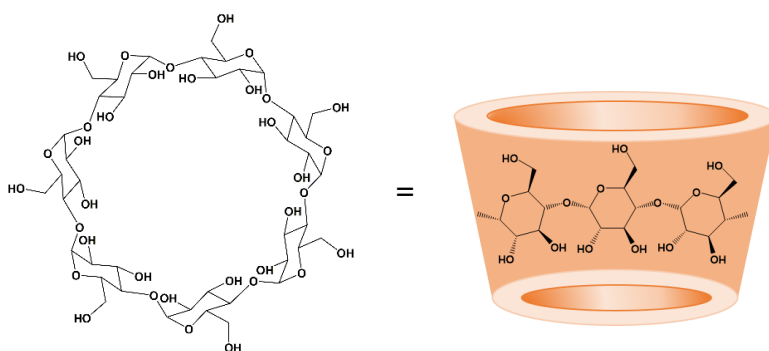


Figure 1. 1 Structure of β -Cyclodextrin

The properties of different cyclodextrin are shown in table no 1.1. CDs have the ability to inclusion complex with variety of drug molecules to change their physicochemical properties thus, CDs are

Introduction

most commonly used as pharmaceutical excipients. An inclusion complex formation takes place in-between guest molecule and central cavity of cyclodextrins. No covalent bonds are created or destroyed during the formation of the inclusion complex and the physicochemical property of guest molecules such as water solubility, crystallinity, and chemical stability can be altered [11].

Table 1. 1 Properties of cyclodextrins in Pharmacopoeia

Monographs [12]

| Properties | α-CD | β-CD | γ-CD |
|---|-------------------------------|------------------------------|-------------------------------|
| Number of glucopyranose units | 6 | 7 | 8 |
| Molar weight (g/mol) | 972 | 1135 | 1297 |
| Solubility in water at 25 °C (%_{w/v}) | 14.5 | 1.85 | 23.2 |
| Outer diameter (Å) | 16.4 ± 0.4 | 5.4 ± 0.4 | 17.5 ± 0.4 |
| Inner diameter (Å) | 4.7-5.3 | 6.0-6.5 | 7.5-8.3 |
| Height of torus (Å) | 7.9 ± 0.1 | 7.9 ± 0.1 | 7.9 ± 0.1 |
| Crystal forms (from water) | Hexagonal plates | Monoclinic parallelograms | Quadratic prism |
| Crystal water, wt % | 10.2 | 13.2-14.5 | 8.13-17.7 |
| Pharmacopoeia Monographs* | Ph.Eur., USP-NF, JPC | Ph.Eur., USP-NF, JPC | Ph.Eur., USP-NF, JPC |

*The European Pharmacopoeia (Ph.Eur.), the United States Pharmacopoeia and the National Formulary (USP-NF), and the Japanese Pharmaceutical Codex (JPC).

Introduction

The drug molecules formed an inclusion complex with CDs that are in dynamic equilibrium in the aqueous solution compared to free drug molecules. The release of complexed drug molecules is carried out by serial dilution or by competitive complexation [13,14]. Thus it is possible that one drug molecule can form an inclusion complex with one or more CDs or vice versa. However, the most common type of inclusion complex is 1:1 drug:CD complex [15].

The equilibrium constant for 1:1 drug:CD complex can be determined from the following equation:

$$K (1:1) = \text{Slope}/S_0 (1-\text{Slope})$$

Where S_0 is the intrinsic solubility of a drug molecule.

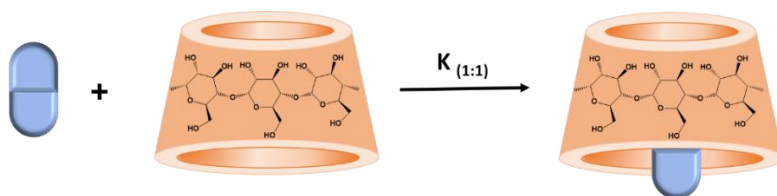


Figure 1. 2 Inclusion complex of drug-CD.

A higher value of K reflects higher stability of the drug:CD inclusion complex. However, a small change in the intrinsic solubility of drug molecules can significantly affect the K value especially in the case of drugs with low water solubility. Thus in such a case, the determination of the complexation efficiency is more important. The complexation efficiency can be determined by the following equation:

$$CE = K 1:1 \times S_0$$

Introduction

1.3 Safety and Regulatory Status of CDs

Unlike γ -CD, α - and β -CD cannot be hydrolyzed by amylase enzyme present in the salivary and pancreatic secretions. Hydrophilic cyclodextrins show low oral bioavailability thus are considered as non-toxic at low to moderate dosage. Moreover, β -CD cannot be administered parentally due to low aqueous solubility and nephrotoxicity. The majority of CDs (α , β , and γ -CD) are considered as food additives and listed as safe materials by the Food and Drug Administration (FDA). Several derivatives of CDs such as hydroxypropyl-beta-cyclodextrin (HP- β -CD) and sulfobutylether β -cyclodextrin (SBE- β -CD) are considered as safe and considered as inactive pharmaceutical excipients [16,17]. The use of different CDs as inactive pharmaceutical excipients has been listed in the pharmacopoeia monographs of different countries (Table 1.1).

1.4 Cyclodextrin-based Nanosponges

The presence of large number of reactive hydroxyl groups on CDs allow them to further modify chemically or crosslinked to give insoluble polymers. One of such polymer is cyclodextrin nanosponges (CDNSs).

Nanosponges can be prepared by organic or inorganic compounds. However, organic NSs prepared from cyclodextrins are preferred for pharmaceutical applications. CDNSs are hyperbranched crosslinked insoluble polymers of CDs prepared by crosslinking with variety of crosslinking agents. The reactive hydroxyl groups of CDs act as monomers for the crosslinking reaction with other polyfunctional chemical moieties such as carbonates, esters, carboxylic acids and

Introduction

diisocyanate. CDNSs are nanosized porous insoluble polymers with high swelling properties. However, the swelling degree of the CDNSs can be altered by changing the cross-linker concentration [18,19].

CDNSs can be utilized to form an inclusion complex with hydrophilic as well as lipophilic drug molecules and can be administered in the form of nanosuspension via several routes to the humans. CDNSs are better as nanocarrier compared to native CDs molecules as it can host more number of guest molecules due to the presence of cyclodextrin cavities and newly formed interstitial spaces between CDs [20]. Moreover, due to the presence of the polymeric network, it is easier to control the release profile of drug molecules from the nanosponges compared to CDs alone thus slow and uniform drug release kinetics can be obtained which is important in case of drugs with low therapeutic index. Over the years, CDNSs have been utilized for the variety of applications such as solubilization of guest molecules, chemical stabilization, taste masking, enhancement in drug absorption, reduction of toxicity and improvement of drug release profile or sustained drug delivery applications [21].

1.4.1 Classification of CDNSs

CDNSs has been classified in different groups depending on the types of crosslinker used for the synthesis of the polymer.

1.4.1.1 Cyclodextrin-based Carbamate Nanosponges

These types of NSs are prepared by crosslinking of cyclodextrins with diisocyanates. The most commonly used diisocyanates are hexamethylene diisocyanate (HDMI) and toluene-2,4- diisocyanate. These types of NSs were developed initially for water treatment

Introduction

applications by Li and Ma [22]. The prepared carbamate NSs were utilized as an alternative for activated carbon and their performance was demonstrated on the absorption of p-nitrophenol. Regardless of low surface area of 1-2 m²/g, a high loading capacity of 20-40 mg/cm³ was observed.

The absorption capacity of carbamate NSs against organic pollutants generated from feed water of power plants was evaluated by Mamba and co-workers [23]. The significant results were obtained as carbamate NSs showed 90 % absorption of volatile compounds and 84 % absorption of dissolved organic carbon fractions was observed.

1.4.1.2 Cyclodextrin-based Carbonate Nanosponges

These are the most preferred nanosponges for drug delivery applications because of their high stability and low toxicity. Carbonate based NSs are prepared by crosslinking of CDs with carbonyl group-containing crosslinkers such as 1-1'-carbonyldiimidazole (CDI), diphenyl carbonate (DPC) and triphosgene.

However, triphosgene is not preferred crosslinker as it is toxic in nature. These NSs exhibit low swelling tendency due to the presence of short crosslinking bridges. Moreover, high chemical stability in acidic as well as alkaline medium was observed. It was also observed that in some cases, the absorption performance of carbonate-based NSs is similar or higher compared to activated carbons. The absorption capacity of carbonate-based NSs was demonstrated by Trotta and group for the removal of chlorinated

Introduction

persistent organic pollutants (POPs) from wastewaters, in comparison with activated carbon [19].

Furthermore, carbonate-based NSs have been extensively utilized for the encapsulation of several water-insoluble drugs such as curcumin [24] doxorubicin [25], resveratrol [26], and babchi Oil [27] to improve their wettability and solubilization.

1.4.1.3 Cyclodextrin-based Ester Nanosponges

These types of NSs are usually prepared from polyesters or polycarboxylic acids such as pyromellitic dianhydride (PMDA) [28], ethylene diamine-tetraacetic dianhydride (EDTA dianhydride) [29], butanetetracarboxylic dianhydride [30] and citric acid [31]. This class of NSs has a unique property as they can absorb large amounts of water (up to 25 times) and form hydrogels. The degree of swelling of ester-based NSs is dependent on the crosslinker concentration. A higher crosslinker concentration leads to low swelling of the polymer because of the higher crosslinking density. In contrast to carbamate and carbonate-based NSs, ester-based NSs are more susceptible to the hydrolytic degradation. This type of NSs can further host cationic guest molecules as well due to the presence of terminal free carboxylic acid groups. The effect of crosslinker concentration on the vibrational dynamics of NSs was evaluated earlier and it was observed that crosslinking is dependent on the crosslinker concentration up to 1:6 mole ratio of CD and PMDA. However, a further increase in the crosslinker concentration (i.e. 1:8 and 1:10) led to decrease in the degree of crosslinking due to possible steric hindrance [32].

Introduction

1.4.1.4 Cyclodextrin-based Ether Nanosponges

The ether-based NSs are prepared by the crosslinking of CDs with crosslinker containing epoxide groups such as epichlorohydrin [33], bisphenol A diglycidyl ether, and ethylene glycol diglycidyl ether [34]. Ether based NSs are highly chemically stable and their swelling properties can be tailored. However, epichlorohydrin is considered toxic in nature. Despite of toxicity, epichlorohydrin has been explored in the pharmaceutical field.

CD-based NSs are utilized widely as tablet disintegrating agents [35], as a drug carrier [36], for the removal of unwanted flavors of food [37], for the inhibition of enzymatic browning of fruit juices [38], and as a stationary phase for chromatographic separations.

A different type of swellable NS called poly(amidoamine) CD nanosponges were synthesized by Ferruti and co-workers [39]. Poly(amidoamine) CD nanosponges were prepared by the polymerization of β -CD with acetic acid 2,2'-bis(acrylamide) in water with the help of lithium hydroxide as a catalyst. In another study, these NSs were utilized in the drug delivery applications and it was observed that approx. 90 % of the encapsulation of Bovine serum albumin was obtained. The presence of carboxylic acid and amines groups in the polymeric network provides a good affinity for proteins and other similar small molecules [40].

Morales-Sanfrutos et al. developed crosslinked polymer of divinyl sulfone (crosslinker) with α and β -CD to demonstrate absorption of aromatic pollutants (i.e. bisphenol α - and β -naphthol) and bioactive compounds (i.e. progesterone and curcumin) [41].

Introduction

1.4.1.5 Functionalized Nanosponges

The presence of the hydroxyl groups of CDs allow the addition of desired functional groups or moieties to generate new kind of NSs. The addition of desired moieties can be carried out in three possible ways: pre-crosslinking functionalization, co-crosslinking functionalization, and post-crosslinking functionalization of CDs.

Two different class of functionalized nanosponges have been studied so far:

- (i) Fluorescent CD-NSs
- (ii) Charged CD-NSs

Fluorescent CD-NSs were prepared using rhodamine and fluorescein as a fluorescent probe on epichlorohydrin-CD polymer by Malanga and group [42]. In a similar study, Ncube et al. demonstrated the synthesis of the fluorescent water-soluble polymer [43]. To carry out cell internalization studies, Lemdo et al. demonstrated the synthesis of fluorescent carbonate and carboxylated NSs by incorporating fluorescein isothiocyanate with preformed NSs by post- crosslinking functionalization. The post-synthetic modification of carbonate-based NSs was carried out by succinic anhydride. The carboxylation of the NSs leads to improved encapsulation and higher intracellular permeability of acyclovir [44].

Charged CD-NSs have been developed in order to promote efficient complexation of the ionic compounds. Moreover, it was also observed that charged NSs are more stable compared to non-charged NSs due to more statistic repulsion between ionic groups.

Introduction

Positively charged β -CDNSs of glycidyl-trimethylammonium chloride and epichlorohydrin were also reported [45].

1.4.1.6 Cyclodextrin-calixarene Nanosponge

This is a new class of cyclodextrin based NSs mainly prepared by the co-polymerization of β -CD and calixarene, covalently crosslinked via triazole units. Lo Meo et al. first demonstrated the synthesis of cyclodextrin-calixarene based NSs for the removal of nitroarenes and commercial dyes [46]. In another study, cyclodextrin-calixarene polymers were developed by Massaro and co-workers for the encapsulation of polyphenolic bioactive compounds (i.e. quercetin and silibinin). It was observed that due to the presence of two different cavities of cyclodextrin-calixarene NSs, different drug molecules can also be co-incorporated simultaneously [47]. Moreover, the presence of free or incompletely coupled azide groups can be utilized for the post-synthetic modification of the NSs.

1.4.1.7 Stimuli-responsive Nanosponges

The stimuli-responsive nanocarriers are responsible for the release of drug molecules at the target site in a response to stimulating signals in order to minimize the drug-related side effects [48]. The controlled drug release at the target site can be obtained using nanocarrier stimulated by different signals ranging from temperature, electromagnetic fields, redox potentials, reactive species and pH levels [49].

Trotta et al. developed glutathione (GSH) responsive nanosponges for the delivery of an anticancer drug [50]. It is well known that cancer cells exhibit higher intracellular GSH content (0.5-10 mM)

Introduction

compared to normal cells (2-20 μM) [51]. The presence of GSH in the nanocarrier allows the delivery of a drug to the target site without affecting the normal tissues. GSH responsive NSs were prepared by the crosslinking of 2-hydroxyethyl disulfide with pyromellitic dianhydride and β -CD. The prepared NSs were used to encapsulate the doxorubicin and its effect on cell viability was determined.

Russo et al. demonstrated the synthesis of pH-responsive polyaminocyclodextrin nanosponges by crosslinking of (6-deoxy)- β CD with different aliphatic polyamine linkers. The performance of polyaminocyclodextrin nanosponges was evaluated in terms of their absorption ability at different pH values for selected guest molecules [52].

1.4.1.8 Molecularly Imprinted Nanosponges

These types of NSs are prepared by the reaction of template molecules (i.e. drug) with functional monomer and crosslinking agents. The template molecules are usually removed after the reaction that led to the generation of cavities corresponds to the target [53,54]. These generated cavities provide molecular recognition property to the molecularly imprinted polymer (MIP). Specific molecule recognition, high selectivity, and affinity for the target molecules are the important properties of MIPs [55].

Shende et al. demonstrated the synthesis of MIPs of PMDA and β -CD as biomimetics for glucose estimation. MIPs are widely utilized in drug delivery applications, as a biosensor for recognition of protein or enzymes, and quantitative assay [56,57]. Trotta and

Introduction

group developed the L-DOPA imprinted CD-NSs for the treatment of neurodegenerative disease in which MIPs were prepared by crosslinking of β -CD and CDI in the presence of the variable amount of L-DOPA [58].

1.4.2 Method for the Preparation of the NSs

1.4.2.1 Solvent-based Method

This method of synthesis involves the use of solvents such as DMF, DMSO, and pyridine in order to dissolve CDs and crosslinker. A mixture of CDs and crosslinker were added into the different molar ratios and reaction is carried out either at room temperature or reflux temperature depending on the type of crosslinker. Carbonate based NSs are prepared at high temperature however, PMDA containing ester-based NSs are prepared at room temperature [59,60].

Once the reaction completed, a gel-like mass was obtained which was washed with water followed by acetone or ethanol. The final purification of NSs was carried out by Soxhlet extraction. It has been also observed that NSs of the desired size range can also be obtained by size reduction techniques such as high-pressure homogenization and ball-milling.

1.4.2.2 Melt/Fusion Method

This method involves the synthesis of NSs without the use of any organic solvents. In this method, CDs and crosslinkers were heated at a higher temperature to carry out a crosslinking reaction [21].

Introduction

The prepared NSs were purified by method as mentioned in section 1.4.2.1.

1.4.2.3 Ultrasound-assisted Synthesis

This method of NSs synthesis is carried out by sonication without the use of any organic solvents. β -CD and crosslinker (i.e. DPC) were added into water and reaction is carried out at 90 °C for five hours with continuous sonication for the entire experiment. Ultrasound-assisted synthesis is helpful to control the crystallinity of the prepared NSs. The purification of prepared NSs is performed as mentioned above [61].

1.4.2.4 Microwave-assisted Synthesis

The reaction time required to synthesize NSs can be reduced by the use of microwave and high crystallinity of NSs can be obtained. In this method, CDs and crosslinker were dissolved in the organic solvent such as DMF and subjected to the microwave irradiation. It was observed that the use of microwave irradiation causes a four-fold reduction in the reaction time. The prepared NSs were purified as mentioned above [62].

1.4.3 Factors Affecting Nanosponges Formation

1.4.3.1 Types of Crosslinker and Polymer

The performance and nature of NSs are depended on the type of crosslinker. The native CDs can be converted into a 3-dimensional nanoporous structure with the reaction with different crosslinkers. Moreover, the type of crosslinker leads to the formation of either hydrophilic or hydrophobic NSs.

Introduction

The hydrophilic NSs can be synthesized by the use of epichlorohydrin as a crosslinker [63]. Due to their hydrophilic nature, these NSs can be used to prepare extended or immediate-release formulations with improved absorption of drugs across the biological membranes. On the other side, hydrophobic NSs can be prepared by a variety of crosslinkers such as carbonyldiimidazole, diphenyl carbonate, pyromellitic dianhydride and diisocyanates [64,65]. Moreover, the nature of crosslinkers is important to decide the applications of the prepared NSs.

1.4.3.2 Degree of Substitution

The number, type and position of the substitution on the polymeric network can affect the complex formation ability of the prepared NSs. The reactive functional groups of different types of cyclodextrins are available to prepare NSs with different crosslinkers. The higher degree of substitution of hydroxyl groups of cyclodextrin with crosslinkers can lead to the formation of a highly crosslinked structure that can form more interconnected networks within the polymer. The higher degree of crosslinking further affects the complexation efficiency as the presence of highly interconnected networks hinder the inclusion of guest molecules within the polymer [66,67].

1.4.3.3 Complexation Temperature

The complexation temperature can significantly affect the stability of the drug-NS complex. The rise in temperature during complexation leads to a decrease in interaction forces (i.e. Van der

Introduction

Waals forces) required for the formation of complex thus altering the stability of the NS complex [68,69].

1.4.4 Characterization of Nanosponges

Several methods have been extensively used to characterize different types of NSs as shown below:

1.4.4.1 Morphological Evaluation

The morphology of blank NSs or drug-loaded NSs can be determined by Transmission Electron Microscopy (TEM), Scanning Electron Microscopy (SEM), and Field Emission Scanning Electron Microscopy (FE-SEM). The shape and size of NSs and drug-NSs inclusion complex can be predicted by the above-mentioned techniques. The change in the crystallinity of the inclusion complex compared to native NSs can be considered as an indication of the formation of inclusion complex [70,71].

1.4.4.2 Polydispersity and Zeta Potential Determination

The hydrodynamic diameter of NS formulations can be determined by dynamic light scattering (DLS) method. The prepared formulation should have nanometer particle size and uniform size distribution for the drug delivery applications. Surface charge of the NSs is expressed in terms of zeta potential. The stability of drug-NSs colloidal suspension is dependent on the zeta potential. Zeta potential values greater than ± 25 mV are considered as good to make a stable suspension [72,73].

Introduction

1.4.4.3 Drug Loading and Entrapment Efficiency

The distribution of the drug within the nanocarrier is determined by the drug loading and the percentage of drug successfully entrapped inside the nanocarrier is predicted by entrapment efficiency. Different techniques such as UV-Visible spectroscopy, and high-performance liquid chromatography (HPLC) are most commonly used to determine drug loading and entrapment efficiency [74].

The following equations are used to determine drug loading (DL) and entrapment efficiency (EE).

$$DL (\%) = [\text{Entrapped Drug}/\text{weight of NSs}] * 100$$

$$EE (\%) = [\text{Entrapped drug}/\text{Total drug}] * 100$$

1.4.4.4 Porosity and Surface Area

The presence of nanocavities and nanochannels in the NSs can be determined by porosity measurement. The helium displacement method is used to determine the true volume due to the ability of helium to penetrate into intra-particle and inter-particle channels of the NSs. The most common method for the determination of the surface area of porous material is Brunauer, Emmett, and Teller (BET) analysis [75,76].

1.4.4.5 Swelling and Water Uptake Studies

The water uptake and swelling studies of the NSs are used to determine the extent of swelling in aqueous media and water uptake capacity mainly in case of the swellable NSs [77,78].

Introduction

The following equations are used to depict the swelling and water uptake of the NSs.

$$\text{Swelling (\%)} = [S_t/R_0]*100$$

Where S_t = reading of cylinder after soaking at a specific time and S_0 = initial reading of cylinder before soaking

$$\text{Water uptake (\%)} = [W_t/W_0]*100$$

Where W_t = weight of hydrogel at a specific time and W_0 = weight of dry NSs.

1.4.4.6 In-vitro Release Studies

The release behavior of a drug from the NSs is determined by in-vitro release profile. Multi-compartment rotating cells or dialysis membranes method is used to predict the drug release profile. For drug release studies, at predetermined time intervals aliquots are withdrawn and replaced with fresh dissolution media that were subjected to further analysis by UV-visible spectroscopy or HPLC [79,80].

1.4.4.7 Fourier Transform Infrared Spectroscopy and Raman Spectroscopy (FTIR)

FTIR and Raman spectroscopy techniques are used to predict the interaction of a drug with the NSs in the solid-state. NSs are characterized by the presence of characteristic peaks in their structure such as carbonate-based NSs prepared from CDI exhibit peaks at $1720\text{-}1750\text{ cm}^{-1}$ (carbonate stretching vibrations). A change or shift in the characteristic peaks of the NSs is considered

Introduction

as possible interaction of the drug molecules within NSs might be due to encapsulation of the drug [81,82].

1.4.4.8 Thermal Analysis

Thermal properties of drug molecules and NSs are determined by differential scanning calorimetry (DSC), and thermogravimetric analysis (TGA). The appearance of new peaks, disappearance of existing peaks, peak shift or peak broadening can be evaluated by DSC. A shift or disappearance of the characteristic peak of a drug molecule is considered as the formation of an inclusion complex. Moreover, TGA analysis can be utilized to predict the change in the weight loss as an indication of the inclusion complex formation [83,84].

1.4.4.9 Crystalline and Amorphous Nature of the NSs

The nature of the NSs or drug molecules in solid-state can be determined by the powder x-ray diffraction (PXRD) studies. Most of the drug molecules exhibit different diffraction patterns compared to the NSs. The inclusion complex formation can be confirmed by the change in the crystallinity of the drug molecules, shifting or disappearance of the diffraction peaks. For instance, the disappearance of the diffraction pattern of crystalline drug molecules is considered as the molecular dispersion of drugs within the NSs. A comparative evaluation of the physical mixture (non-inclusion complex) of drug and NSs with inclusion complex can also be carried out to determine the change in the diffraction pattern [85,86].

Introduction

1.4.4.10 In-vitro Stability Studies

The determination of the in-vitro stability of the colloidal suspension of the drug-NSs inclusion complex is important in order to avoid the sedimentation or aggregation of the particles. The stability of suspension is can be evaluated by the DLS method in order to determine the size and particle size distribution upon storage at different temperatures. Moreover, particles with nanometer size range and narrow size distribution offer long term stability due to the slow sedimentation rate. Furthermore, polymeric stabilizers or cryoprotectants can also be incorporated in the formulation to impart the stability during freeze-drying [87].

1.5 Applications of the Nanosponges

NSs are extensively utilized for several pharmaceutical and non-pharmaceutical applications as discussed below:

1.5.1 Solubilization of Poorly Water-soluble Drug Molecules

Solubilization of drug molecules is an important parameter for drug delivery applications for instance, in oral drug delivery drugs should dissolve rapidly to form a solution in order to absorb through the gastrointestinal tract (GIT). Thus, the low solubility of drug molecules remains a challenge in the drug delivery applications. Inclusion complex formation of poorly water-soluble drugs with NSs can increase the wettability subsequently the solubilization of the guest molecules. The presence of the internal cavities can host hydrophobic drug molecules and hydroxyl groups of CDs at the outer surface are hydrophilic in nature thus can act as a hydrophilic drug-CD complex [88]. The change in the crystallinity of guest molecules

Introduction

after inclusion complex formation can also be attributed to the high dissolution [89]. Conte et al. developed topical formulation of ester-based NSs containing Benzoporphyrin-derivative monoacid ring A (BDPMA), All-trans retinoic acid and Diclofenac sodium to increase the solubilization, photostability, and localized action of the encapsulated drug molecules [90]. An increase in the aqueous solubility and oral bioavailability of telmisartan with the help of ternary complex of NSs is also reported earlier. The inclusion complex of telmisartan with NSs exhibited 20 fold enhancement in the aqueous solubility and 54 % increase in the oral bioavailability [91].

1.5.2 Modulation of Drug Release Profile

Conventional dosage forms are associated with a major drawback of frequent dosing that can cause dose-related side effects. NSs offer several advantages in such cases as they can provide a slow and uniform drug release profile for a longer period of time. Drug loaded NSs provide sustained drug release to decrease the dosing frequency and alter pharmacokinetic profile that can subsequently decrease drug-related side effects. Swaminathan and co-workers demonstrated the synthesis of the itraconazole inclusion complex with CDNSs in order to achieve the sustained drug release profile compared to itraconazole alone [86]. Dexamethasone encapsulated carbonate-based NSs were prepared to increase the drug dissolution and corneal permeability for ocular delivery. In-vitro release profile suggested a significant increase in the release of dexamethasone from NSs was observed compared to drug alone. A higher corneal

Introduction

permeability of dexamethasone inclusion complex was reported compared to the marketed formulation [92].

1.5.3 Nanosponges as a Drug Delivery Carrier

NSs are considered as the drug delivery carrier for a variety of drug molecules such as hydrophobic drugs, hydrophilic drugs or macromolecules. Short biological half-life, poor aqueous solubility, low permeability, and low chemical stability are the major challenges while designing a drug delivery dosage form. For instance, dissolution in a biological fluid is a rate-limiting step for hydrophobic drug molecules. CDNSs offer several advantages as they can accommodate drugs inside the cyclodextrin cavities as well as nanochannels formed between CDs and crosslinkers thus can also provide the desired drug release profile. Moreover, the presence of drug molecules inside the CDs cavities can protect it from the outer environment.

NSs are considered as biocompatible and nontoxic for the pharmaceutical applications. In 2014, the EU Commission report suggested the use of NSs as promising drug delivery vehicles for the pharmaceutical use, thanks to the versatility of the NSs. NSs have been utilized as diluents or fillers for the preparation of solid oral dosage form. In parenteral formulation, freeze-dried NSs containing drugs can be reconstituted with sterile water for injection or saline to administer via intravenous route. Drug-NSs inclusion complex containing hydrogel can be used as topical drug delivery systems. Morales-Sanfrutos and group developed the divinyl sulfone crosslinked cyclodextrin nanosponges as a drug delivery carrier for progesterone and curcumin [41]. Nanosponge based dry suspension

Introduction

of gabapentin for the controlled delivery in pediatric patients was developed by Rao and Bhingole. In-vivo pharmacokinetic studies confirmed the uniform and consistent delivery of gabapentin [93].

1.5.4 Protein Delivery

The delivery of proteins and peptides is associated with several challenges such as sensitivity towards various enzymes, poor bioavailability, the tendency of denaturation, short-half life and high molecular mass. The use of NSs for the delivery of proteins and peptides are reported earlier as NSs can accommodate protein with variable mass and can protect it from the sensitive outer environment. Deshmukh et al. reported the synthesis of carbonate-based NSs containing calcium carbonate for the treatment of hypocalcemia, impregnated with lysozyme to determine the antimicrobial potential [94]. In another study swellable cyclodextrin-based poly (amidoamine) nanosponges (PAA-NS) were prepared for the delivery of Bovine serum albumin (BSA) as a model protein [40].

1.5.5 Protection from Degradation

The encapsulation of drug molecules within the NSs allow protection from light, chemical and enzyme induced degradation. The protection of various chemical entities from light degradation has been studied extensively. Camptothecin is a poorly water soluble drug most commonly used for the treatment of the cancer. However, camptothecin is susceptible to the hydrolytic degradation due to the presence of a lactone ring. Swaminathan et al. prepared the inclusion complex with NSs to increase the shelf life of camptothecin [95]. The protection of resveratrol against UV-light

Introduction

was also reported by Pushpalatha and co-workers. It was observed that almost 2 fold protection from light degradation was observed after the encapsulation of resveratrol with ester and carbonate-based NSs [96].

1.5.6 Gas Delivery

It has been reported that CDNSs acts as a reservoir for various gas molecules such as oxygen, carbon dioxide, and 1-methyl cyclopropane. The use of carbonate-based NSs as a carrier for the oxygen delivery was first reported by Cavalli and group [97]. Recently, Femminò et al. prepared water-soluble and insoluble ester-based NSs containing oxygen for the treatment of injury associated with ischemia/reperfusion [98].

1.5.7 Water Purification

Treatment of the polluted water is another interesting application of NSs. Polluted water contains several harmful organic and inorganic chemicals that can cause severe damage to the humans, animals and the nature. The most common metallic impurities are copper, zinc, and lead. Aromatic hydrocarbons and alkyl-phenolic compounds are organic impurities commonly present in industrial discharge [99]. Li and Ma prepared polyurethane-based NSs for the removal of organic impurities presented in the polluted water [22]. Euvrard and group demonstrated the absorption capability of ester-based NSs for the treatment of polluted water containing heavy metals and organic impurities [100].

Introduction

1.6 Literature Survey

1.6.1 Literature Related to Nanosponges

Over the last 20 years, nanosponges have been used extensively in the pharmaceutical applications. Some of the examples are reported in the table below.

Table 1. 2 Nanosponges for the several pharmaceutical applications.

| S.No. | Drug | Property enhanced | Remarks | Ref. |
|--------------|--------------------------|--|--|-------------|
| 1. | Curcumin and Resveratrol | Controlled drug delivery and enhanced ex-vivo permeation | Ester-based NSs were developed for breast cancer treatment. The controlled release profile of both drug molecules was observed up to 8 hours. Ex-vivo skin permeation studies confirmed the 11.5 fold enhancement for curcumin and 2.5 fold enhancement for the resveratrol compared to their respective free drugs. | [101] |

Introduction

| S.No. | Drug | Property enhanced | Remarks | Ref. |
|--------------|-------------|---|--|-------------|
| 2. | Norfloxacin | Intestinal permeability and antibacterial activity | Carbonated-based NSs were prepared. A higher permeation of Norfloxacin with NSs was reported compared to free drug. NSs based formulation of norfloxacin showed high mucoadhesive property followed by a high antimicrobial activity. | [102] |
| 3. | Doxorubicin | pH-responsive nanocarrier, improved internalization and controlled drug release | Cyclic nigerosyl-1-6-nigerose (CNN)-PMDA NSs for stimuli-responsive drug delivery. Prepared Doxorubicin NSs showed a sustained release of DOX (32.5%) after 21 days. Cytotoxicity study confirmed the 8 fold enhancement in the IC ₅₀ . | [103] |

Introduction

| S.No. | Drug | Property enhanced | Remarks | Ref. |
|--------------|-------------|---|---|-------------|
| 4. | celecoxib | Improved solubilization and oral bioavailability | Drug loaded Acrylamide NSs showed up to 40 fold higher solubilization of celecoxib. The in-vivo pharmacokinetic data suggested high skin permeation of celecoxib due to an increase in the permeability of drug-NSs complex. | [104] |
| 5. | Paclitaxel | Increase in the chemical stability and oral bioavailability | Carbonate-based NSs were prepared for cancer treatment. Relative oral bioavailability was enhanced 2.56 fold compared to plain paclitaxel. Higher cytotoxicity was observed, and prepared formulations were safe compared to other reported formulations. | [105] |

Introduction

| S.No. | Drug | Property enhanced | Remarks | Ref. |
|--------------|-------------|---|--|-------------|
| 6. | Tamoxifen | Improvement in solubility, bioavailability, and cytotoxicity | Tamoxifen loaded CDNSs were prepared which showed more than 40 % solubilization compared to free drug. Higher cytotoxicity of tamoxifen NSs formulation was observed with 1.45 fold higher oral bioavailability. | [106] |
| 7. | Quercetin | Higher solubilization, photostability, and antioxidant activity | Quercetin loaded carbonate-based NSs formulation showed 20 fold higher solubilization of drug. Photostability studies confirmed the protection of quercetin, better antioxidant activity was observed with drug loaded NSs compared to free quercetin. | [107] |

Introduction

| S.No. | Drug | Property enhanced | Remarks | Ref. |
|--------------|--------------------|--|--|-------------|
| 8. | Imiquimod | Controlled release and high anti-proliferative Activity | Imiquimod loaded ester-based NSs showed controlled release profile. In vitro cell line studies confirmed the reduction in the proliferation of HS fibroblast and controlled in-vitro skin permeation compared to others. | [108] |
| 9. | γ -Oryzanol | Enhanced photostability and antioxidant property, better skin permeability | γ -Oryzanol containing NSs showed that photostability, antiradical activity, inhibition of lipid peroxidation were comparatively higher for drug-inclusion complex. γ -Oryzanol loaded NSs 30 fold higher skin permeation than o/w emulsion of the same formulation. | [109] |

Introduction

| S.No. | Drug | Property enhanced | Remarks | Ref. |
|--------------|--|---|---|-------------|
| 10. | Erlotinib | Enhanced solubilization, and drug release. High anti-tumor activity | Erlotinib containing carbonate NSs were prepared which showed more than 8 fold higher solubilization than the free drug. Biological studies showed better internalization and more than 2 fold higher cytotoxicity than the free drug. | [110] |
| 11. | Rutin, phloridzin and chlorogenic acid | Enhanced protection from heat and light, controlled release | Carbonate and urethane-based NSs were prepared. Carbonate based NSs showed better encapsulation of rutin while urethane-based NSs good results with phloridzin and chlorogenic acid. All the NSs formulation showed consistent release over a period of 24 hours. | [111] |

Introduction

| S.No. | Drug | Property enhanced | Remarks | Ref. |
|--------------|-----------------------------|--|---|-------------|
| 12. | Dexa-methasone (DEX) | Solubility enhancement | Two different types of carbonate-based NSs mainly crystalline and paracrystalline NSs of dexamethasone were prepared to improve its solubilization. | [112] |
| 13. | Flurbiprofen | Improved solubilization and modulation of drug release | Preliminary results suggested good solubilization of Flurbiprofen with carbonate-based NSs. Hemolytic and cytotoxicity studies confirmed the safety of the nanocarrier. | [113] |
| 14. | Acetyl salicylic acid (ASA) | Improvement in the oral bioavailability | ASA loaded ester-based NSs showed slow and uniform drug release for 24 hours. In-vivo studies suggested higher anti-inflammatory activity compared to free drug. | [114] |

Introduction

| S.No. | Drug | Property enhanced | Remarks | Ref. |
|--------------|-----------------------|--|--|-------------|
| 15. | Rilpivirine HCl (RLP) | Enhancement of solubility and oral bioavailability | RLP loaded carbonate and ester-based NSs showed higher drug solubilization which was confirmed by contact angle study. In-vivo pharmacokinetic studies confirmed the increase in the plasma concentration and biological half-life of drug-NSs complex than free drug. | [115] |
| 16. | Efavirenz | Improvement in the solubility and oral bioavailability | Efavirenz loaded NSs exhibited 8-fold higher solubility in water compared to free drug. In-vivo pharmacokinetic studies showed close to 2-fold higher blood concentration of the drug on oral administration. | [116] |

Introduction

1.6.2 Literature Related to the Selected Drug Molecules

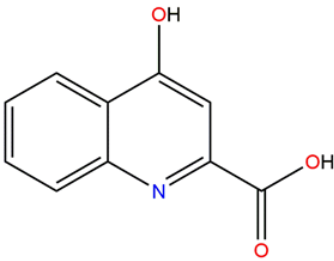
1.6.2.1 Profile of Kynurenic Acid

Kynurenic acid (KYNA) is synthesized endogenously via the kynurenine metabolic pathway because of the metabolism of the tryptophan. However, Dietary food products such as broccoli, potato, and spices also showed the presence of KYNA [117,118]. KYNA acts as an excitatory amino acid antagonist and exhibits neuroprotective properties. László and beal demonstrated the neuroprotective activity of KYNA [119]. Moreover, KYNA also acts as glutamate receptor antagonist which was reported by Carpenedo and group [120]. It has been widely reported that KYNA exhibits antioxidant and free radical scavenging activity. Majorly, KYNA is synthesized inside the central nervous system (CNS). However, presence of KYNA is also reported in the human blood and peripheral organs. Several neurological disorders such as Parkinson's disease, multiple sclerosis, and Huntington's disease are associated with decreased production of KYNA [121,122].

However, KYNA exhibits poor aqueous solubility and limited blood-brain barrier (BBB) permeability, which limits the therapeutic application of KYNA [123]. Moreover, it is also reported that KYNA can cross the blood-brain barrier (BBB) to a limited extent and systemic administration of KYNA leads to the accumulation in the brain [124]. The concentration of KYNA in the mammalian brain is around 10–150 nM which was reported by Moroni and co-workers [125].

Introduction

Table 1. 3 Properties of Kynurenic Acid

| Name | Kynurenic acid |
|----------------------|--|
| Chemical name | 4-hydroxyquinoline-2-carboxylic acid |
| Molecular formula | C ₁₀ H ₇ NO ₃ |
| Molecular weight | 189.168 g/mol |
| Chemical structure |  |
| CAS number | 492-27-3 |
| Description | White crystalline powder |
| Melting point | 282.5 °C |
| Log P | 1.16 |
| Solubility | Poor water solubility (0.017 mg/ml), soluble in DMSO (20 mg/ml). |
| Therapeutic category | Natural Antioxidant, Parkinson's Disease, Multiple Sclerosis, and Huntington's Disease |

Introduction

Researchers have demonstrated applications of KYNA on systemic administration and its permeation across BBB. KYNA loaded core-shell nanoparticles of bovine serum albumin (BSA) were prepared by Varga and group. They also demonstrated that KYNA loaded BSA nanoparticles on peripheral administration, produce electrophysiological effects within the CNS [126]. Hornok and co-workers demonstrated the pharmacological activity of KYNA loaded micelles on systemic administration [123]. The solubility of KYNA is a greater concern in the drug delivery thus researchers also tried different methods to improve its solubilization. KYNA loaded silica nanoparticles were prepared by López and co-workers to improve the solubilization of KYNA [127]. Prodrugs of KYNA with different ester derivatives were also prepared to improve its solubility and permeability [128]. Thus, problems associated with KYNA can be countered by preparing an inclusion complex with NSs as a delivery carrier.

1.6.2.1.1 Metabolic Pathway of KYNA

Apart from being one of the 20 amino acids that constitute proteins, tryptophan is also a precursor for the synthesis of serotonin and L-kynurenine under physiological conditions.

L-kynurenine is an intermediate metabolite of the complex metabolic pathway that ends with NAD⁺, kynurenic acid, and xanthurenic acid. More than 95% of tryptophan is metabolized through the kynurenine pathway. Tryptophan is transported across the blood-brain barrier (BBB) with the aid of the large neutral amino acid transporter. Within the brain, the metabolism of tryptophan proceeds via the serotonin pathway and the kynurenine pathway.

Introduction

The metabolites of this pathway are collectively called kynurenines. The kynurenine metabolic pathway endogenously metabolizes tryptophan into KYNA, 3-hydroxykynurenine (3-HK) and quinolinic acid (QUIN) by kynurenine aminotransferase, kynurenine 3-monooxygenase, and kynureninase enzymes, respectively. The 3-HK is a potent free radical generator and QUIN acts as N-methyl-D-aspartate (NMDA) receptor agonist. However, KYNA is an ionotropic glutamate and alpha 7-nicotinic receptor antagonist [129].

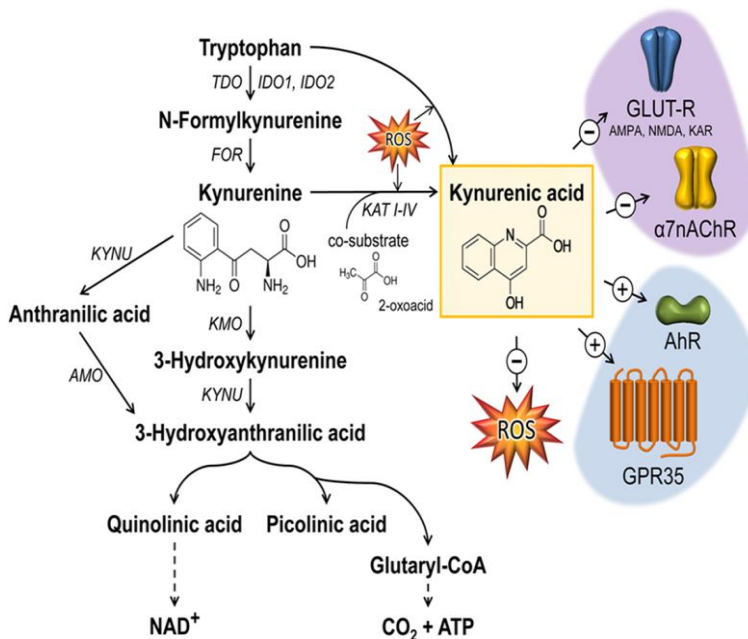


Figure 1.3: Kynurenine Pathway [130]

Introduction

1.6.2.1.2 Analytical Methods for the Determination of KYNA

KYNA has been evaluated by several methods. The most commonly used methods are based on HPLC and fluorescence spectroscopy. The table lists some of the examples of KYNA determination.

Table 1. 4 Analytical methods of KYNA

| Type of Column | Mobile Phase | Detector and λ_{\max} | References |
|---|--|---|-------------------|
| Hypersil GOLD C18 column (50 mm x 2.1 mm i.d.) | 15 mM potassium phosphate (pH 6.4), with 2.7% (v/v) acetonitrile (Isocratic Elution) | UV diode array detector (PDA); 286-360 nm | [131] |
| Synergi 4 μ m reverse-phase Fusion-RP80A column (250 \times 4.6 mm) | 27% methanol: 73% 10 mM sodium dihydrogen phosphate (pH 2.8) (Isocratic Elution) | UV-Vis detector; 220 nm Fluorescence (LS 30) detector; 254/404 nm | [132] |
| TSK-Gel ODS-80 Ts (250 \times 4.6 mm i.d., 5 μ m) | 0.1% TFA in H ₂ O:ACN (90:10 v/v) (Isocratic Elution) | UV-PDA detector; 220 nm | [133] |

Introduction

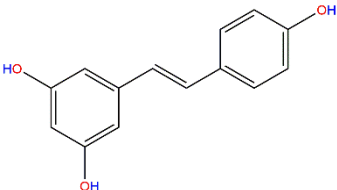
1.6.2.2 Profile of Resveratrol

Resveratrol (RES) is a naturally occurring polyphenolic compound of stilbenes family. In 1939, RES was first isolated from *Veratrum grandiflora* O. loes. Later, it has been discovered in a variety of edible sources such as peanuts, mulberries, grapes, pistachios, and plums [134]. Several studies suggested that RES has a number of potential health benefits, such as antioxidant, anti-cancer, anti-inflammatory, anti-obesity, and heart/brain-protective effects.

It is also observed that RES is helpful to combat coronary heart diseases such as myocardial infarction, arrhythmias, hypertension, atherosclerosis, and thrombosis [135]. Several biochemical mechanisms have been suggested for the activity of RES in heart diseases like antioxidant activity, inhibition of cyclooxygenase-I (COX-I) enzyme [136]. For brain-related diseases, antioxidant activity of RES, its ability to interfere with signaling pathways, and the ability to rise sirtuin production are responsible [137]. Moreover, RES exhibited the ability to induce apoptosis, caspase activation, arrest of cell cycle and decrease of the metastasis that is responsible for the anti-carcinogenic activity [138]. Anti-obesity activity of RES is due to decrease in lipid production, promotion of lipolysis, and reduction of lipid accumulation. RES also shows COX-II inhibition activity which is responsible for the anti-inflammatory effect [139]. The pharmaceutical use of RES is limited due to low water solubility, and chemical instability.

Introduction

Table 1. 5 Properties of resveratrol

| Name | Resveratrol |
|----------------------|--|
| Chemical name | Trans-3,5,4'- Trihydroxystilbene |
| Molecular formula | C ₁₄ H ₁₂ O ₃ |
| Molecular weight | 228.24 g/mol |
| Chemical structure |  <p>The chemical structure of Resveratrol is a stilbenoid, specifically a trans-stilbenoid. It consists of two phenolic rings connected by a trans-stilbene bridge. The left ring is a 3,5-dihydroxyphenyl group, and the right ring is a 4'-hydroxyphenyl group. The hydroxyl groups are shown in red and blue.</p> |
| CAS number | 501-36-0 |
| Description | White powder |
| Melting point | 261 to 263 °C |
| BCS classification | Class II |
| Log P | 3.1 |
| Solubility | Poor water solubility (0.03 g/L), soluble in DMSO (16 g/L) and ethanol (50 g/L) |
| Therapeutic category | Natural Antioxidant, Anti-Carcinogenic, Anti-Inflammatory, and Anti-Obesity |

Introduction

Despite of low aqueous solubility, RES showed good permeability thus can be considered as Biopharmaceutical Classification System (BCS) class II drug [140]. Moreover, RES is chemically unstable at elevated temperature, pH change, and exposure to the UV light. More precisely, UV exposure of RES for 120 minutes leads to conversion of 90.6% of trans-isomer into cis-isomer which is therapeutically inactive [141].

Thus, the above-mentioned properties of RES make it a suitable candidate to study solubilization, release behavior, chemical stability with NSs based carriers.

1.6.2.2.1 Pharmacokinetics of Resveratrol

Several in-vitro and in-vivo studies were carried out to determine the absorption, metabolism, and bioavailability of RES. Andlauer and co-workers demonstrated the intestinal permeability of RES in rat small intestine perfusion model which suggested that 46% of the lumenally administered resveratrol was extracted by the small intestine whereas vascular side showed 21% of administered RES and intestinal tissue showed the presence of 2% of administered RES [142]. In-vivo metabolism of RES was first evaluated by Bertelli and group in rodent models which suggested that the peak concentration of RES was reached within 60 minutes after ingestion of wine [143]. Moreover, bioavailability determination in humans was carried out in 2001 by Soleas and group. They suggested that plasma concentration of RES is very low (1-5 ng/mL) [144].

Introduction

Goldberg and group demonstrated that oral administration of RES leads to peaks plasma concentration within 30 minutes, however, it gets eliminated rapidly from the body (within 4 hours) [145]. Lancon and group reported the hepatic uptake of RES in human hepatoblastoma cell lines (HepG2; tumor cells) and human hepatocytes (normal cells) to evaluated resveratrol transport in normal versus cancer cells. The authors suggested that RES showed transport via passive diffusion and a carrier-mediated transport mechanism [146]. Burkon and Somoza studied the distribution and excretion of RES and discovered that more than 90 % of free RES bound to plasma and it is also reported that renal excretion is the major route for the elimination of RES [147]. Walle et al. demonstrated that total excretion (via urine and faces) of orally administered RES was 71-98% compared to intravenously administered RES which showed 54-91% of total excretion [148].

1.6.2.2.2 Analytical Methods for the Determination of RES

The detection of RES was carried out majorly by HPLC. Some of the examples of the HPLC methods are shown below:

Table 1. 6 Analytical methods of RES

| Type of Column | Mobile Phase | Detector and λ_{max} | References |
|---|--|--|-------------------|
| Ultrasphere-ODS column (250 mm x 10 mm, 5 mm) | Water/acetonitrile (50:50, v/v). (Isocratic Elution) | UV-Vis detector; 307 nm | [149] |

Introduction

| Type of Column | Mobile Phase | Detector and λ_{max} | References |
|--|--|------------------------------|------------|
| Hypersil ODS2 C18 (5 μ m, 4.6 \times 250 mm) | 0.5% (v/v) acetic acid in methanol and distilled water (50:50 v/v), (Isocratic Elution) | UV-Vis detector; 303 nm | [150] |
| Waters Nova Pack C18 (150 \times 3.9 mm) | Acetonitrile/phosphate buffer pH 4.8–4.9 (25:75, v/v). (Isocratic Elution) | UV-Vis detector; 310 nm | [151] |
| ODS2-C18 reverse-phase (250 \times 4.6 mm, 5 mm) | Methanol: phosphate buffer pH 6.8 (pH adjusted with 0.5% v/v orthophosphoric acid solution (63:37%, v/v). (Isocratic Elution) | UV-PDA Detector; 306 nm | [152] |

1.6.2.3 Profile of Oxyresveratrol

Oxyresveratrol (OXY) is a polyphenolic derivative of stilbenes family obtained from mulberry fruits (*Morus alba* L.) and *Artocarpus lakoocha* Roxburgh (*Moraceae*). OXY showed various pharmacological activities such as antioxidant property, hepatoprotection, neuroprotection, antiviral (mainly herpes simplex virus type I; HSV-I), anti-inflammatory, anti-tumor and cholesterol-lowering property [153,154].

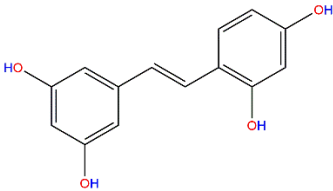
Introduction

The anticancer activity of OXY due to inhibition of protein kinase C, cytochrome P450 (CYP), and 1B1 which act as a tumor promoter. Moreover, OXY promotes apoptosis which is also responsible for anti-carcinogenic activity [155]. Neuroprotection activity of OXY due to its ability to interference with signaling pathways, ability to decrease cytochrome c release followed by reduction of caspase-3 activation [156]. Moreover, in Alzheimer's disease OXY causes a reduction in the β -amyloid induced neurotoxicity [157]. OXY inhibits replication of the virus in the early and late phase which is responsible for the antiviral activity of OXY. OXY also demonstrated the antioxidant activity to prevent oxidative stress-induced apoptosis. Excessive production of reactive oxygen species (ROS) such as H_2O_2 or O_2^- can cause oxidative stress that leads to cell death as a result of apoptosis [158]. The anti-inflammatory effect of OXY was also reported earlier on leukocyte migration which is considered as a key step of inflammatory responses.

It was observed that OXY showed inhibition of chemokine receptor type-4 mediated chemotaxis and extracellular kinase pathway in immune cells [159]. Despite the several pharmaceutical properties, several problems associated with OXY limit its uses as nutraceuticals. OXY is technically unstable molecules as it is photosensitive and undergoes oxidative degradation in aqueous solutions. Moreover, the low bioavailability of OXY further limits its applications [160].

Introduction

Table 1. 7 Properties of oxyresveratrol

| Name | Resveratrol |
|----------------------|---|
| Chemical name | trans-2',3,4', 5-tetrahydroxystilbene |
| Molecular formula | C ₁₄ H ₁₂ O ₄ |
| Molecular weight | 244.24 g/mol |
| Chemical structure |  |
| CAS number | 29700-22-9 |
| Description | Off-white powder |
| Melting point | 196 to 204 °C |
| Log P | 1.1 |
| Solubility | Freely soluble in DMSO, Methanol, Ethanol, and water |
| Therapeutic category | Natural Antioxidant, Anti- Carcinogenic, Anti- Inflammatory |

These above-mentioned problems can be overcome by the use of CDNSs based drug delivery system.

Introduction

1.6.2.3.1 Pharmacokinetics of Oxyresveratrol

It has been observed that OXY exhibits low permeation that leads to low bioavailability on oral administration. Mei and co-workers demonstrated the absorption of OXY in caco-2 cell models. The studies suggested that OXY shows passive diffusion across caco-2 cells which subsequently involved in the efflux mediated transport by P-glycoprotein (P-gp) that is responsible for the low bioavailability of the OXY. The degradation of the OXY is another reason for the low bioavailability at alkaline pH [161]. OXY showed high tissue distribution mainly in the heart, liver, spleen, lung, and kidney on oral administration as reported by Bertram and Davies [162]. OXY also undergoes significant hepatic first-pass metabolism and metabolizes mainly by glucuronidation and sulfation. Human intestinal microsomes are also responsible for the metabolism of the OXY. The metabolic pathway of the OXY was demonstrated by Huang and group. Based on the LC-MS/MS analysis, various conjugated metabolites of OXY including glucuronide, methyl, and sulfate were identified. These metabolites of OXY are excreted via urinary and biliary excretion. It is also reported that a small amount of OXY is excreted unchanged with very short plasma half-life of $0.73 \pm 0.09 \text{ h}^{-1}$ [163]. Moreover, Huang et al. reported that administration of a traditional Chinese plant showed cumulative excretion of OXY in bile and urine was 0.29%, and 0.84%, respectively [164].

Introduction

1.6.2.3.2 Analytical Methods for the Determination of OXY

Some of the examples of methods for the determination of OXY in the literature.

Table 1. 8 Analytical methods of OXY

| Type of Column | Mobile Phase | Detector and λ_{\max} | References |
|---|--|---|-------------------|
| C18 column (VertiSep™ pHendure 4.6 x 250mm, 5- μ m) | Acetonitrile and 0.5% v/v aqueous acetic acid (27:73, v/v) (Isocratic Elution) | UV-Vis detector; 320 nm | [165] |
| Zorbax SB-C18 column (250 x 4.6 mm, 5 μ m) | (A) acetonitrile and (B) 0.5% aqueous acetic acid (v/v) (Gradient Elution) | UV-Vis detector; 320 nm | [166] |
| Agilent ZORBAX Eclipse Plus C18:250 x 4.6 mm i.d., 5mm) | Acetonitrile and Milli-Q water (Gradient Elution) | UV-Vis detector; 325 nm | [167] |
| Phenomenex® Luna® C18 (250 x 4.60 mm) | Acetonitrile, water and formic acid (30 : 70 : 0.04 v/v) (Isocratic Elution) | UV-Vis detector; 320 nm | [168] |

Introduction

1.6.2.4 Profile of Curcumin

Turmeric is the rhizome part of the plant *curcuma longa*. Turmeric contains several polyphenolic compounds collectively called curcuminoids. The most common curcuminoids are curcumin, demethoxycurcumin, and bisdemethoxycurcumin. Curcumin is a major component among the curcuminoids having antibacterial, anti-inflammatory, hepato-protective, antioxidant, and anti-cancer activity [169,170].

Curcumin (CUR) is a chemically unstable drug molecule with photosensitivity, pH-sensitivity, and low aqueous solubility. This leads to the poor absorption and low bioavailability which limits the therapeutic applications of curcumin [171].

The antioxidant activity of CUR is due to its scavenging activity against reactive oxygen species (ROS), and reactive nitrogen species. Moreover, the anticancer activity of CUR is attributed to the ability to control DNA damage and ROS mediated lipid oxidation due to the antioxidant property [172,173].

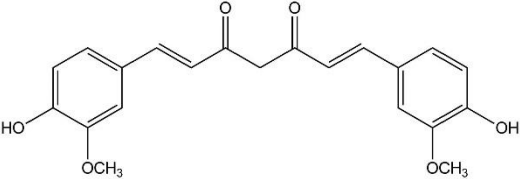
CUR also exhibits anti-inflammatory properties due to the inhibition or downregulation of various molecular pathways mainly cyclooxygenase and lipoxygenase that are responsible for the inflammatory responses [174,175].

CUR is used in various liver-related disorders due to its hepato-protective activity. CUR promotes the activity of hepatocellular enzymes to promote the detoxification, improved the anti-oxidants level, and hepatic histo-architecture [176]. Moreover, it is also

Introduction

reported that CUR exhibit antimicrobial activity against several Gram-positive and Gram-negative bacteria [177].

Table 1. 9 Properties of curcumin

| Name | Curcumin |
|----------------------|---|
| Chemical name | (1E,6E)-1,7-Bis(4-hydroxy-3-methoxyphenyl)-1,6-heptadiene-3,5-dione |
| Molecular formula | C ₂₁ H ₂₀ O ₆ |
| Molecular weight | 368.38 g/mol |
| Chemical structure |  |
| CAS number | 458-37-7 |
| Description | Bright yellow-orange powder |
| Melting point | 170-183 °C |
| Log P | 3.62 |
| Solubility | Insoluble in water but freely soluble in DMSO, Methanol, and Ethanol |
| Therapeutic category | Natural Antioxidant, Anti-Carcinogenic, Anti-Inflammatory, Antibacterial |

Introduction

1.6.2.4.1 Pharmacokinetics of Curcumin

It is reported in the literature that CUR shows low oral bioavailability. Pharmacokinetic and bioavailability data suggested low oral absorption and rapid body clearance of CUR [178]. Sharma and group reported that 1g/kg CUR was administered to the rats which showed 75 % excretion through feces with very little amount in urine [179]. In another study, Ravindranath and Chandrasekhara reported that the 60 % oral absorption of administered CUR in rats was observed [180].

CUR is metabolized mainly via glucuronidation and sulfation. It is also reported that metabolites of CUR exhibit low activity compared to parent CUR. For instance, tetrahydro-curcumin is a major metabolite of CUR which is less effective against cyclooxygenase-1, and 5-lipoxygenase compared to equivalent concentration of the CUR [181].

1.6.2.4.2 Analytical Methods for the Determination of CUR

Some of the examples of methods for the determination of CUR in the literature.

Table 1. 10 Analytical methods of CUR

| Type of Column | Mobile Phase | Detector and λ_{\max} | References |
|--|--|---|-------------------|
| Diamonsil C18 column (4.6 × 100 mm, 5 μm) | Acetonitrile– 5% acetic acid (75:25, v/v) (Isocratic Elution) | UV-Vis detector; 420 nm | [182] |

Introduction

| Type of Column | Mobile Phase | Detector and λ_{\max} | References |
|---|---|-------------------------------|------------|
| Alltima C18 column | Acetonitrile and 2% v/v acetic acid (40:60, v/v) (Isocratic Elution) | UV-Vis detector; 425 nm | [183] |
| Zorbax SB-C18 column (250 mm \times 4.6 mm i.d., 5 μm) | Acetonitrile (A) and water containing 0.4% (v/v) acetic acid (B) (Gradient Elution) | UV-Vis detector; 430 nm | [184] |
| Vydac [®] , RP-18, 250 mm \times 4.6 mm, 5 μm , | Acetonitrile: 0.1% trifluoroacetic acid (TFA) (50:50 v/v) (Isocratic Elution) | UV-Vis detector; 420 nm | [185] |

Chapter 2

AIMS

Aims

2. Aims

The PhD work presented here summarizes research focused on the synthesis, and characterization of the dextrin based drug delivery systems for various pharmaceutical applications. The work presented in this thesis divided into five different parts comprising new potential applications of dextrin based polymers in the field of drug delivery.

Project 1: Kynurenic Acid Loaded Cyclodextrin Nanosponge.

Kynurenic acid (KYNA) showed that it possesses antioxidant, neuroprotective and free radical scavenging properties. However, low aqueous solubility of kynurenic acid limits its therapeutic activity. Moreover, pH-dependent solubility also causes variation in the bioavailability. In the present study, cyclodextrin nanosponges were developed to improve the solubility and therapeutic activity of kynurenic acid. The formation of kynurenic acid loaded nanosponge was confirmed by different characterization techniques. The effect of β -CD and NSs on the solubilization of the KYNA was studied.

The change in the properties of KYNA after encapsulation within the NSs was studied. The effect of solubilization on the drug release was also demonstrated. In-vitro antioxidant activity of KYNA and KYNA loaded NSs was carried out to confirm the difference in the activity after drug encapsulation. The effect of blank NSs and KYNA loaded NSs on the viability of the SHSY-5Y neuroblastoma cell line was studied. Thus, these studies demonstrated that nanosponges can be used as a carrier for the delivery of kynurenic acid.

Aims

This work was published in *Carbohydrate Polymer*, 2019, 224, 115168.

Project 2: Comparative Evaluation of Resveratrol and Oxyresveratrol Loaded Nanosponges.

Resveratrol (RES) and Oxyresveratrol (OXY) are natural polyphenolic stilbenes with several important pharmacological activities such as antioxidant, anti-inflammatory, and anti-tumor activity. However, low solubility, photosensitivity, and aqueous instability are the major limitations in their drug delivery applications. In the present work, we demonstrated the encapsulation of resveratrol and oxyresveratrol with nanosponge to improve solubility and stability. Several characterization techniques were used to confirm the encapsulation of both drug molecules within the nanosponges. UV-exposure studies on RES and OXY loaded NSs were carried out to determine the change in the drug concentration after UV-exposure. A comparison of antioxidant and anticancer activity of RES and OXY loaded NS against DU-145 prostate cancer cell lines was also demonstrated.

This work was published in *Pharmaceutics*, 2019, 11, 545.

Project 3: Determination of Encapsulation Constant and Activity against Colon Cancer by OXY Loaded NSs

Oxyresveratrol (OXY) is a naturally occurring stilbene derivative with numerous biological activity and can be obtained from a variety of natural sources. In this work, we demonstrated a novel method to determine the encapsulation constant of OXY with different NSs. The OXY encapsulation within the NSs was confirmed with several

Aims

methods. The stability of OXY in simulated biological fluids (Gastric and Intestinal Fluid) was also demonstrated. The activity of OXY on colon cancer was determined using HCT116 and HT29 cell lines.

This work is submitted to carbohydrate polymer.

Project 4: Stimuli-responsive Drug Delivery Carrier for Resveratrol.

Resveratrol (RES) is a polyphenolic compound that is found in a variety of natural sources such as grape juice, red wine, peanuts, mulberries, and other plant extracts. It is reported that RES exhibits anticancer activity along with anti-inflammatory, antioxidant activity, and cardiovascular benefits. However, poor aqueous solubility, low bioavailability, and photosensitivity of RES are the major challenges in the delivery of the RES. In the present work, we demonstrated the encapsulation of resveratrol with GSH responsive nanosponge to improve solubility, and selective drug release. Moreover, stimuli-responsive nanocarriers allow the delivery of the drug at the target site in the response to redox gradient. The presence of GSH in the nanocarrier allows the delivery of drug to the target site without affecting the normal tissues.

Several characterization techniques were used to evaluate RES loaded GSHNSs. Moreover, Cell internalization study was carried out to determine the preferential internalization of nanocarrier in cancer cells with high GSH compared to normal cells. Consistently, in-vitro cell cytotoxicity studies were performed using RES loaded GSH responsive nanosponges to determine the difference of anticancer activity compared to free RES. Taken, together, our preliminary studies support the view that GSH

Aims

responsive nanosponges can be used as an effective carrier for the delivery of RES.

Project 5: Development of Biotin-functionalized Cyclodextrin Nanosponges.

This work was focused on the development of biotin functionalized ester-based cyclodextrin nanosponges. Biotin is considered as a prominent biomolecule for the targeting of the cancer cells. It is observed that the biotin receptor is overexpressed on cancer cells more than folate and vitamin B-12 receptors in many cancer such as Leukemia, ovarian, Colon, mastocytoma, lung, renal, and breast cancer cell lines.

The characterization of the biotin-functionalized NSs was varied out by FTIR and elemental analysis. The concentration of biotin on the nanocarrier was determined by the HABA-Avidin assay kit. The prepared biotinylated NSs were used to encapsulate the curcumin (CUR) to determine the effect on the aqueous solubilization of the CUR.

This work is in the continuous process to further demonstrate the biological activity of the CUR-loaded biotinylated NSs

Chapter 3

Material and

Methods

Material and Methods

3. Material and Methods

3.1 Chemicals

α -cyclodextrin (α -CD), β -cyclodextrin (β -CD), and γ -cyclodextrin (γ -CD) were the kind gift from Roquette Italia (Cassano Spinola, Italy). Before use, β -CD was desiccated overnight in an oven at 80 °C for the removal of absorbed moisture. Resveratrol, Kynurenic acid, Curcumin, 1,1'-carbonyldiimidazole, Thiobarbituric (TBA) acid, 2,2-diphenyl-1-picrylhydrazyl (DPPH), triethylamine, pyromellitic dianhydrides, 2-hydroxyethyl disulfide, acetone, ethanol were purchased from Sigma-Aldrich (Milan, Italy). Oxyresveratrol was purchased from TCI Europe. Deionized and milliQ® water were obtained using a Millipore Direct-QTM 5 production system. Cell culture reagents were purchased from Gibco/Invitrogen (Life Technologies, Paisley, UK). Unless otherwise specified, all other chemicals and reagents used were of analytical grade.

Material and Methods

3.2 Characterization Techniques

3.2.1 Determination of Particle Size, Polydispersity Index, and Zeta Potential

Dynamic light scattering (DLS) method was used to determine the particle size and polydispersity index of selected drug molecules and drug loaded NSs. A Malvern Zetasizer Nano instrument at a fixed scattering angle of 90° was used and all the samples were analyzed at 25 °C after suitable dilution by milli-Q water. Zeta potential of all the samples was also determined by placing an additional electrode within the same instrument. All the results were recorded in triplicate.

3.2.2 Differential Scanning Calorimetry (DSC)

Thermal stability of selected drug molecules, blank NSs, physical mixture, and drug loaded NSs were determined by a TA instruments Q200 DSC (New Castle, DE, USA). Individual samples (2-3 mg) were placed in an aluminum pan and scanned from 30 to 300 °C at the scanning rate of 10 °C/min under a nitrogen purge of 50 mL/min.

3.2.3 Thermogravimetric analysis (TGA)

Selected drug molecules, blank NSs, and drug loaded NSs were subjected to thermogravimetric analysis using a TGA 2050 thermogravimetric analyzer (TA instruments, USA) from 40 to 700 °C at 10 °C/min.

Material and Methods

3.2.4 Fourier Transform Infrared Spectroscopy (FTIR)

The presence of functional groups in selected drug molecules, blank NSs, physical mixture, and drug loaded NSs were determined using a PerkinElmer 100 FTIR with an attenuated total reflectance (ATR) accessory. Data were recorded from 4000-650 cm^{-1} at a resolution of 4 cm^{-1} and 8 scans/spectrum. Collected data were analyzed by spectrum software version 10.03.05 (PerkinElmer, Waltham, MA, USA).

3.2.5 X-ray Powder Diffraction Studies (PXRD)

The nature of selected drug molecules, blank NSs, physical mixture and drug loaded NSs was determined using the Malvern Panalytical X'Pert diffractometer. Cu K α 1 as a source of radiation and data were collected over an angular range from 5 to 45° (diffraction angle) at a step size of 0.017 ° and a time per step of 100.33 s. The values of the diffraction angle were reported as 2θ .

3.2.6 Morphology Evaluation

Field Emission Scanning Electron Microscopy (FE-SEM): Surface property and morphology of blank NSs and drug loaded NSs was determined by ZIESS Supra 40 FE-SEM microscope. NS suspension (3-4 drops) was placed on a copper stub and air-dried later, sputter-coated with gold. Samples were analyzed at 3 kV accelerating voltage at a working distance of 10 mm.

Transmission electron microscopy (TEM): A JEOL JEM 3010 (300 KV) transmission electron microscope was used to acquire TEM images of blank NS and drug loaded NSs. Samples were placed on a copper

Material and Methods

grid and excess of water was removed by evaporation at room temperature and later analyzed on TEM.

3.2.7 BET Analysis

The prepared blank NSs and drug loaded NSs were characterized by nitrogen adsorption-desorption isotherms at 77 K with the help of automatic adsorption instrument (ASAP 2010, Micromeritics). All the samples were degassed at 300 °C and then cooled to nitrogen boiling temperature (77 K). Samples were exposed to a series of precisely controlled doses of nitrogen gas (from 0 to 1 of nitrogen relative pressure). Each pressure was recorded and the quantity of adsorbed gas was determined by universal gas law. The adsorption of gas starts, filling the micropores followed by mesopores and macropores, respectively. Once, the adsorption finishes desorption of gas takes place. Data collected from the above process was used to describe the adsorption and desorption isotherms.

Material and Methods

3.3 Kynurenic Acid (KYNA) Loaded Cyclodextrin Nanosponges

3.3.1 Synthesis of β -cyclodextrin Nanosponges (β -CDNSs)

Ester-based nanosponges were prepared by β -cyclodextrin (β -CD) and 1,1'-carbonyldiimidazole (CDI) as a crosslinking agent. Briefly, β -cyclodextrin (β -CD) was dissolved in N,N-dimethylformamide (DMF) and CDI was added in a different molar ratio of 1:2, 1:4 and 1:6 (Table 3.1). Three different types of NSs were prepared according to the variable molar ratio (i.e. β -CD:CDI). The reaction was carried out at 90 °C with continuous stirring on a magnetic stirrer. The reaction was completed within 3 hours and after that, it was kept overnight for incubation to carry out further crosslinking.

Table 3. 1 Quantities of chemical for the synthesis of nanosponges.

| Samples | Cyclodextrin (β -CD) | | CDI | | DMF | β -CD:CDI Molar Ratio |
|----------------|-----------------------------|--------|-------|--------|------|-----------------------------|
| | (g) | (mmol) | (g) | (mmol) | (mL) | |
| β -CDNS1 | 5 | 4.405 | 1.426 | 8.794 | 30 | 2 |
| β -CDNS2 | 5 | 4.405 | 2.852 | 17.588 | 30 | 4 |
| β -CDNS3 | 5 | 4.405 | 4.278 | 26.382 | 30 | 6 |

The solid monolithic mass of nanosponge was collected, and crushed in a mortar to obtain small particles. Collected NSs were washed several times with water to remove unreacted components using Buchner funnel followed by ethanol. The nanosponges were subjected to the Soxhlet extraction with ethanol in order to purify them for a period of 24-48 hours. Later, nanosponges were air-dried and stored in a desiccator at room temperature for further use. The

Material and Methods

prepared CDI-nanosponges were abbreviated as β -CDNS1, β -CDNS2, and, β -CDNS3, respectively.

3.3.2 Swelling Degree of Nanosponges

Nanosponges were dried overnight in an oven at 90 °C and known amounts of different nanosponges were placed in water. At a predetermined time intervals, the swollen nanosponges were taken out and the excess quantity of water was removed by blotting the nanosponges on the filter paper. The weight of swollen nanosponges was recorded and this procedure was repeated several times until a constant weight was achieved.

The percentage of a swelling degree was calculated using the following equation.

$$\% \text{ Swelling Degree} = (W_s - W_d) / (W_d) \times 100$$

Where W_s is the weight of swollen nanosponges and W_d is the weight of dry nanosponges.

3.3.3 Determination of Percentage Crosslinking

A calibration curve was recorded using beta-cyclodextrin (β -CD and diphenyl carbonate (DPC) as a carbonate standard using a KBr pellet method. β -CD and DPC were mixed together in an increasing molar ratio from 1:1 to 1:8. The weight of all the pellets was kept constant and FTIR spectra were recorded. A calibration curve was recorded by taking a ratio of two bands as a standard i.e. I_{1774} (C=O stretching vibration of crosslinker) and I_{2929} (C-H stretching vibration of β -CD). The calibration curve obtained from the ratio of I_{1774} and I_{2929} peak was found to be linear with a regression coefficient of 0.9986.

Material and Methods

3.3.4 Solubilization of the KYNA

The aqueous solubility of KYNA alone, and in the presence of β -CD or NSs (β -CDNS1 to β -CDNS3) was studied. An excess quantity of KYNA with a fixed amount of β -CD or different nanosponges was suspended in water (2 mL). The vials were stirred overnight on a mechanical shaker at room temperature. Later, the supernatant was collected from suspension after centrifugation at 6000 rpm for 15-20 minutes. The collected supernatant was filtered through a 0.45 μ m syringe filter and KYNA content was determined by HPLC as mentioned in section 3.2.6.

3.3.5 Preparation of KYNA Loaded Nanosponges

Individual nanosponges (β -CDNS1 to β -CDNS3) were suspended in water to make a final concentration of 10 mg/mL. The required amount of KYNA was added into the nanosponge suspension at different weight ratios of 1:3, 1:4 and 1:5 (w/w), respectively. The KYNA-NS suspension was subjected to sonication for 10-15 minutes and kept for overnight stirring at a magnetic stirrer at room temperature. Later, to remove the un-complexed drug the suspension was centrifuged at 6000 rpm for 15 minutes. The supernatant was collected and freeze-dried with 5 % trehalose (cryo-protectant; % w/v). The freeze-dried formulations of KYNA with NSs were abbreviated as KYNA- β -CDNS1, KYNA- β -CDNS2, and KYNA- β -CDNS3, respectively.

Physical mixtures of KYNA with NSs were also prepared by mixing KYNA (2.5 mg) with different nanosponges (10 mg) by trituration in

Material and Methods

a mortar for 30 min at room temperature. The physical mixture formulations were abbreviated as PM1, PM2, and PM3, respectively.

3.3.6 Quantitative Determination of KYNA

The quantitative determination of KYNA was carried out by an HPLC system (PerkinElmer, Waltham, USA) equipped with a UV detector (Flexar UV/Vis LC spectrophotometer). A phenomenex C18 analytical column (4.6 mm x 250 mm, 5 μ m) was used. The mobile phase consisted of a mixture of 0.14 % (v/v) TFA (trifluoroacetic acid) in water and acetonitrile (90:10 v/v). The mobile phase was filtered and degassed ultrasonically before the use. A flow rate of 1 ml/min was maintained and the samples (20 μ L) were injected through the column. The quantification was carried out on a UV-Visible detector set at 330 nm. A calibration curve was recorded in the concentration range of 1-25 μ g/mL with a regression coefficient of 0.9995.

3.3.7 KYNA Loading within the NSs

The KYNA loaded NSs were suspended into a vial containing 1 mL of DMSO-water mixture (50:50) and sonicated for 1-2 hours. The suspension was centrifuged at 6000 rpm and the supernatant was collected. Later, it was filtered and analyzed on the HPLC after suitable dilution with the mobile phase.

3.3.8 Characterization of the KYNA Loaded NSs

The Particle Size, Polydispersity Index, and Zeta Potential of KYNA loaded NSs were determined by DLS (Malvern Zetasizer Nano). The thermal properties of all the samples were evaluated using a TA

Material and Methods

instruments Q200 DSC (New Castle, DE, USA). The functional group determination of samples was carried out by PerkinElmer 100 FTIR (PerkinElmer, Waltham, USA). Diffraction studies of all the samples were performed using an X-ray diffractometer (Malvern Panalytical X'Pert diffractometer, UK). The morphological evaluation of blank NSs and KYNA loaded NSs was carried out by FE-SEM. Surface area and porosity of blank NSs and KYNA loaded NSs was determined by BET analysis.

3.3.9 In-vitro Drug Release Profile of KYNA

The accurate weight amount of KYNA loaded NS (20 mg KYNA loaded NS containing 1.5 mg KYNA) or equivalent KYNA alone (1.5 mg) was dispersed in 3 mL of phosphate buffer pH 7.4 and sealed into a dialysis bag made up of a cellulose membrane (12,400 MWCO). The bag was submerged into 30 mL of phosphate buffer pH 7.4 at 37 ± 0.5 °C with a rotation speed of 50 rpm. At predetermined time intervals, 1 mL of aliquots were withdrawn and replaced with the same amount of fresh phosphate buffer to maintain sink condition. Later, all the samples were analyzed on HPLC. Drug release data were represented as % cumulative drug release vs. time.

The release profile of KYNA and KYNA loaded NS was fitted with different release kinetic models to determine the mechanism of drug release. The zero-order release kinetic model was plotted between % cumulative drug release vs. time, first-order release kinetic model was plotted between log cumulative % of drug remaining vs. time, Higuchi–Connors model was plotted between cumulative % drug

Material and Methods

release vs. square root of time and Korsmeyer–Peppas model was plotted between log cumulative % drug release vs. log time.

3.3.10 Evaluation of Antioxidant Activity

Thiobarbituric Acid Reactive Substances (TBARS) Assay:

This assay is based on the evaluation of oxidative decomposition of polyunsaturated fatty acid in acidic medium. Oxidative decomposition leads to the generation of malondialdehyde (MDA), which reacts with TBA to form TBA-MDA adduct. KYNA (1 mg/mL stock solution in N-methyl pyrrolidone) and KYNA loaded NS (PBS pH 7.4) were prepared in the concentrations of 50 μ M and 100 μ M. The reaction was carried out by taking 0.1 mL of linoleic acid (1 % w/v) in a test tube, followed by addition of 0.2 mL of sodium dodecyl sulfate (SDS) (4 % w/v), 1.5 mL of phosphoric acid (1.0 % v/v), 1.0 mL of TBA (0.6 % w/v), 0.1 mL of water and 0.1 mL of KYNA solution or KYNA loaded NS. The reaction was performed at 100 °C for 45 minutes later it was cooled down on an ice bath. Later, The reaction mixture was mixed with 1-butanol (4 mL) to extract TBA-MDA adduct. All the samples were analyzed by UV-Visible spectrophotometer (Lambda 25, PerkinElmer, Waltham, USA) at 535 nm. The concentration of MDA in the reaction mixture was determined from a calibration curve of an MDA precursor 1,1,3,3-tetraethoxypropane (TRP), which was recorded under the same experimental conditions. The antioxidant activity of KYNA was evaluated by determining the reduction in the MDA generation which was presented as μ g of MDA generation per mg of lipid.

DPPH Scavenging Activity:

Material and Methods

The DPPH scavenging activity of KYNA loaded NS or KYNA alone was recorded. The different concentrations of KYNA and KYNA loaded NS (10-100 μM) were prepared, of which 2 mL of samples were mixed with a 0.5 mL of ethanolic solution of DPPH (0.004 % w/v). The reaction mixture was incubated for 60 minutes at room temperature and analyzed by UV-visible spectrophotometer at 525 nm. Ethanol (0.5 mL) was used as control (without drug). The DPPH inhibition activity of KYNA samples was compared with a known positive standard of the same concentrations (i.e. L-ascorbic acid).

The following equation was used to calculate the percentage of DPPH scavenging activity.

$$\text{DPPH Inhibition (\%)} = (A_c - A_s) / (A_c) \times 100$$

Where A_c is the absorbance of the control, and A_s is the absorbance of the sample.

H₂O₂ Scavenging Activity:

The H₂O₂ scavenging activity of KYNA and KYNA loaded NS was demonstrated. Briefly, different concentrations of KYNA and KYNA loaded NS (10-100 μM) were prepared. 0.5 mL of KYNA or KYNA loaded NS were mixed with 0.5 mL of KI (1M), 0.5 mL of TCA (0.1%; w/v), 0.5 mL of phosphate buffer pH 7.4, 0.5 mL of H₂O₂ (10 mM) at room temperature for 10 minutes. The phosphate buffer pH 7.4 (0.5 mL) was used as a control (without drug). The absorbance was recorded by UV-Vis spectrophotometer at 350 nm.

The percentage of H₂O₂ scavenging activity was calculated by the following equation.

Material and Methods

$$\text{H}_2\text{O}_2 \text{ Scavenging Activity (\%)} = (A_C - A_S) / (A_C) \times 100$$

Where A_C is the absorbance of the control, and A_S is the absorbance of the sample.

3.3.11 Cell Viability Studies

SHSY-5Y human neuroblastoma cell lines were used to carry out 3-(4,5-dimethylthiazol-2-yl)-2,5-diphenyltetrazolium bromide (MTT) assay, to determine the cell viability for KYNA, KYNA loaded NS and NS alone. SHSY-5Y human neuroblastoma cells were cultured as a monolayer in RPMI 1640 medium accompanied by 10 % fetal calf serum (FCS), 100 U/mL penicillin, and 100 $\mu\text{g/mL}$ streptomycin at 37 °C and cells were maintained under 5 % CO_2 atmosphere. SHSY-5Y cell lines were seeded into a 96-well plate and incubated for 24 hours at 37 °C in a 5 % CO_2 humidified atmosphere. Cells were treated with different concentrations of KYNA or KYNA loaded NS (1-100 μM) for a period of 24 hours. Blank NSs were dispersed in 0.9 % NaCl saline solution followed by suitable dilution with culture media and treated with the cells as mentioned above. After 24 hours, cell viability was determined by recording the absorbance at 570 nm. Cell medium alone was considered as a control and the reading obtained from treated cell were represented as % cell viability.

3.3.12 Stability Studies

The in-vitro stability of blank NS and KYNA loaded NS in 0.9 % NaCl saline solution was evaluated. All the samples were incubated at 4 °C for a period of one week. The average diameter and zeta

Material and Methods

potential of blank NS and KYNA loaded NS were studied at different time intervals.

3.4 Resveratrol (RES) and Oxysresveratrol (OXY) Containing Cyclodextrin Nanosponges

3.4.1 Synthesis of Carbonate-based Nanosponges

Carbonate-based cyclodextrin nanosponges were according to the procedure mentioned earlier in the section 3.3.1. β -Cyclodextrin-CDI nanosponges (1:4 molar ratio) were used to perform this study.

3.4.2 Solubilization of RES and OXY

To study the solubilization of RES and OXY, an excess quantity of RES and OXY was suspended in water (5 mL) and a fixed quantity of nanosponge was added into it. Samples were kept for stirring for 24 hours in dark at room temperature. The samples were centrifuged at 6000 rpm for 20 minutes, and the supernatant was collected. The collected supernatant was filtered and analyzed on HPLC to determine RES and OXY content as stated in section 3.3.4.

3.4.3 Preparation of RES and OXY Loaded Nanosponge

An aqueous suspension of nanosponges (10 mg/mL) was mixed with the required amount of RES or OXY at different weight ratios of 1:2, 1:4, and, 1:6 (w/w; drug: nanosponge). Samples were sonicated for a few minutes and kept for stirring for 24 hours in dark at room temperature. All the samples were subjected to mild centrifugation and dialyzed for few minutes to remove the uncomplexed drug. Dialyzed samples were freeze-dried to obtain free-flowing powder samples.

Material and Methods

3.4.4 Quantitative Determination of RES and OXY by HPLC

The quantity of RES and OXY was determined by an HPLC system (PerkinElmer, Waltham, USA) equipped with a UV detector (Flexar UV/Vis LC spectrophotometer) with the help of reversed-phase phenomenex C18 analytical column (4.6 mm x 250 mm, 5 μ m) for both drugs. Two separate mobile phases were used for the determination of RES and OXY. A mixture of 0.5 % acetic acid in methanol and water (52:48, v/v) was used for RES and a mixture of acetonitrile and 0.5 % aqueous acetic acid (27:73, v/v) was used for OXY. The isocratic elution was performed at room temperature, with a flow rate of 1 mL/min and an injection volume of 20 μ L. The UV detector was used with λ_{max} of 305 nm for RES and 326 for OXY. The calibration curve was recorded between peak area and concentration of RES and OXY. OXY showed a good correlation coefficient of 1 at the concentration range of 2-10 μ g/mL and RES showed a correlation coefficient of 0.9997 at the concentration range of 0.5-2.5 μ g/mL.

3.4.5 Determination of RES or OXY Loading

The concentration of RES or OXY within the NSs were determined by taking the required amount into a vial containing 1 mL of ethanol and sonicated for 1-2 hour. Later, the suspension was centrifuged followed by filtration and analyzed on HPLC for RES or OXY content after suitable dilution with the respective mobile phase.

3.4.6 Characterization of Drug Loaded NSs

The Particle Size, Polydispersity Index, and Zeta Potential of drug-loaded NSs were determined by DLS (Malvern Zetasizer Nano). The

Material and Methods

thermal properties of all the samples were evaluated using a TA instruments Q200 DSC (New Castle, DE, USA). The functional group determination of samples was carried out by PerkinElmer 100 FTIR (PerkinElmer, Waltham, USA). Drugs alone, blank NS and drug-loaded NSs were subjected to diffraction studies using an X-ray diffractometer (Malvern Panalytical X'Pert diffractometer, UK). The morphology of RES and OXY loaded NS was determined by a JEOL JEM 3010 (300 KV) transmission electron microscopy (TEM; JEOL, MA, USA).

3.4.7 In-Vitro Drug Release Profile

The drug release study of OXY and RES was carried out by a dialysis bag prepared by cellulose membrane (cut-off = 12,400 Da). Drug loaded NSs (20 mg RES-NS containing 1 mg RES or 20 mg OXY-NS containing 2 mg OXY) or equivalent quantity of free drugs (1 mg RES or 2 mg OXY) were dispersed into 2 mL of phosphate buffer pH 7.4 and filled into the dialysis bag. Dialysis bag was immersed into 30 mL of phosphate buffer pH 7.4 at 37 ± 0.5 °C with a constant rotation speed of 50 rpm during the experiment. 5 mL of aliquots were withdrawn at predetermined time intervals and RES or OXY content in aliquots was determined by the HPLC as described earlier. Data were represented as % cumulative drug release vs. time.

The mechanism of drug release was determined by fitting the drug release profile into different release kinetic mathematical models. The zero-order release model, first-order release model, Higuchi-Connors model, and Korsmeyer-Peppas model were used.

Material and Methods

3.4.8 Photodegradation Study

The photodegradation study of RES and OXY was carried out under a UV lamp (CAMAG UV LAMP 4; wavelength 320-400 nm). All samples were irradiated under UV light from a fix distance of 10 cm and analyzed on HPLC at different time intervals according to the HPLC method specified in section 3.4.4. Data were presented as a ratio of change in drug concentration (C) against initial drug concentration (C₀) versus time.

3.4.9 Antioxidant Activity of RES and OXY

DPPH assay was performed to determine the antioxidant activity of OXY, RES, OXY loaded NS and RES loaded NS. A series of concentrations (10-100 µM) of drug alone (RES or OXY) in ethanol and drug-loaded NS in water were prepared. 1mL of DPPH solution (0.004 % w/v ethanolic solution) was mixed with 1 mL of drug alone or drug-loaded NSs and incubated for 30 minutes. All the samples were analyzed by a UV-visible spectrophotometer (PerkinElmer Lambda 25) at 525 nm. Ethanol (1 ml) was used as a control (without drug). The following equation was used to calculate the percentage of DPPH inhibition.

$$\% \text{ DPPH Inhibition} = \frac{\text{Control absorbance value} - \text{Sample absorbance value}}{\text{Control absorbance value}} \times 100$$

3.4.10 Cytotoxicity Studies

DU-145 cell lines were grown as a monolayer culture in RPMI 1640 medium supplemented with 10 % fetal bovine serum, 2 mmol/L L-

Material and Methods

glutamine and 100 U/mL penicillin-streptomycin at 37 °C and cells were maintained under 5 % CO₂ atmosphere.

The percentage inhibition of cell viability by RES and OXY loaded NS was evaluated using MTT assay against DU-145 prostate cancer cells and compared with respective free drugs. DU-145 cells (2 x 10³/well) were seeded into a 96-well plate and incubated for 24 hours at 37 °C in a 5 % CO₂ humidified atmosphere. Different concentrations (10-100 µM) of OXY and RES loaded NSs were added into the cell culture and incubated for 96 hours. The Blank NS was also dispersed in RPMI 1640 medium and treated with the cells as mentioned above. After 96 hours, the absorbance was recorded at 570 nm using a microplate reader. The control (i.e. cells that have received no drugs) were normalized to 100%, and the readings from treated cells were expressed as % of viability inhibition. Eight replicates were used to determine each data point and five experiments were performed.

Material and Methods

3.5 Determination of Complexation Constant and Activity Against Colon Cancer by OXY Loaded NSs

3.5.1 Synthesis of NSs of Different Cyclodextrins

CDI-based nanosponges with different cyclodextrins (α -, β -, and γ -) were prepared. Briefly, 100 mL of anhydrous DMF was placed in a round-bottomed flask and 10 g of the appropriate CD was added until complete dissolution. Then, the required quantity of CDI was added at a molar ratio of 1:4 or 1:8 (CD:linker). The solution was allowed to react for 4 h at 90 °C. The prepared NSs were purified according to the method mentioned earlier in section 3.3.1. Below, the different CD-NS will be called "X-CDI 1:Y" where X is the type of CD and Y the linker ratio.

3.5.2 Determination of Apparent Encapsulation Constant

To obtain the apparent encapsulation constant, the methodology described by Benesi-Hildebrand was used with slight modifications [186].

The following points need to be considered to determine the encapsulation constant:

i) CD-NSs have a random number of cavities, it was assumed that each cavity, which has its own microscopic encapsulation constant, to give an overall (macroscopic) apparent encapsulation constant. Using this approximation only a 1:1 complex could be evaluated, where R^2 is the degree of alteration between each microscopic constant.

Material and Methods

$$\frac{\sum_{i=0}^n K_n}{n} = K_{Fapp}$$

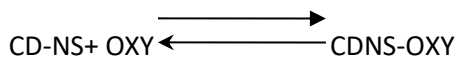
where n is the number of the microscopic cavities and K_n the constant for each cavity and K_{Fapp} the macroscopic apparent complexation constant.

ii) However, It is not possible to determine the molecular weight of CD-NSs accurately but it is possible to know the molecular weight of the guest (in our case, OXY).

iii) As since our CD-NSs are insoluble, and also the complex, the quantity encapsulated can be eliminated from the dissolution. So, we can measure the [OXY] before and after the equilibrium. Its variation is proportional to the CDNS-OXY formed.

$$[OXY]_{Final} - [OXY]_{Initial} \propto [CDNS - OXY]_{Formed}$$

So, assuming a 1:1 complex, the following equilibrium was applied



The apparent encapsulation constant, K_{Fapp} is given by:

$$K_{Fapp} = \frac{[CDNS - OXY]}{[OXY][CDNS]}$$

where [CDNS], [OXY] and [CDNS-OXY] are equilibrium concentrations.

To calculate K_{Fapp} , eppendorfs with increasing OXY (or RES) concentration (from 2 to 400 μ M) at 1 % CD-NSs in water were mixed in a Thermomixer Comfort® (Eppendorf) at 25 °C and 800

Material and Methods

rpm for 48 hours to measure the respective absorbances (t_0). After this time, the eppendorfs were centrifuged in refrigerated conditions at 7500 x g for 15min. The concentration of the OXY was determined by the HPLC method. Briefly, 15 μ L of OXY at different concentrations were injected into Shimadzu LC-2210cHT (Shimadzu, Japan) HPLC with a Kromasil C18 (150mm x 4.6 μ m) column (AnálisisVínicos, Spain) at 25 °C. The mobile phase was acetonitrile:water:acetic acid (27:73:0.5 v/v at 1 mL/min). The UV signal was obtained at 301 nm. The calibration curve showed linearity with a coefficient of correlation value 0.99. The absorbance of the supernatant was measured in an appropriate dilution. Finally, the expression corresponding to the Benesi–Hildebrand method was used to determine the K_{Fapp} value.

$$\frac{1}{A - A_0} = \frac{1}{(A_\infty - A_0)K_{Fapp}[OXY]} + \frac{1}{A_\infty - A_0}$$

where [OXY] denotes the OXY concentration; A_0 is the absorbance of OXY in solution without CDNS (at the initial time); A_∞ is the absorbance when all CD-NSs are complexed with OXY; and A , is the absorbance of any sample at each OXY concentration indicated (at 48 h). K_{Fapp} would be obtained by fitting $(1/A-A_0)$ vs $1/[OXY]$, being " $1/(A_\infty-A_0)K_{Fapp}$ " the slope and " $1/A_\infty-A_0$ " the intercept; the quotient between intercept and slope gives K_{Fapp} .

3.5.3 Drug Loading and Encapsulation Efficiency

OXY loaded NSs were prepared in the following way: OXY (100 mg) was taken into 150 mL of water and sonicated for 15 minutes. Later, 500 mg of NSs were added into it and kept for stirring for 24 hours

Material and Methods

in dark. This suspension was centrifuged and the nanospheres containing OXY were collected and dried overnight in an oven at 60 °C.

The weighed amount of OXY loaded NS (10 mg) was added to 1 mL of ethanol. This was sonicated for 3 hours and then centrifuged to remove the solid part. The supernatant was diluted and its absorbance was measured at 301 nm in a UV-Vis spectrophotometer (PerkinElmer Lambda 25).

3.5.4 Characterization of OXY Loaded NSs

The characterization of OXY loaded NSs was carried out by several methods as mentioned below:

The thermal properties of samples were evaluated by TA instruments Q200 DSC (New Castle, DE, USA), and TGA 2050 thermogravimetric analyzer (TA instruments, USA). Functional groups were determined out by PerkinElmer 100 FTIR (PerkinElmer, Waltham, USA).

3.5.5 In-vitro Drug Release Profile

The drug release profile of OXY from NSs and OXY alone was carried out by a dialysis membrane (cut-off 12000 Da) submerged in different stirred flasks at 37 °C with 40 mL of 0.1M phosphate-sodium-potassium buffer at pH 7.4 and 5.5 respectively. The donor phase was filled with 2 mL of buffer containing drug-loaded NSs (20 mg OXY-NSs containing 1.5 mg OXY) or equivalent free OXY. Samples were withdrawn from the receptor phase at predetermined

Material and Methods

time intervals and replaced with the same amount of buffer. The samples were diluted and its absorbance was recorded at 301 nm.

3.5.6 In-vitro Digestion Studies

Free OXY (225 μM) and OXY (225 μM) with 1% w/v NSs suspension were mixed for a period of 24 hours to perform the complexation. Later, samples were subjected to in-vitro digestion to determine the behavior of the complexes. Initially, the samples were prepared in saline solution at pH 3 with pepsin-HCl to simulate the gastric phase. Later, samples were incubated in a water bath shaker at 37 °C for 1 hour. The incubation was stopped by adding Na_2CO_3 to increase the pH to 6.9. In the subsequent intestinal phase, the pH was adjusted to 6.9 and a pancreatin/autoclaved bile extract/lipase mixture followed by incubation at 37 °C for 2 hours. The tubes containing OXY samples were placed in an ice bath to stop digestion and the contents were mixed vigorously. Later, samples were filtered using cellulose filters (0.22 μm) and analyzed using an HPLC method as described earlier to determine the amount of OXY. The results were compared using the initial amount of OXY.

3.5.7. In-vitro Cell Cytotoxicity Studies

HT-29 and HCT116 colon cancer cell lines were purchased from ATCC (Manassas, VA, USA). Cancer cell lines were seeded into a 96-well plate and incubated for 24 hours at 37 h in a 5 % CO_2 atmosphere. The cells were treated with OXY, OXY-NS or NS alone (previously sterilized by autoclave) in the concentration range of 1-100 μM for 72 hours. Then, cell viability was evaluated using MTT by recording the absorbance at 570 nm according to the

Material and Methods

manufacturer's protocol. The cells treated with culture medium alone were considered as a control and normalized to 100%, and the readings obtained from treated cells were expressed as % of viability inhibition. Eight replicates were used to determine each data point and five different experiments were performed.

Material and Methods

3.6 Stimuli-responsive Cyclodextrin Nanosponges for Resveratrol

3.6.1 Synthesis of Glutathione-responsive Cyclodextrin Nanosponges

Glutathione-responsive nanosponges (GSHNSs) were prepared by a method developed by our group earlier. Briefly, 4.0 g (3.52 mmol) of anhydrous β -CD (desiccated in an oven at 100°C, up to constant weight) was dissolved in 16 mL of DMSO in a 100 mL round bottom flask followed by the addition of 0.400 g (2.59 mmol) of 2-hydroxyethyl disulfide and 4.0 mL (28.70 mmol) of trimethylamine with continuous stirring for approximately 30 minutes. Finally, 11.01 g (48.96 mmol) of pyromellitic dianhydride was added to the solution to carry out the reaction. Gelation was achieved within a few minutes which was incubated for 24 hours at room temperature to complete the reaction. At the end of reaction, a solid monolith block was obtained which was crushed with mortar to obtain a coarse powder followed by extensive washing with water and air-dried. The purification of prepared GSHNSs was carried out by Soxhlet extraction with acetone (for approximately 24 h). After air-drying, a white powder was collected and stored in a desiccator at room temperature.

3.6.2 Elemental Analysis

Elemental analysis was performed to determine the quantity of sulfur in the prepared GSHNSs. CHNS elemental analysis (Thermo Electron Corporation Flash EA 1112 series CHNS-O Analyzer) was performed in the triplicate and calculated values were compared with the theoretical value of the sulfur. Approximately 2.5 mg of

Material and Methods

individual sample was placed in a tin capsule with an equal amount of V_2O_5 (catalyst).

3.6.3 Preparation of Drug Loaded and Fluorescent NSs

Before performing drug loading, nanosuspension of NSs was prepared by a top-down approach. Briefly, a weighed amount of NS (10 mg/mL) was suspended in distilled water or saline (for cell Line studies) under stirring at room temperature. The suspension was then dispersed using a high shear homogenizer (Ultraturrax®, IKA, Königswinter, Germany) for 10 min at 24,000 rpm. Further size reduction was performed using high-pressure homogenizer (HPH) for 90 minutes at a back pressure of 500 bar using an EmulsiFlex C5 instrument (Emulsiflex C5, Avestin, USA). The prepared nanosuspension was purified by dialysis using a cellulose membrane (cut-off = 12,400 Da) and stored at 4 °C.

RES loaded GSHNSs were prepared by adding the required quantity of RES in a nanosuspension of GSHNSs (10 mg/mL) at different weight ratios of 1:2, 1:4, and, 1:6 (w/w; drug: nanosponge). Samples were sonicated for 10-15 minutes and kept for continuous stirring in dark for 24 hours at room temperature. The supernatant was collected after mild centrifugation and dialyzed for few minutes to remove the uncomplexed drug. Fluorescent NSs were prepared in similar manner by taking 10 mg/mL NS suspension in 0.9 % NaCl with 0.1 mg/mL coumarin-6 (C-6). Free coumarin-6 was removed by mild centrifugation.

Material and Methods

3.6.4 Quantitative Determination and Drug Loading

The quantitative determination of RES was carried out by HPLC method mentioned in section 3.4.4. The RES loaded GSHNSs were taken into a vial containing 1 mL of ethanol and sonicated for 1-2 hours. Later, it was filtered and analyzed on HPLC for RES content.

3.6.5 Characterization of Drug loaded NSs

The Particle Size, Polydispersity Index, and Zeta Potential of RES loaded GSHNSs or C-6 loaded GSHNSs were determined by DLS (Malvern Zetasizer Nano). The thermal properties of samples were evaluated by TA instruments Q200 DSC (New Castle, DE, USA). Functional groups were determined by PerkinElmer 100 FTIR (PerkinElmer, Waltham, USA). The diffraction pattern was recorded using an X-ray diffractometer (Malvern Panalytical X'Pert diffractometer, UK). The morphology of samples was determined by a JEOL JEM 3010 (300 KV) transmission electron microscopy (TEM; JEOL, MA, USA) and Field Emission Scanning Electron Microscope (FE-SEM; ZIESS Supra 40).

3.6.6 In-Vitro Drug Release Profile of RES-GSHNSs

A suspension of RES-GSHNSs (10 mg) was prepared in 1 mL of phosphate buffer pH 7.4 and sealed into a dialysis bag (12,400 MWCO). The bag was immersed into 10 mL of phosphate buffer pH 7.4 at 37 ± 0.5 °C with a rotation speed of 50 rpm. The effect of GSH on the drug release was also studied by adding 10 mM GSH and 20 mM GSH in the dissolution media. The aliquots (1 mL) were withdrawn at different time intervals and replaced with the same

Material and Methods

amount of fresh phosphate buffer. Later, all the samples were filtered with a 0.4 μm syringe filter and analyzed on HPLC.

3.6.7 In-Vitro Biological Assays

Normal fibroblast cells, human ovarian cancer OVCAR3, non-tumorigenic epithelial MCF10A, and breast cancer MDAMB231 cells were purchased from ATCC (<http://www.lgcstandards-atcc.org>) and cultured under standard conditions (37 $^{\circ}\text{C}$, 5% CO_2) in RPMI 1640 (cod. R8758) or MEM (cod. M2279) medium, respectively, supplemented with 10% heat-inactivated FBS (cod. ECS0180L; Euroclone Spa, Milano, Italy), 1% Glutamine (cod. G7513), 1% non-essential amino acids (cod. M7145) and 1% penicillin and streptomycin (cod. P0781).

3.6.7.1 Cell Internalization Study

The internalization of coumarin-6 loaded GSHNSs was studied. Normal Fibroblast cell, OVCAR3, MCF10A, and MDAMB231 were cultured in 6-well plate for 24 hours. Internalization of coumarin-6 loaded GSHNSs was studied at different time intervals of 30 minutes, 2 hours, and 24 hours using confocal laser microscope (488 nm exciting laser band 505 to 530 nm bandpass emission filters).

3.6.7.2 Cell Viability Study

To determine cell viability, cells adherent on coverslips were treated with different concentrations of RES loaded GSHNSs (10-200 μM) and stained with fluorescent dye CellTrackerTM (CellTrackerTM Blue-CMAC-7-amino-4-chloromethylcoumarin; cod. 2110; Life Technologies Ltd) in serum-free medium for 30 minutes, and the

Material and Methods

blue fluorescence, an indicator of cell viability, was immediately imaged under the fluorescence microscope (LeicaDMI6000 Microsystems AG, Wetzlad, Germany).

3.6.7.3 Propidium Iodide Staining

Cells plated on coverslips were treated as described earlier. Necrotic cells were detected by using 0.2 µg/mL propidium iodide incubated for 10 minutes in dark at 37 °C (PI; cod. 4170, Sigma Aldrich). At the end of the experiment, fluorescent dye stained coverslips were observed under the fluorescence microscope.

The effect of GSH inhibitor on the different cells using above mentioned studies was also determined.

Material and Methods

3.7 Synthesis of Biotin-functionalized Ester-based NSs and Encapsulation of Curcumin

3.7.1 Synthesis of Ester-based NSs

The ester-based nanosponges (NS) were synthesized by cross-linking of β -CD with pyromellitic dianhydride (PMDA) as a cross-linking agent in a 1:4 molar ratio. Briefly, 6.108 g of β -CD was dissolved in 25 mL of anhydrous dimethyl sulfoxide. Then, 6.3 mL of triethylamine was added into it followed by the addition of the PMDA (4.695 g) with vigorous stirring. The reaction was completed within a few minutes and the solid mass of NSs was obtained. Subsequently, the solid NS was ground in a mortar and series of washing were performed with deionized water and acetone through Buchner filtration. Finally, NSs were purified by Soxhlet extraction in acetone for 24 hours and air-dried to collect coarse powder.

3.7.2 Biotin-Functionalization of the NSs (Bio-NSs)

200 mg of biotin (0.8 mmol) was activated by 306 mg of EDC (1.6 mmol) and 195 mg of DMAP (1.6 mmol) in 30 mL of dry DMF. 1 g of NS was added into the reaction mixture and kept for stirring at 45 °C for 48 hours. After the reaction mixture was cool down and solid mass was collected after filtration with continuous washing by ethanol and water. Collected solid mass was dispersed in water and subjected to extensive dialysis for 72 hours. Later, Bio-NSs were freeze-dried and subjected to the characterization.

Material and Methods

3.7.3 Elemental Analysis of Bio-NSs

Elemental analysis was performed to determine the quantity of sulfur in the prepared Bio-NSs. CHNS elemental analysis (Thermo Electron Corporation Flash EA 1112 series CHNS-O Analyzer) was performed in the triplicate and calculated values were used to determine the percentage distribution of the sulfur within the NSs. Approximately 2.5 mg of individual sample was placed in a tin capsule with an equal amount of V₂O₅ (catalyst).

3.7.4 Determination of the Biotin Concentration by HABA-Avidin Assay

The spectrophotometric measurement of the concentration of biotin on the surface of NSs was performed by 4'-hydroxyazobenzene-2-carboxylic acid/avidin (HABA/avidin) reagent. 5 mg of Bio-NS was suspended into 1 mL of water and powdered HABA/avidin reagent was reconstituted in deionized water to make a solution in a concentration of 10 mg/mL. 900 μ L of HABA-Avidin solution was added to 100 μ L of Bio-NSs and mixed thoroughly. The UV-Vis spectrum was recorded immediately at 500 nm. The following equation was used to determine the biotin content as per the manufacturer's protocol.

$\Delta A_{500} = 0.9 \times (\text{Absorbance of HABA/Avidin as control}) - (\text{Absorbance of Bio-NSs with HABA/Avidin as sample})$

$$\text{Biotin Concentration } (\mu\text{mol/mL}) = (\Delta A_{500}/34) \times 10$$

Material and Methods

3.7.5 Quantitative Determination of the CUR

The quantity of CUR was determined by an HPLC system (PerkinElmer, Waltham, USA) equipped with a UV detector (Flexar UV/Vis LC spectrophotometer) with the help of reversed-phase phenomenex C18 analytical column (4.6 mm x 250 mm, 5 μ m). A mobile phase containing a mixture of methanol and 1 % acetic acid (75:25, v/v) with a flow rate of 1 mL/min and an injection volume of 20 μ L was used at room temperature. CUR detection was carried out at a wavelength of 428 nm. CUR showed a good correlation coefficient of 0.9993 at the concentration range of 1-10 μ g/mL.

3.7.6 Solubilization of Curcumin (CUR)

An excess quantity of CUR was suspended in water (2 mL), and with a fixed amount of β -CD or Bio-NSs was added into it. Samples were kept for stirring for 24 hours in dark at room temperature. The samples were centrifuged at 6000 rpm for 20 minutes, and the supernatant was collected. The collected supernatant was filtered and analyzed on HPLC to determine CUR content as mentioned above.

3.7.7 CUR Loading with Bio-NSs

A weighed amount of Bio-NSs (10 mg/mL) was suspended in distilled water under stirring at room temperature. The suspension was then dispersed using a high shear homogenizer (Ultraturrax®, IKA, Königswinter, Germany) for 10 min at 24,000 rpm followed by the size reduction using high-pressure homogenizer (HPH) for 90 minutes at a back pressure of 500 bar using an EmulsiFlex C5 instrument (Emulsiflex C5, Avestin, USA). The prepared

Material and Methods

nanosuspension was purified by dialysis using a cellulose membrane (cut-off = 12,400 Da). 3 mL of Bio-NSs (10 mg/mL) was mixed with CUR (10 mg) and sonicated for 10-15 minutes. The suspension was kept for continuous stirring in dark for 24 hours at room temperature. The supernatant was collected after mild centrifugation and dialyzed for few minutes to remove the uncomplexed drug. Later, supernatant was freeze-dried and stored. The quantity of CUR in Bio-NSs was determined by dispersing 5 mg of CUR-loaded Bio-NSs in 1 mL of ethanol. Samples were sonicated for 2 hours and supernatant was analyzed on HPLC.

3.7.8 Characterization of the BIO-NSs and CUR Loaded Bio-NSs

The thermal properties of samples were evaluated by TA instruments Q200 DSC (New Castle, DE, USA). Functional groups were determined out by PerkinElmer 100 FTIR (PerkinElmer, Waltham, USA).

3.7.9 In-vitro Release Profile of CUR Loaded Bio-NSs

A suspension of CUR-loaded Bio-NSs (10 mg of CUR-BIO-NSs containing 1.2 mg of CUR) or CUR alone (1.2 mg) was prepared in 1.5 mL of phosphate buffer pH 7.4 and sealed into a dialysis bag (12,400 MWCO). The bag was immersed into 30 mL of phosphate buffer pH 7.4 with 0.1 % sodium lauryl sulfate (SLS) at 37 ± 0.5 °C with a rotation speed of 50 rpm. The aliquots (2 mL) were withdrawn at different time intervals and replaced with the same amount of fresh phosphate buffer. Later, all the samples were analyzed to determine the CUR content.

Chapter 4
Results and
Discussion

Results and Discussion

Results and Discussion

4. Results and Discussion

4.1 Kynurenic Acid Loaded Nanosponges for Controlled Drug Delivery

4.1.1 Physicochemical Characterization of NSs and KYNA Loaded NSs

β -CD has a large number of hydroxy groups that make it a suitable candidate for the crosslinking reaction. During the synthesis a carbonate bond between CDI and the hydroxyl groups of β -CD that leads to the formation of NSs. A schematic of the structure of the NSs is shown in figure 4.1.

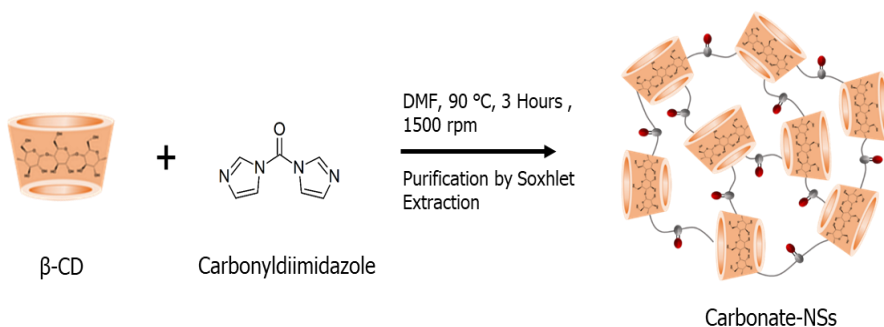


Figure 4. 1 Schematic representation of CDI-based cyclodextrin nanosponges.

The swelling study suggested that β -CDNS2 showed moderate swelling (251 %), compared to β -CDNS1 (200 %) and β -CDNS3 (168 %). However, no evident trend was observed.

Results and Discussion

The percentage crosslinking of prepared NSs was evaluated from the ratio of the two peaks i.e. I_{1774} which corresponds to the carbonyl group stretching of the crosslinker and I_{2929} which corresponds to the C-H stretching of β -CD (Figure 4.2).

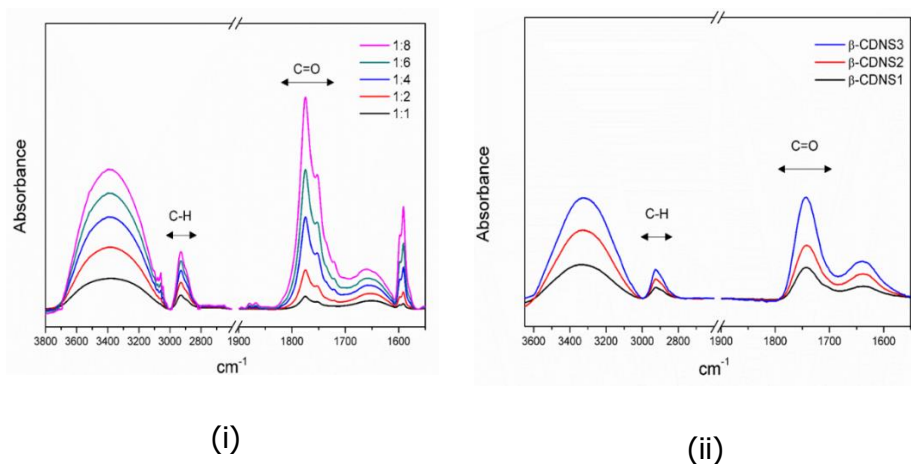


Figure 4. 2 FTIR spectra of (i) calibration standards and (ii) nanosponges.

A high ratio of selected peaks (i.e. I_{1774}/I_{2929}) was obtained due to increment in the I_{1774} band of the carbonyl group because of the high crosslinker concentration.

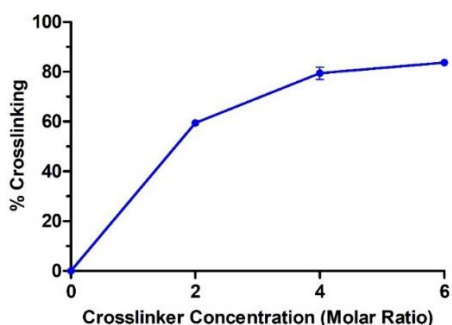
The % crosslinking of the prepared NSs was calculated from the following equation.

$$\% \text{ Crosslinking (\% CL)} = (\text{Sample } I_{1774}/I_{2929} \text{ Value}) / (\text{Reference } I_{1774}/I_{2929} \text{ Value}) * 100$$

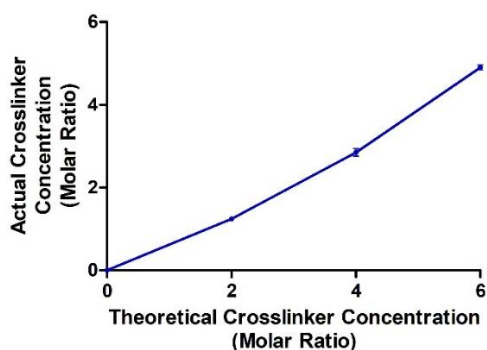
Results and Discussion

Table 4. 1 The percentage cross-linking determination

| NSs | Standard | | Sample | | % CL |
|-----------------|---|---|--|---|---------|
| | Molar Ratio (Crosslinker : β -CD) | Reference I_{1774}/I_{2929} Value | Sample I_{1774}/I_{2929} Value | Calculated Molar Ratio (Crosslinker : β -CD) | |
| β -CDINS1 | 2 | 2.20 | 1.31 | 1.24 | 59.49 % |
| β -CDINS2 | 4 | 3.67 | 2.90 | 2.84 | 79.42 % |
| β -CDINS3 | 6 | 5.93 | 4.93 | 4.89 | 83.70 % |



(i)



(ii)

Figure 4. 3 (i) The percentage crosslinking at different molar ratio (n=3). (ii) Theoretical vs. actual crosslinker concentration (n=3).

It suggested that higher crosslinker concentration leads to higher crosslinking of the nanosponges. The highest crosslinking was achieved with β -CDNS3 (83.7 %) followed by β -CDNS2 (79.42 %) and β -CDNS1 (59.49 %). No significant change in the % crosslinking between β -CDNS2 and β -CDNS3 was observed. It might be due to

Results and Discussion

the fact that majority of free functional groups were involved in the crosslinking.

The solubilization of KYNA is depicted in Figure 4.4. Low aqueous solubility of KYNA (16.4 $\mu\text{g/ml}$) was observed which was enhanced to two-fold with β -CD. Moreover, KYNA solubility was significantly increased to 5.3 folds with β -CDNS1 and 6.77 folds with β -CDNS2. However, no further enhancement in the KYNA solubilization was observed with β -CDNS3 (5.65 folds) because of the higher cross-linker concentration that might have formed more complex nanochannel which hindered the drug encapsulation.

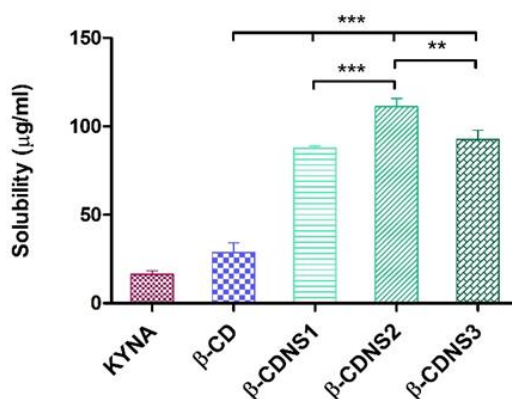


Figure 4. 4 Solubilization of KYNA with different NSs.

Drug loading study was performed with the different weight ratios of drug to NSs i.e. 1:3, 1:4 and 1:5 w/w (KYNA:NS). A weight ratio of 1:4 showed maximum drug loading of 19.06 % compared to 12.7 % at 1:3 w/w and 19.19 % at 1:5 w/w, respectively. A significant difference in the drug loading in between 1:3 w/w and 1:4 w/w was observed. However, further increase in the weight ratio of KYNA:NS

Results and Discussion

(1:5 w/w) does not show significant improvement in the drug loading due to saturation solubility of KYNA.

The drug loading study suggested that the better results were observed with β -CDNS2 thus further studies were carried out on KYNA loaded NS (1:4 w/w). Table 4.2 showed the average particle size and zeta potential of nanosponge formulations.

Table 4. 2 Physicochemical properties of Blank NSs and KYNA loaded NSs.

| Properties | Blank NSs (β -CDNS2) | KYNA loaded NSs (KYNA- β -CDNS2) |
|------------------------------|--------------------------------|---|
| Particle Size (nm) | 224.43 \pm 3.72 | 255.8 \pm 7.88 |
| PDI | 0.35 \pm 0.040 | 0.32 \pm 0.043 |
| Zeta Potential (mV) | -26.3 \pm 1.91 | -23 \pm 0.945 |
| Encapsulation Efficiency (%) | - | 95.31 % |

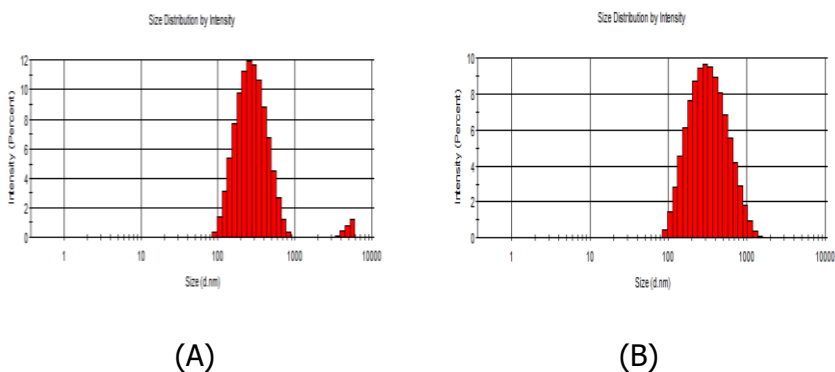


Figure 4. 5 Particle size distribution of blank NSs (A) and KYNA loaded NSs (B).

Results and Discussion

KYNA alone showed an endothermic melting peak at 277.15 °C as shown in figure 4.6. Moreover, NSs were found to be stable over the temperature range of 30-300 °C without any significant thermal transition. Physical mixture (PM2) showed endothermic transition similar to KYNA alone with lesser intensity that might be due to the possible dilution with NS.

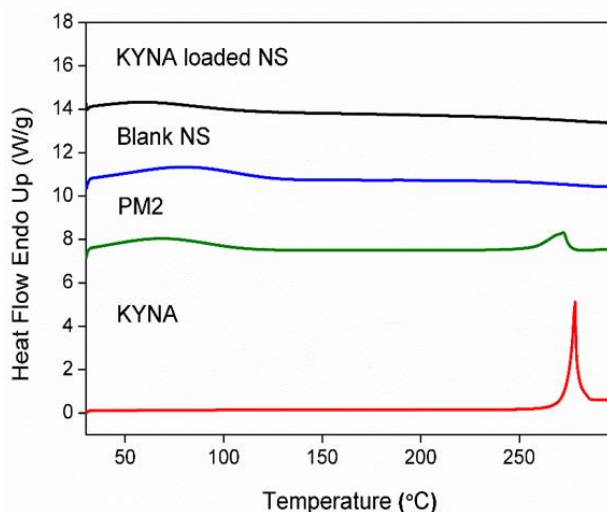


Figure 4. 6 DSC thermogram of the different samples.

An endothermic pattern similar to blank NS was observed in case of KYNA loaded NS which did not show any significant thermal transition might be due to possible amorphization of KYNA, thus confirming the encapsulation of KYNA within the nanosponges.

FTIR spectra of KYNA, blank NS, physical mixture and KYNA loaded NS were showed in figure 4.7. The FTIR spectrum of KYNA showed strong characteristic vibration peaks at 3095 cm^{-1} (-N-H stretching), 2940 cm^{-1} (-C-H stretching), 1660 cm^{-1} (-C=C stretching), 1362 cm^{-1} (-OH bending), 1121 cm^{-1} (-C-O stretching).

Results and Discussion

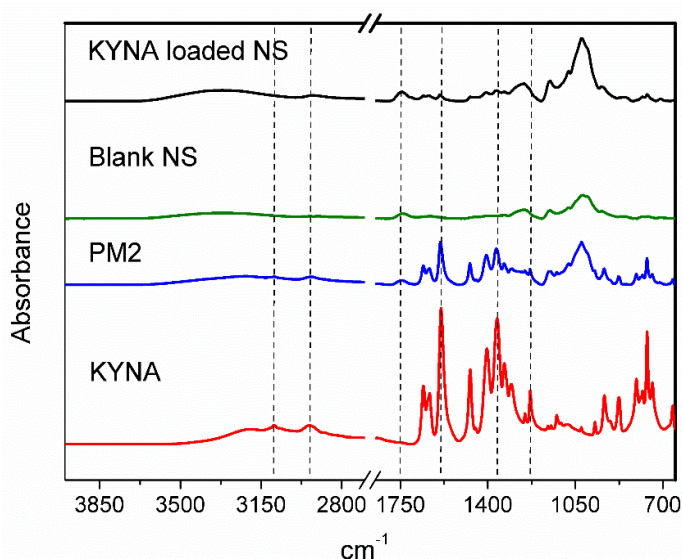


Figure 4. 7 FTIR spectra of the different samples.

It is well reported that CDI-based NSs show characteristic carbonate stretching peak at 1739 cm^{-1} . Moreover, the superposition of FTIR peaks of both KYNA and NSs was observed in the case of a physical mixture. FTIR spectrum of physical mixture does not show any significant shift or suppression, confirming no interaction or encapsulation of KYNA with NSs. In contrast, FTIR spectrum of KYNA loaded NS showed disappearance of peaks at 3095 cm^{-1} (-N-H stretching), and a significant shift in the absorption band at 3318 cm^{-1} (-OH stretching), and 1743 cm^{-1} (-C=O stretching). A change in the characteristic FTIR peaks indicates possible interaction of KYNA with NSs because of the possible encapsulation of drug.

The PXRD studies demonstrated the amorphous or crystalline nature of the different samples (figure 4.8). KYNA is crystalline in nature which was confirmed by the PRXD pattern that showed sharp and

Results and Discussion

intense peaks at a 2θ angle of 8.01, 9.90, 12.62, 16.07, 24.79, 28.22, 31.68, and 39.89.

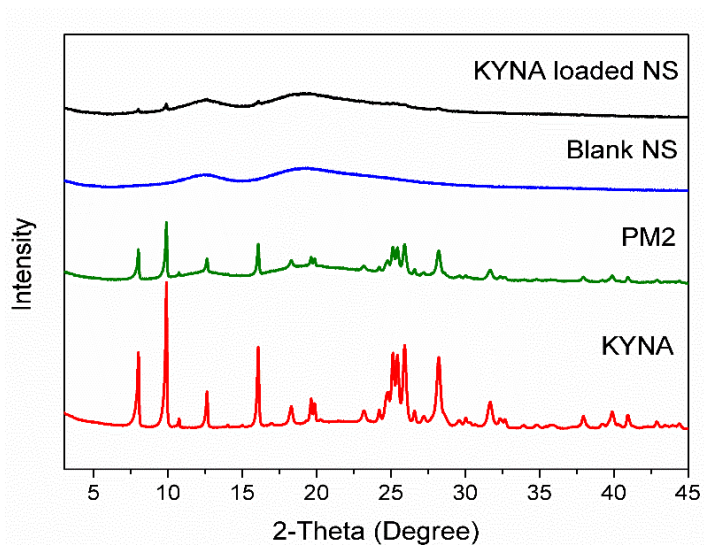


Figure 4. 8 XRD pattern of the different samples.

The XRD of blank NS did not show any sharp peaks which confirmed the amorphous nature of NSs. The characteristic diffraction peaks of KYNA were disappeared in case of KYNA loaded NSs which indicated a loss in the crystallinity and consequent amorphization of KYNA because of the encapsulation of KYNA inside the NSs. However, physical mixture showed characteristic diffraction peaks of KYNA with lesser intensity which remained in the crystalline form. Thus, confirming that property of KYNA remained unchanged in physical mixture. FE-SEM analysis was formed to determine the morphology of the samples (figure 4.9). Both blank NS and KYNA loaded NS showed small spherical shaped particles of diameter around 200 nm with appropriate size distribution. FE-SEM data was in the agreement with the DLS data.

Results and Discussion

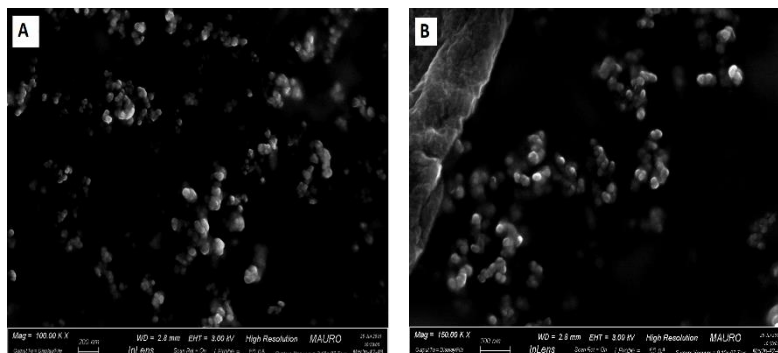


Figure 4. 9 FE-SEM images of (A) Blank and (B) KYNA-loaded NSs

The porosity and surface area of blank and drug-loaded NSs were determined by BET analysis. N₂ adsorption-desorption isotherm and pore distribution curve of blank and KYNA loaded NS is shown in figure 4.10. A type IV isotherm with hysteresis loop was observed for both blank and KYNA loaded NS.

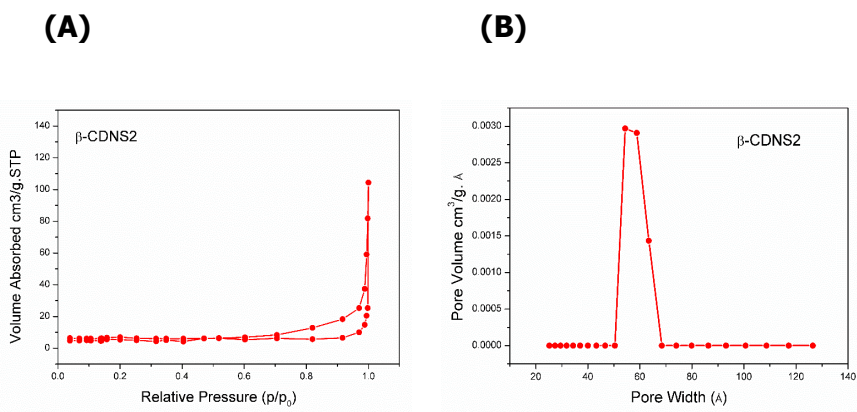


Figure 4. 10 N₂ absorption-desorption (A) and porosity curve of β -CDNS2 (B).

The presence of a hysteresis loop could be attributed to the mesoporous structure of the NS. Moreover, the pore distribution of

Results and Discussion

NSs further suggests the mesoporosity of NSs as the pore diameter was 50-70 Å (5-7 nm).

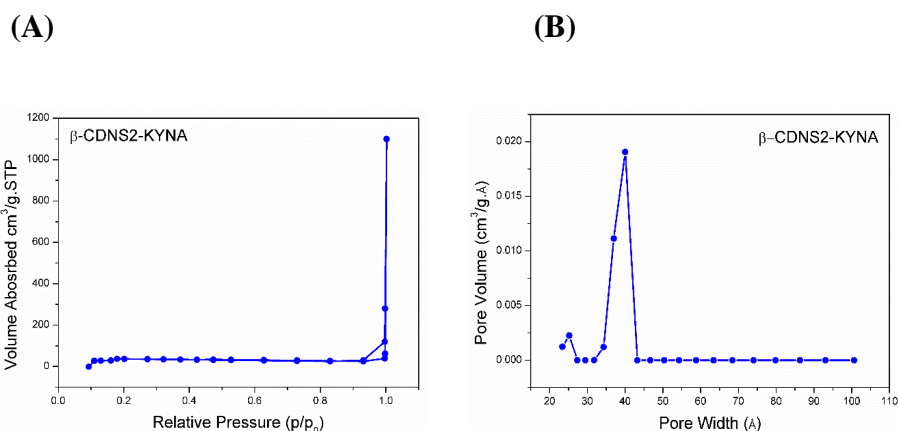


Figure 4. 11 N₂ absorption-desorption (A) and porosity curve of KYNA loaded NSs (B).

The surface area of blank NS was less than 1 m²/g. Moreover, BET analysis of KYNA loaded NS showed a type IV isotherm with hysteresis loop similar to blank NS (figure 4.11). However, porosity of KYNA loaded NS (35-45 Å) was reduced which might be due to encapsulation of KYNA within the NSs.

4.1.2 Release Profile of KYNA

KYNA loaded NSs showed a slow and uniform drug release profile without any initial burst effect (figure 4.12). The presence of KYNA inside the cavities of nanospheres is responsible for a slower drug release profile. Moreover, the absence of an initial burst release could be attributed that the drug was not partially encapsulated or adsorbed on the surface of nanospheres. The mechanism of KYNA

Results and Discussion

release from the NSs was determined by fitting the release profile in different kinetics models such as zero order, first order, Higuchi-Connors, Hixen-Crowell, and Korsmeyer-Peppas. It was observed that the release profile of KYNA was best fitted to Higuchi-Connors release kinetic model ($R^2 = 0.995$) indicating that drug release was diffusion-controlled.

In the case of KYNA alone, it was observed that KYNA showed a rapid and uncontrolled release profile in which equilibrium was achieved within a few minutes. A slow and steady release profile is important parameter in drug delivery in order to avoid dose-related toxic effects. Therefore, controlled drug delivery, which can be achieved by encapsulation of KYNA within NSs, is required.

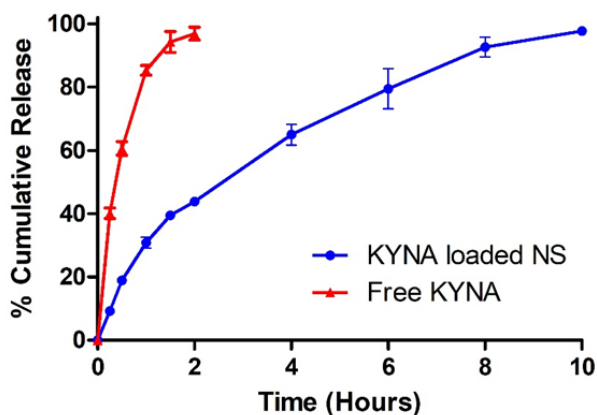


Figure 4. 12 In-vitro release kinetics of KYNA.

4.1.3 Antioxidant Activity of KYNA Loaded NSs

Several phenolic compounds demonstrate antioxidant activity due to their ability to react rapidly with reactive oxygen species. Moreover, KYNA shows antioxidant activity might be because of the

Results and Discussion

presence of an aromatic hydroxyl group that readily provides protons to react with free radicals (Figure 4.13).

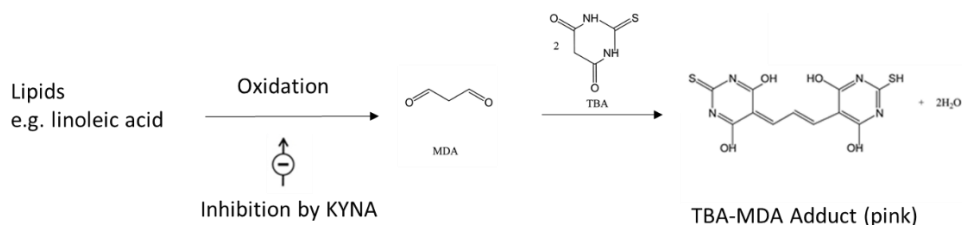


Figure 4. 13 A schematic of the formation of TBA-MDA Adduct.

Moreover, aromatic ring or carboxylic acid present in the structure of KYNA acts as an electron-withdrawing group which helps to stabilize the free radical produced by donation of the proton. The degree of lipid peroxidation can be determined by the generation of MDA as a result of fatty acid degradation. The generated MDA reacts with TBA to produce a pink TBA-MDA adduct. The amount of MDA produced by the degradation of fatty acid is shown in figure 4.14. Results suggested that significant reduction in MDA generation was observed ($P < 0.0001$) compared to free KYNA. A decreased production of MDA could be attributed to the inhibiting and scavenging activity of KYNA on ROS produced during oxidation process.

Results and Discussion

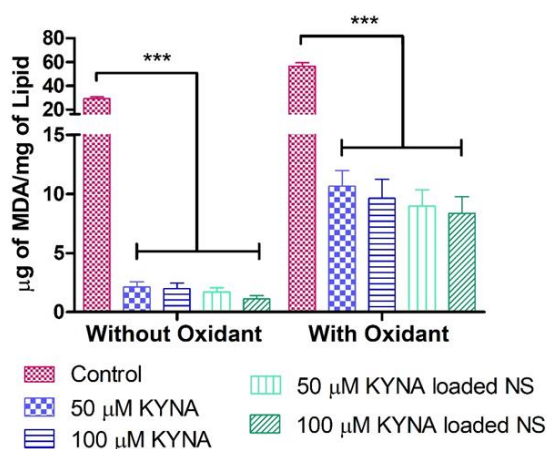


Figure 4. 14 The inhibition of lipid peroxidation by KYNA loaded NS in the absence of oxidizing agent (left) and in the presence of the oxidizing agent (right). *** P < 0.0001.

Oxidizing agents promote the generation of MDA during lipid peroxidation. We demonstrated the effect of KMnO_4 as an oxidizing agent on the MDA generation and high production of MDA was observed due to rapid oxidation of fatty acid. However, a significant decrease in the MDA concentration was observed with KYNA alone and KYNA loaded NSs even in the presence of the oxidizing agent, demonstrating its antioxidant potential. KYNA loaded NSs were found to be comparatively more effective than KYNA alone, might be because of the higher solubilization of KYNA with NSs.

The DPPH consists of a free radical that can be stabilized after accepting the protons which can be determined by the reduction in the absorbance at 517 (figure 4.15). The effect of different concentrations of the KYNA on DPPH inhibition was studied and it was observed that KYNA showed a dose-dependent increase in the

Results and Discussion

DPPH inhibition. Moreover, the KYNA loaded NS showed a significant reduction ($P < 0.001$) in the DPPH concentration compared to KYNA alone (figure 4.16).

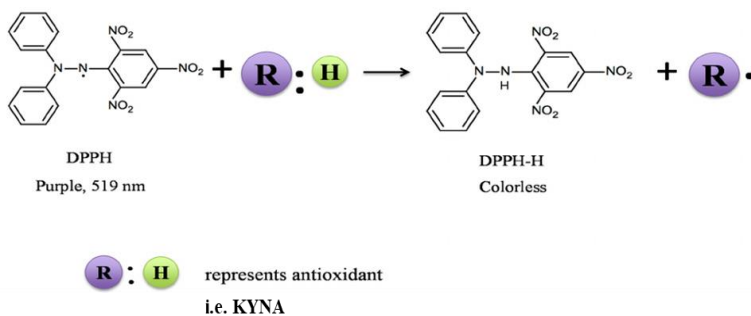


Figure 4. 15 A schematic of DPPH inhibition by KYNA.

It was clear that the KYNA loaded NSs showed higher antioxidant activity compared to KYNA alone which could be attributed to the rapid availability of KYNA due to higher solubilization thus readily provided protons to DPPH.

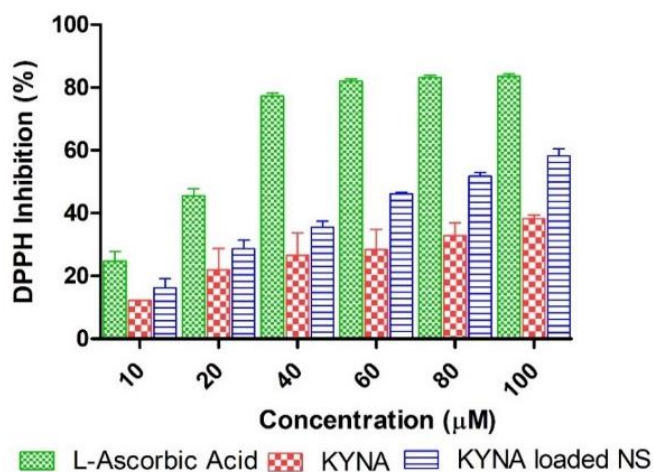


Figure 4. 16 The Percentage DPPH inhibition of KYNA, KYNA loaded NS and L-ascorbic acid.

Results and Discussion

Moreover, the antioxidant property of KYNA was further evaluated by hydrogen peroxide scavenging activity.

The hydroxyl radicals generated from hydrogen peroxide are the most common reactive oxygen species (ROS) that lead to the oxidative degradation of biomolecules such as DNA, RNA, and proteins resulting in the cell death. A schematic of hydrogen peroxide inhibition is demonstrated in figure 4.17.

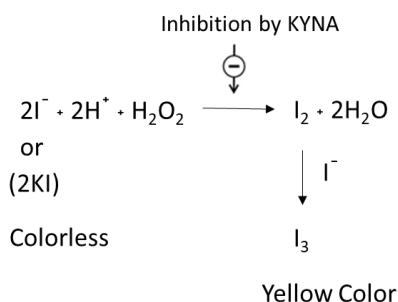


Figure 4. 17 A schematic of H₂O₂ inhibition by KYNA.

The hydrogen peroxide scavenging effect of KYNA and KYNA loaded NSs is shown in figure 4.18. It was observed that all the samples showed concentration-dependent inhibition in H₂O₂ mediated oxidation. Moreover, KYNA loaded NSs demonstrated higher H₂O₂ inhibition ranging from 17 % to 78 % compared to KYNA alone which showed 4 % to 55 % of activity at the same tested concentration. We also studied the effect of a natural antioxidant i.e. L-ascorbic acid and compared with KYNA alone or KYNA loaded NSs. It was clearly evident that L-ascorbic acid showed higher H₂O₂ inhibition activity. We also determined the effect of NSs alone using different methods as described above. However, no significant antioxidant activity was observed.

Results and Discussion

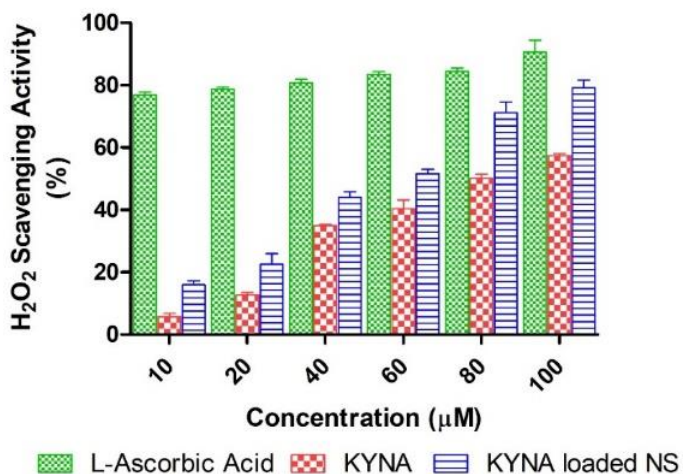


Figure 4. 18 The H_2O_2 scavenging activity of KYNA, KYNA loaded NS and L-ascorbic acid.

4.1.4 In-vitro Cell Viability of KYNA Loaded NSs

The effect of blank NSs on the viability of SHSY-5Y cells was studied to demonstrate the biocompatibility of the NSs. Blank NSs were tested in the concentration range of 5-500 $\mu\text{g}/\text{mL}$ and results obtained suggested that NSs are biocompatible without any significant toxicity (figure 4.19).

Results and Discussion

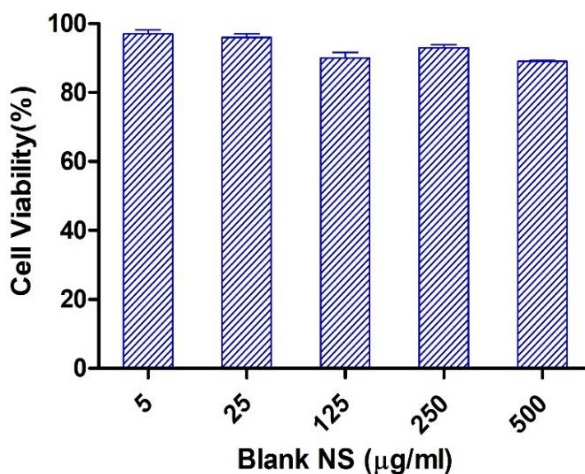


Figure 4. 19 Cytotoxicity of the blank NSs.

Higher cell viability was observed at high NSs concentration (500 $\mu\text{g/mL}$) which was around 90 % after 24 hours. The in-vitro cell viability results are depicted in figure 4.20. The survival of SHSY-5Y cells was evaluated with KYNA and KYNA loaded NSs. It was observed that KYNA and KYNA loaded NSs do not induce toxicity to the SHSY-5Y cells thus confirming their neuro-protective nature. The results obtained from MTT assay confirmed that cell viability was more than 90 % for KYNA alone and KYNA loaded NSs over the concentration range of 10-100 $\mu\text{g/mL}$.

These results strengthen the reports suggested that KYNA can be utilized as a neuro-protector in several neurological diseases.

Results and Discussion

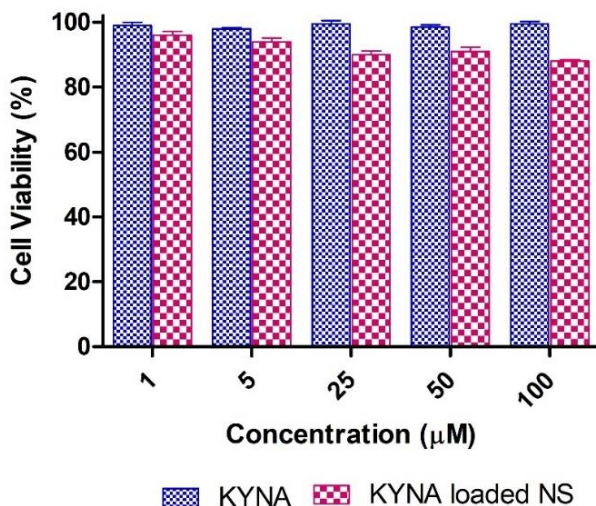


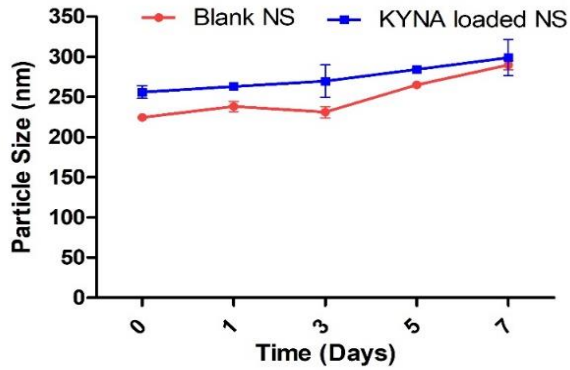
Figure 4. 20 Cytotoxicity of the KYNA loaded NSs.

4.1.5 Storage Stability of KYNA Loaded NSs

The change in the particle size and zeta potential of blank NSs and KYNA loaded NSs was studied to determine their stability at 4 °C for a week. Figure 4.21(A), and 4.21(B) demonstrated the change in the particle size and zeta potential respectively. It was observed that all the samples were stable over the testing period. Moreover, Blank NSs showed little change in the particle size starting from 224 nm to 289.7 nm after one-week. Furthermore, KYNA loaded NSs also showed similar trend in the particle size starting from 255.8 nm and reaching 298.8 nm. Zeta potential of blank NSs and KYNA loaded NSs does not depict a significant change during the storage and found to be in the desired range. These findings clearly confirmed that NSs and KYNA loaded NSs were protected from aggregation and remained stable for the period of a week.

Results and Discussion

(A)



(B)

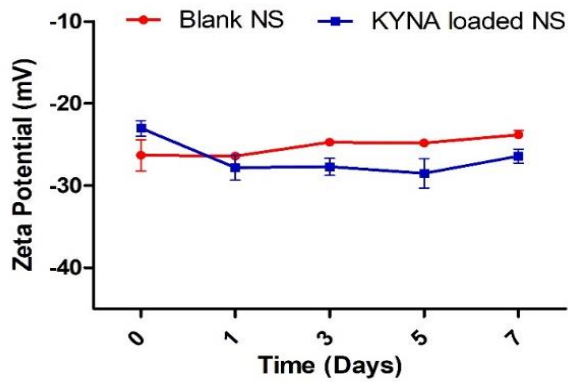


Figure 4. 21 The in-vitro stability study of blank NS and KYNA loaded NS to determine particles size (A) and zeta potential (B). All the values present in terms of mean \pm SD ($n = 3$).

Results and Discussion

4.2 Comparative Evaluation of the Anticancer Activity of RES and OXY

4.2.1 Physicochemical Characterization of RES and OXY Loaded NSs

The therapeutic activity of several drug molecules is limited due to their low aqueous solubility which affects their bioavailability thus remains a major challenge in drug delivery. This work is focused on the improvement in aqueous solubility, photostability and enhanced cytotoxicity of RES and OXY loaded NSs.

Figure 4.22 demonstrated the aqueous solubility of RES and OXY alone and with NSs. RES is a poorly water-soluble drug with aqueous solubility of 0.04 mg/mL. Moreover, the aqueous solubility of OXY was 0.6 mg/mL. Aqueous solubility of both the drug molecules was enhanced significantly with NSs. Indeed, RES exhibited poor aqueous solubility and high solubilization of RES was achieved compared to OXY. An increase in the solubility of RES and OXY might be due to the formation of inclusion complex with CDs present in the structure of the NSs.

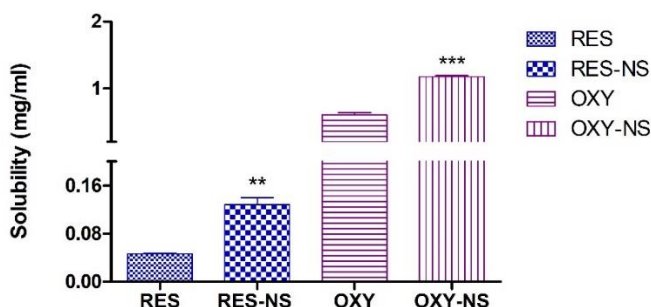


Figure 4. 22 Solubilization of the RES and OXY within the NSs. ** $p < 0.001$; RES vs. RES-NS and *** $p < 0.0001$; OXY vs. OXY-NS.

Results and Discussion

Drug loading study was performed with the different weight ratios of RES or OXY to NSs i.e. 1:2, 1:4 and 1:6 (w/w; Drug:NS). A weight ratio of 1:4 w/w showed maximum drug loading of 13.84 % compared to 9.47 % at 1:2 w/w and 14 % at 1:6 w/w, respectively. Moreover, OXY also showed similar trend with 11.93 % at 1:2 w/w, 16.06 % at 1:4 w/w and 16.78 % at 1:6 w/w of drug loading was observed. For both RES and OXY, A significant difference in the drug loading in between 1:2 w/w and 1:4 w/w was observed. However, further increase in the weight ratio of RES or OXY to NSs (1:6 w/w) does not show significant change in the drug loading due to achieving the saturation solubility of respective drugs.

As per the drug loading data, RES loaded NS (RES-NS) and OXY loaded NS (OXY-NS) at 1:4 w/w ratio were selected for further studies. The physicochemical properties of the prepared RES-NS and OXY-NS are shown in table 4.3.

Table 4. 3 Physicochemical properties of RES-NS and OXY-NSs.

| Properties | RES-NS | OXY-NS |
|-------------------------------------|---------------|---------------|
| Particle Size (nm) | 213.4 ± 2.45 | 220 .3 ± 7.24 |
| PDI | 0.32 ± 0.02 | 0.29 ± 0.08 |
| Zeta Potential (mV) | 23.6 ± 0.25 | 22.3 ± 0.90 |
| Encapsulation Efficiency (%) | 77.73 % | 80.33 % |

Results and Discussion

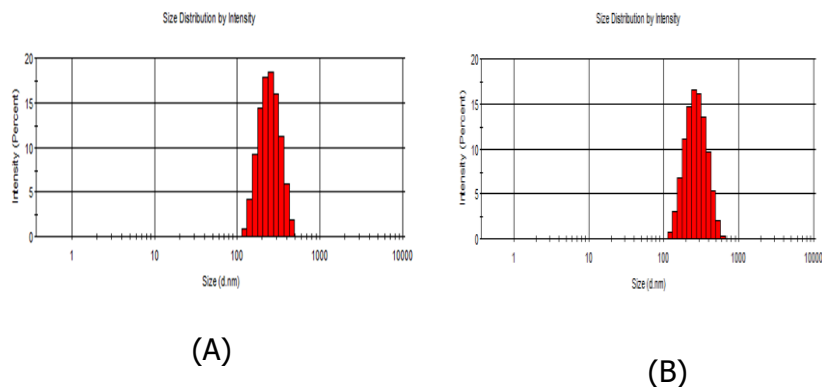


Figure 4. 23 Particle size distribution of RES-NS (A) and OXY-NS (B).

Carbonate-based NSs are characterized by the presence of stretching vibrations of the carbonyl group at 1743 cm^{-1} (figure 4.24). Moreover, RES is characterized by the presence of different FTIR vibrations at 3209 cm^{-1} (O-H stretching), 3019 cm^{-1} (C-H stretching of phenyl ring), 1605 cm^{-1} (C=C stretching), 1322 cm^{-1} (O-H bending). It was observed that RES-NS showed disappearance of characteristic peaks of RES however, a significant shift was observed at 3300 cm^{-1} (O-H stretching). Structure of OXY is similar to the RES thus it also showed similar characteristic vibrations at 3192 cm^{-1} (O-H stretching), 3038 cm^{-1} (C-H stretching of phenyl ring), 1611 cm^{-1} (C=C stretching), 1325 cm^{-1} (O-H bending). However, a significant shift was also observed at 3200 cm^{-1} (O-H stretching) in OXY-NS. The change or shift in the characteristic vibrations of RES-NS or OXY-NS could be attributed to the formation of inclusion complex. Physical mixture of both RES and OXY showed presence of individual characteristic peaks in contrast to the their respective inclusion complex.

Results and Discussion

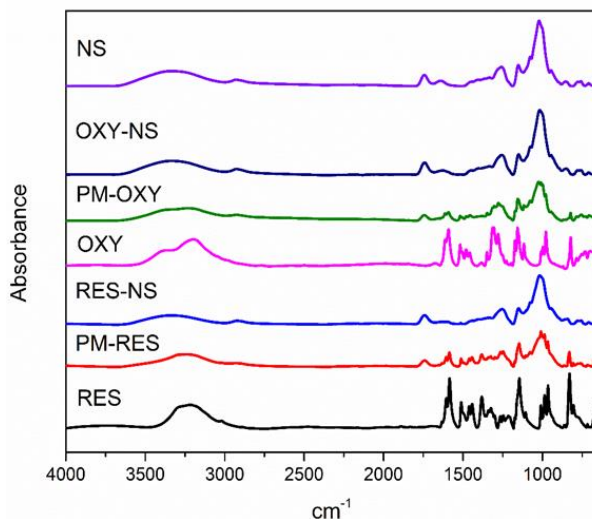


Figure 4. 24 FTIR spectra of RES, OXY, PM-RES, PM-OXY, RES-NS, OXY-NS and blank NS.

DSC thermograms of the samples are shown in figure 4.25.

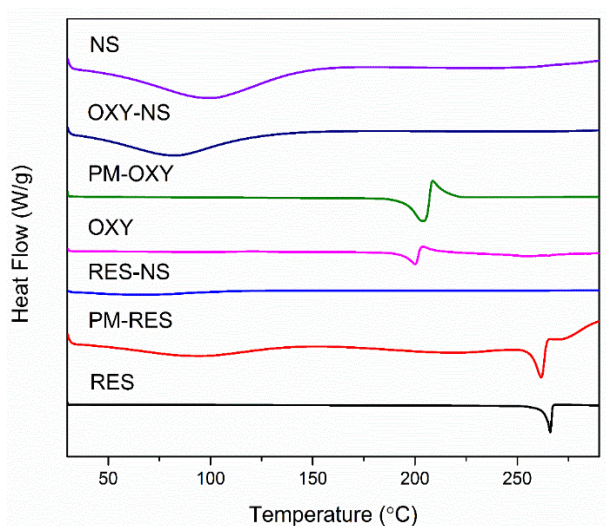


Figure 4. 25 DSC thermograms of RES, OXY, PM-RES, PM-OXY, RES-NS, OXY-NS and blank NS.

Results and Discussion

It was evident that Blank NSs are thermally stable without any significant melting transitions. However, RES and OXY showed prominent endothermic transitions at 266.49 °C and 203.37 °C, respectively. Moreover, in case of physical mixture of both drug molecules no change was observed in the endothermic melting. However, The endothermic melting transitions of RES and OXY were masked completely in the case of RES-NS and OXY-NS. It might be because of the possible encapsulation of RES and OXY within NSs. Moreover, the encapsulation of RES and OXY leads to their amorphization within the NSs which was further validated by PXRD.

PXRD study was performed to determine the nature of different samples as shown in figure 4.26. RES and OXY, are crystalline in nature which was confirmed by PXRD.

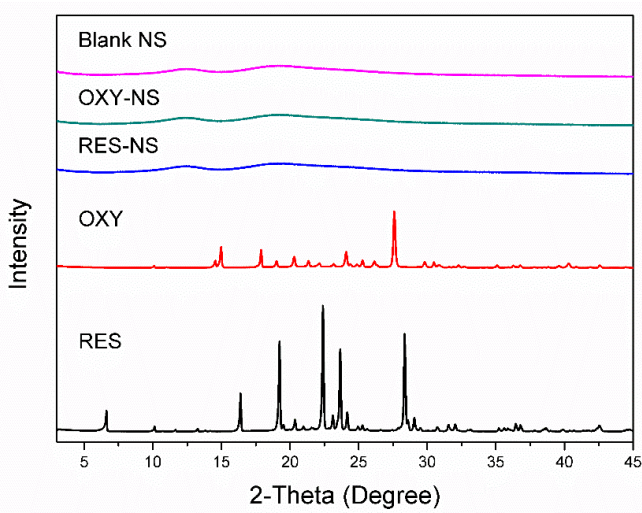


Figure 4. 26 PXRD pattern of RES, OXY, RES-NS, OXY-NS and blank NS.

Results and Discussion

RES showed a sharp and intense diffraction pattern with characteristic peaks at a 2θ angle of 6.61, 16.38, 19.24, 22.38, 23.10, and 28.33. Similarly, OXY also showed sharp peaks at a 2θ angle of 14.56, 17.87, 20.30, 21.34, 24.09, and 27.60. However, it was observed that NSs alone are amorphous in nature. RES-NS and OXY-NS do not exhibit any intense peaks in their respective PXRD pattern, which confirmed that RES and OXY were molecularly dispersed within the NSs resulting in their amorphous state.

The shape and size of RES-NS and OXY-NS were determined by the TEM (figure 4.27). TEM images confirmed the small and uniform particle size of RES-NS and OXY-NS. Moreover, TEM results are in agreement with DLS data (200-250 nm).

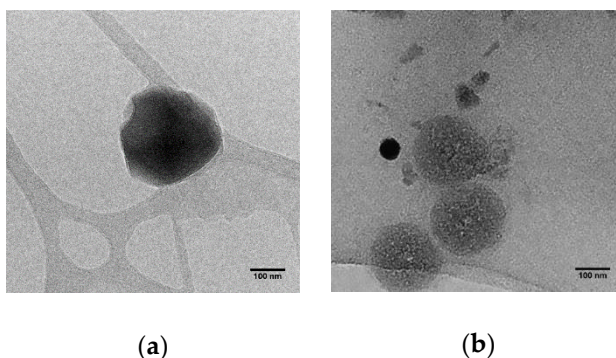


Figure 4. 27 TEM images of (a) RES-NS and (b) OXY-NS.

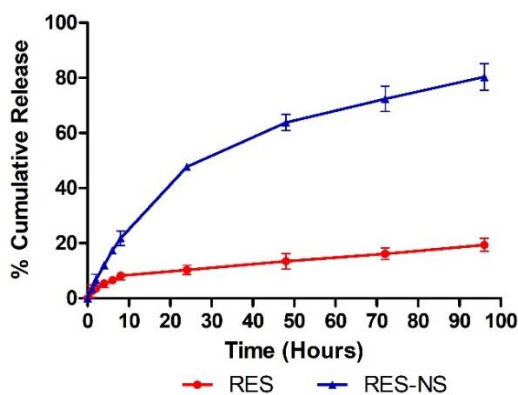
4.2.2 Release Profile of RES and OXY Loaded NSs

The in-vitro release profile of RES-NS and OXY-NS was studied in phosphate buffer pH 7.4 as shown in figure 4.28. RES alone showed very low release even after 90 hours due to low solubility in the

Results and Discussion

dissolution media. However, RES-NS showed almost 5-fold (47.74 %) higher drug release. Indeed, the higher release profile of RES-NS could be attributed to enhanced solubilization and a subsequent amorphization of RES after encapsulation within NSs.

(A)



(B)

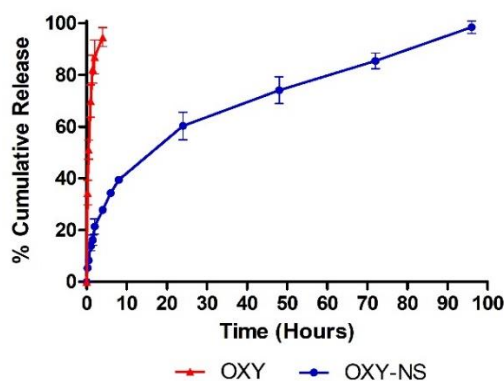


Figure 4. 28 The release profile of (a) RES vs. RES-NS and (b) OXY vs. OXY-NS.

Results and Discussion

In contrast, a rapid and uncontrolled release profile was observed with OXY in which equilibrium was achieved within a few hours. However, OXY-NS exhibited a slow and uniform release profile compared to OXY alone. No burst effect was observed with OXY-NS with nearly 60 % of drug release in the first 24 hours. A slower release of OXY might be due to encapsulation of drug which leads to strong complexation within the NSs. Moreover, Both RES-NS and OXY-NS showed a slow and consistent release profile without an initial burst effect which can be helpful to decrease dose-related side effects.

The release profile of RES-NS and OXY-NS was fitted with different release kinetic models to demonstrate the mechanism of drug release as shown in table 4.4. The release profile of RES-NS and OXY-NS was best fitted to Higuchi-Connors release kinetics models which indicates that RES and OXY were released from the NSs by the means of diffusion. It is well reported that diffusion acts as driving force to release the drug from the NSs.

Table 4. 4 Release kinetic models for RES-NS and OXY-NSs.

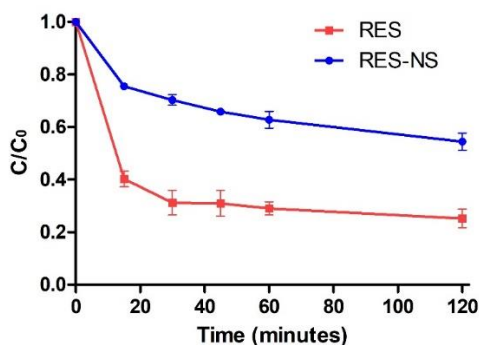
| Models | RES-NS | OXY-NS |
|-------------------------------|----------------------|----------------------|
| | R² | R² |
| Zero Order | 0.904 | 0.9311 |
| First Order | 0.9596 | 0.9136 |
| Higuchi-Connors | 0.9852 | 0.9828 |
| Korsmeyer-Peppas Model | 0.6052 | 0.7076 |

Results and Discussion

4.2.3 Photodegradation Study

RES and OXY both are photosensitive drug molecules and undergo degradation after exposure in UV-light (figure 4.29).

(A)



(B)

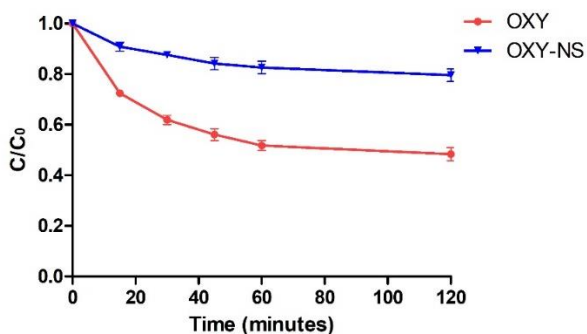


Figure 4. 29 Photodegradation study of (a) RES vs. RES-NS and (b) OXY vs. OXY-NS.

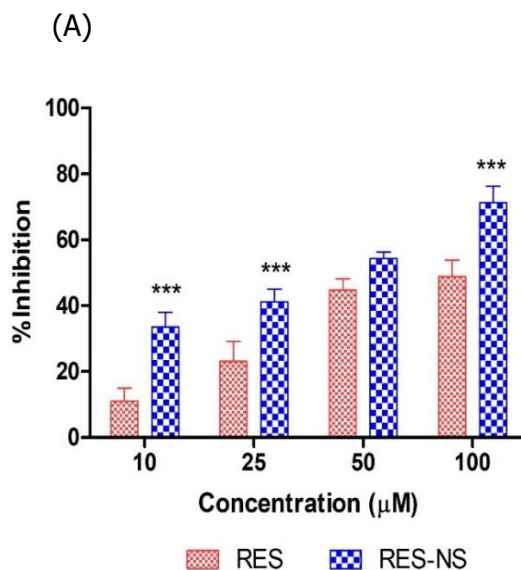
RES and OXY alone were directly exposed to UV-light that lead to their degradation up to 59.7% and 27.5%, respectively within 15

Results and Discussion

minutes. Moreover, RES-NS and OXY-NS showed lesser degradation compared to respective drugs alone. RES-NS showed two-fold and OXY-NS showed three-fold protection from degradation after UV-exposure. Indeed, it was evident that encapsulation of RES and OXY within the NSs provides protection from degradation by preventing the exposure of drugs to the UV-light.

4.2.4 DPPH Assay of RES and OXY Loaded NSs

RES and OXY also exhibit antioxidant property which was determined by their inhibition potential against DPPH. DPPH accepts protons or electrons from the antioxidants and this leads to discoloration of the DPPH. Antioxidant activity of RES and OXY can be measured quantitatively by determining the change in the absorbance values of DPPH compared to control. DPPH inhibition of RES, OXY, RES-NS, and OXY-NS is shown in figure 4.30..



Results and Discussion

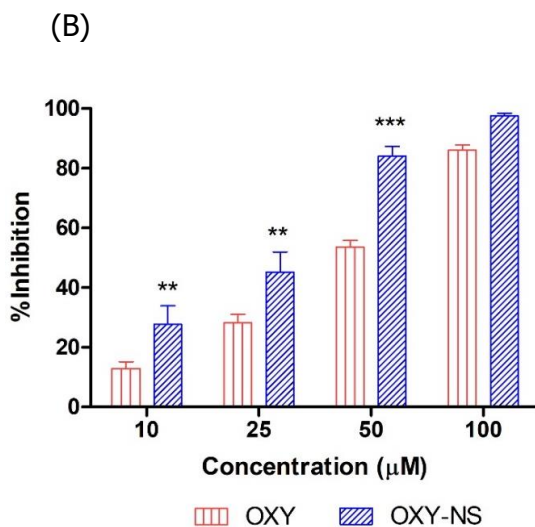


Figure 4. 30 DPPH inhibition activity of (a) RES vs. RES-NS and (b) OXY vs. OXY-NS. ** $p < 0.01$ and *** $p < 0.001$.

It is clearly evident that OXY showed better antioxidant activity than RES alone which could be attributed to the presence of an additional hydroxyl group in OXY which helps to stabilize the DPPH free radical. Moreover, RES-NS and OXY-NS showed significant improvement in the antioxidant activity compared to individual drugs that might be due to high solubilization potential of the NSs by which RES and OXY readily provide protons for the reaction with DPPH.

4.2.5 Anticancer Activity of RES and OXY Loaded NSs

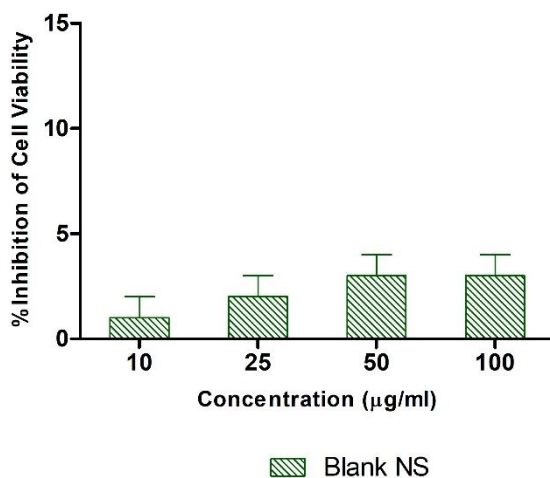
The cytotoxicity of RES-NS and OXY-NS was confirmed against DU-145 prostate cancer cells. Cells were treated with increasing concentrations of the different samples over a period of 96 hours as shown in figure 4.31. It was observed that all the samples exhibited

Results and Discussion

a dose-dependent increase in the cytotoxicity. Moreover, RES-NS and OXY-NS showed higher toxicity compared to RES and OXY alone. A significant difference ($p < 0.05$) of cytotoxicity in-between RES-NS and RES was observed after 96 hours at the concentrations of 25, 50 and 100 μM , respectively. Furthermore, OXY-NS showed significant cytotoxicity ($p < 0.05$) compared to OXY alone at the highest concentration.

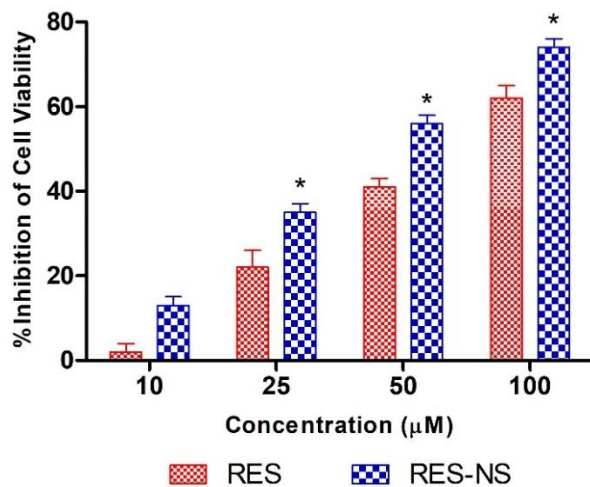
The cytotoxicity of the blank NSs was determined after 96 hours and it was observed that NSs alone are safe and do not exhibit any toxic effects. The low particle size and high solubilization of RES and OXY within the NSs that leads to change in the physicochemical properties could be responsible for the high anticancer activity.

(A)



Results and Discussion

(B)



(C)

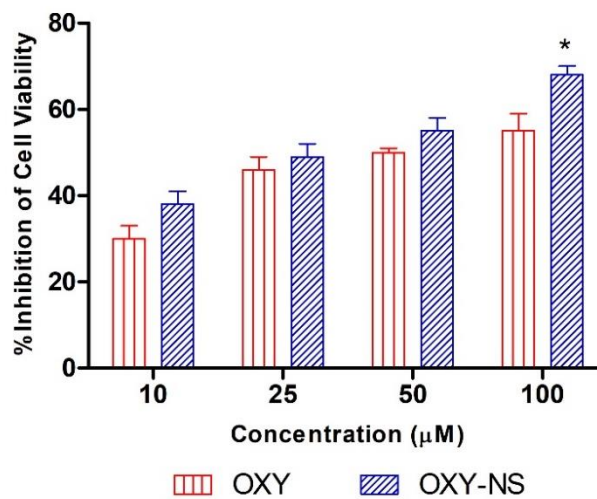


Figure 4. 31 Cell cytotoxicity study of (A) Blank NS, (B) RES vs. RES-NS, and (C) OXY vs. OXY-NS after 96 hours. *p<0.05.

Results and Discussion

4.3 Determination of Encapsulation Constant of the NSs and Activity Against Colon Cancer by OXY Loaded NSs

4.3.1 Encapsulation Constant of the NSs

The encapsulation constant of NSs is usually determined by phase solubility diagram. However, there are certain drawbacks associated with this method such as necessity to determine the molecular weight of the polymer and assuming that no water-soluble molecule that will form complex with insoluble NSs will be solubilized. Indeed, solubility enhancement is limited which might be due to the fact that total complexation capacity of the NSs is not determined because it is insoluble in nature.

For these reasons, we tried a better model to determine the encapsulation constant. The increasing concentrations of OXY were mixed with 1 % β -CDI 1:4 NSs and incubated for a period of 48 hours. The effect of NSs on the OXY concentrations is shown in figure 4.32. A graph was plotted in between $1/(A-A_0)$ vs $1/[OXY]$ to determine the decrease in the OXY concentration due to encapsulation and precipitation. A K_{Fapp} value was calculated as described in material and methods which was around $3917.89 \pm 392.79 \text{ M}^{-1}$. Other NSs were also tested in a similar manner and K_{Fapp} value was determined (Table 4.5). A high correlation coefficient (R^2) suggests a homogeneous complexation power between all the available cavities.

Moreover, among the α -, β - and γ -CDI 1:4 NSs, α - and γ -CDI 1:4 NSs showed similar and lower K_{Fapp} values compared to β -CDI 1:4 NSs. It might be due to the availability of inadequate number of

Results and Discussion

cavities for the complexation of OXY, as natural CDs. β -CDI 1:4 NSs were used for further study due to the better complexation efficiency.

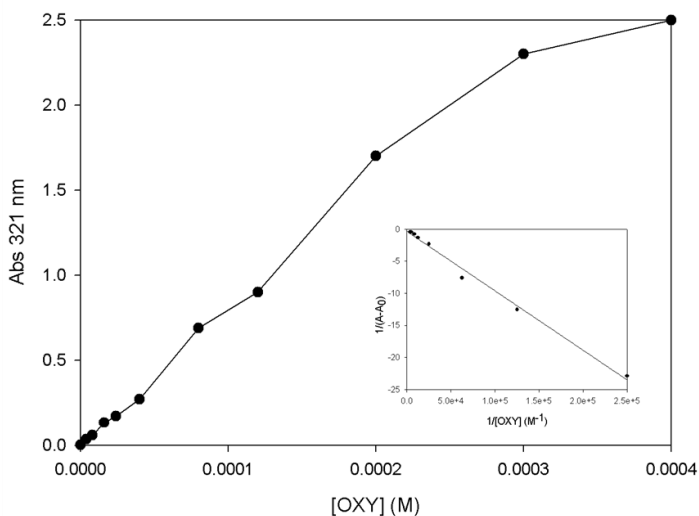


Figure 4. 32 Effect of increasing OXY concentration on absorbance at 48 h with 1% of β -CDI 1:4 in water at 25 °C. Insert. Benesi-Hildebrand plot of OXY complexed to β -CD-CDI 1:4. The β -CDI 1:8 nanosponge showed the highest K_{Fapp} , perhaps due to its higher number of CDs per gram.

Table 4. 5 Apparent K_{Fapp} (M⁻¹), SD (+/-) values and correlation coefficients for OXY/CD complexes at 25 °C in water.

| Guest | CDNS | K_{app} | SD | R^2 |
|-------|-------------------|-----------|--------|-------|
| OXY | β -CDI 1:4 | 3917.89 | 392.79 | 0.99 |
| OXY | β -CDI 1:8 | 5575.52 | 560.55 | 0.98 |
| OXY | α -CDI 1:4 | 1595.08 | 155.51 | 0.99 |
| OXY | γ -CDI 1:4 | 1718.64 | 173.86 | 0.99 |

Results and Discussion

4.3.2 Physicochemical Characterization of the OXY Loaded NSs

CDI-NSs are characterized by the presence of carbonate peaks which was observed at 1746 cm^{-1} (figure 4.33). OXY alone showed characteristic peaks at 3192 cm^{-1} (O-H stretching), 3038 cm^{-1} (C-H stretching of phenyl ring), 1591 cm^{-1} (aromatic C=C stretching). Moreover, Major characteristic peaks of OXY were masked with NSs. The aromatic stretching peak was also observed with OXY loaded NSs with lower intensity might due to the possible encapsulation of OXY with nanosponges.

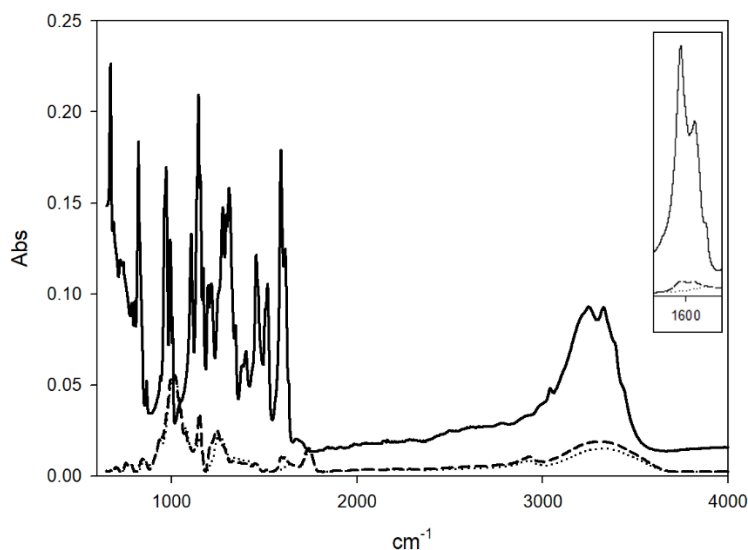


Figure 4. 33 FTIR spectra of OXY, β -CDI 1:4 and OXY-loaded β -CDI 1:4. Legend: (—) OXY, (···) β -CDI 1:4 and (-·-·-) OXY loaded β -CDI 1:4.

DSC method can be used to evaluate the formation of inclusion complex and it can be differentiated with the physical mixture of the same components. The disappearance of the characteristic endothermic melting peak is considered as the formation of the

Results and Discussion

inclusion complex. DSC results of β -CDI 1:4 NSs, OXY and OXY loaded NSs are shown in figure 4.34. β -CDI 1:4 NSs showed an endothermic peak at 100 °C, due to evaporation of the water. Moreover, NSs are found to be stable and no melting or degradation was observed. OXY alone showed endothermic melting peak at 199.94 °C, which was completely masked in the DSC thermogram of OXY loaded NSs. These findings suggest encapsulation of OXY within the NSs. The disappearance of the endothermic melting peak could be the result of the amorphous state of OXY.

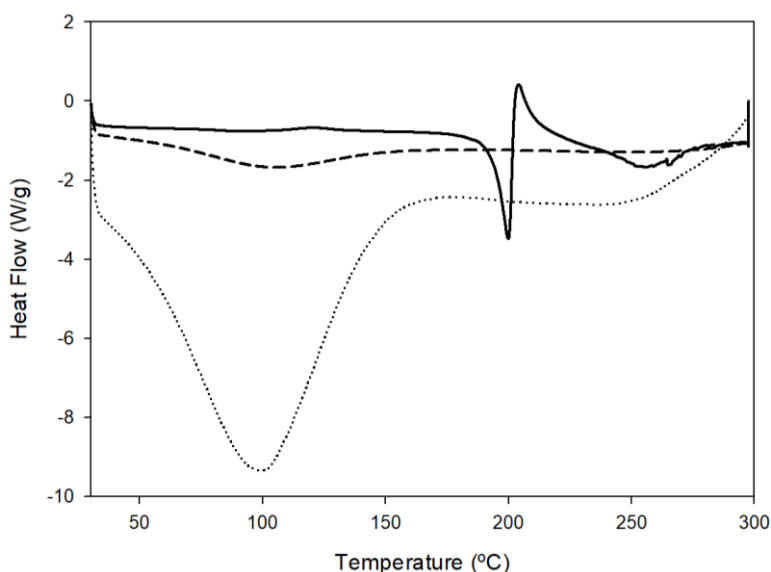


Figure 4. 34 DSC thermogram of OXY, β -CDI 1:4 and OXY-loaded β -CDI 1:4. Legend: (—) OXY, (···) β -CDI 1:4 and (-·-·-) OXY loaded β -CDI 1:4.

The thermal stability of the OXY, NSs, and OXY loaded NSs was determined by TGA study (figure 4.35). TGA of blank NSs showed two degradation peaks (possibly due to different intramolecular binding strengths) with a mass reduction of 79.29 %. Moreover,

Results and Discussion

OXY alone showed early degradation starting after 200 °C. Furthermore, OXY degradation was shifted towards the higher temperature in case of OXY loaded NSs and the presence of OXY not only decreased the mass reduction (69.62%), but the two degradation peaks of NSs became one. Such observations lend weight to the complexation.

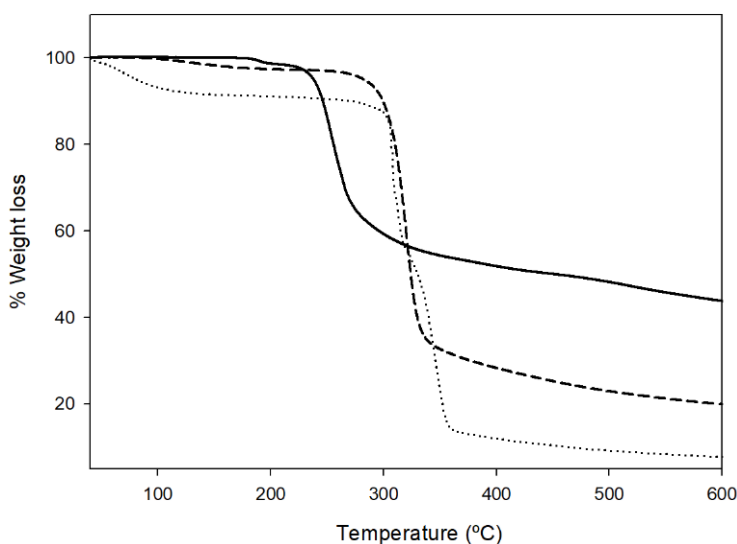


Figure 4. 35 TGA curves of OXY, β -CDI 1:4 and OXY-loaded β -CDI 1:4. Legend: (—) OXY, (···) β -CDI 1:4 and (-·-·-) OXY loaded β -CDI 1:4.

4.3.3 In-vitro Drug Release Profile

The in-vitro release profile of OXY loaded NSs was determined in physiological buffer pH 7.4 and pH 5.5. Samples of OXY were collected and analyzed to determine the % OXY release over the period of experiment (figure 4.36).

Results and Discussion

The release profile of OXY loaded NSs showed slow and consistent drug release for more than 80 hours. OXY loaded NSs showed 45 % and 39 % of drug release at pH 7.4 and pH 5.5, respectively within 12 hours. A slow and uniform drug release profile could be attributed to the the formation of inclusion complex of OXY with NSs due to the presence of CD cavities.

These data represent a good approximation to real release conditions and confirm the potential of β -CDI 1:4/OXY complexes for nutraceutical applications.

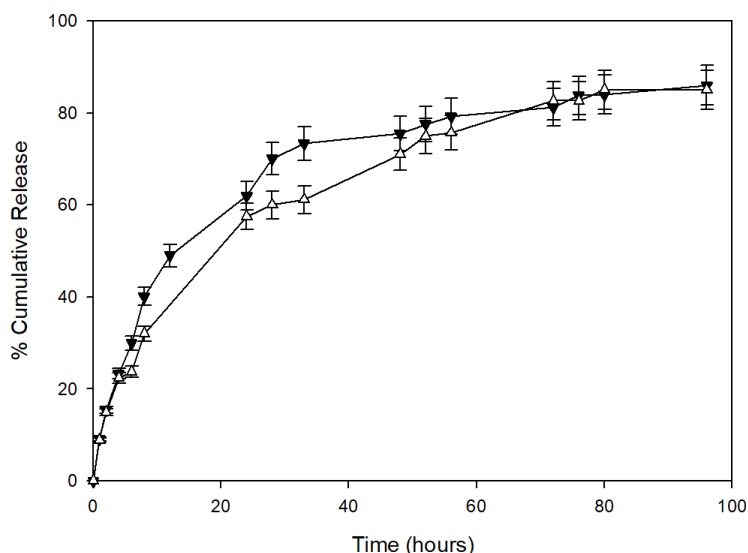


Figure 4. 36 In-vitro release profile of OXY or complex at pH 7.4 and 5.5 at 37 °C. Legend: (Δ) OXY loaded β -CDI 1:4 at pH 7.4 and (\blacktriangle) OXY loaded β -CDI 1:4 at pH 5.5.

4.3.4 In-vitro Digestion Study of OXY

To determine the bioaccessibility of OXY from OXY loaded NSs after digestion in simulated gastric media, in-vitro digestion study was

Results and Discussion

performed for OXY and OXY loaded NSs (figure 4.37). It was observed that OXY amount was reduced to 89 % after digestion in stomach media while high amount of OXY was observed with OXY loaded NSs. Later, amount of OXY alone further reduced to 75 % of the initial amount after digestion in intestine media. However, OXY loaded NSs showed an increase in the concentration of the OXY (154 % of initial value) by the end of the digestion step.

When the ratio (r) of OXY in the soluble part, between CD-NS and free OXY, was calculated, the initial amount of OXY in the free sample was higher than in the complexed sample ($r \approx 0.6$) this is because a part of OXY is loaded in CD-NS in the insoluble part. However, after the intestine step the complexed OXY was released from CD-NS, perhaps by the displacement due to bile salts changing the ratio ($r \approx 1.3$) and increasing the OXY for absorption.

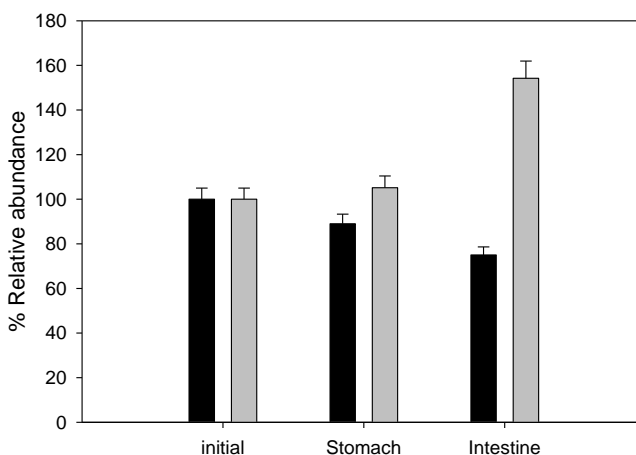


Figure 4. 37 Relative abundance of OXY after stomach and intestine digestion without (black) and with (gray) CD-NS. The data are normalized using initial OXY abundance.

Results and Discussion

Although the initial bioaccessibility of the free OXY sample was better than that of the complexed sample in the intestine step, the release of OXY from CD-NS and its additional protection increased these values suggesting that CD-NS complexation could be a good option for OXY administration.

4.3.5 Activity of OXY Against Colon Cancer

We compared the ability of OXY solution and OXY loaded NSs to inhibit the growth of different colon cancer cell lines in vitro. Cells were incubated for 72 hours and it was observed that OXY-NS always inhibited cancer cell viability to a higher extent than OXY. Indeed, OXY alone induced a small inhibition of HT29 viability only at the higher concentration, being ineffective against the other cell lines. Instead, OXY loaded NSs effect was concentration-dependent with the high difference among the different cell lines, being HT29 (figure 4.38) more susceptible than HCT116 (figure 4.39). The viability inhibition at the higher concentration was $79\pm 3\%$, and $55\pm 4\%$ for HT29, and HCT116, respectively. Furthermore, Blank NS does not give any significant toxicity compared to OXY-NS. Against both types of cancers, OXY loaded CD-NS presented better results than free OXY. These data suggest a slower release of OXY from the complexes than from the free drug, which is a desirable characteristic. In general, the complexation of drugs provides higher or would provide consequent changes in the physicochemical properties of OXY. In this case, they might be responsible for the higher toxicity towards cancer cells.

Results and Discussion

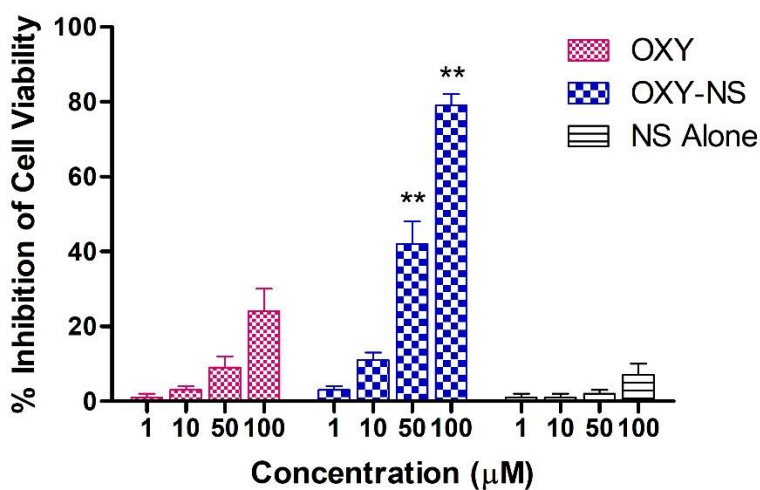


Figure 4. 38 Cytotoxicity of OXY, OXY-NS, and NS alone on HT29 cell lines. ** $p < 0.01$; OXY vs. OXY-NS.

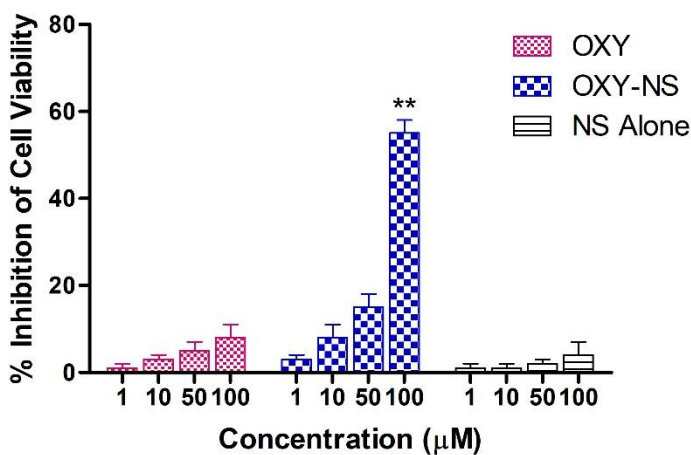


Figure 4. 39 Cytotoxicity of OXY, OXY-NS, and NS alone on HCT116 cell lines. ** $p < 0.01$; OXY vs. OXY-NS.

Results and Discussion

4.4 Stimuli-responsive Drug Delivery System of Resveratrol

4.4.1 Physicochemical Characterization of the GSHNSs and RES-GSHNSs

GSH-responsive nanosponges were prepared from pyromellitic dianhydride and 2-hydroxyethyl disulfide as crosslinker. A schematic of the structure of the GSHNSs is shown in figure 4.40.

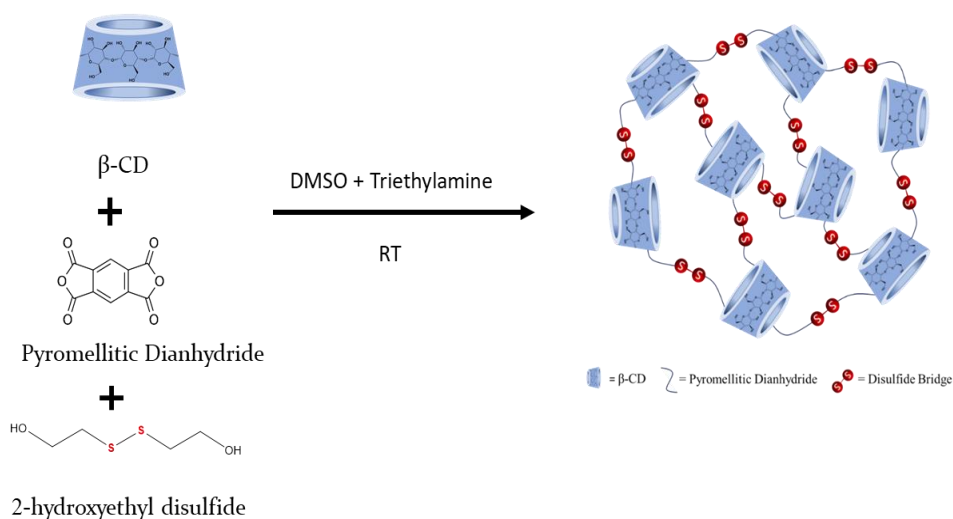


Figure 4. 40 Structure of the GSHNSs.

We first performed an elemental analysis to characterize unloaded (blank) GSHNSs. The elemental analysis confirmed the presence of disulfide groups in the nanostructures. Additionally, CHNS analysis demonstrated carbon and hydrogen contents of 54.42% and 5.33%, respectively. The sulfur content was 0.75 %. However, it was lower than the expected value of 0.97%, suggesting that 2-hydroxyethyl disulfide has less reactivity as crosslinking agent than pyromellitic dianhydride.

Results and Discussion

The solubilization of RES alone and in the presence of nanosponge (GSHNSs) is shown in figure 4.41. The aqueous solubility of RES was 0.04 mg/mL and the encapsulation of RES with GSHNSs leads to 5-fold enhancement of the aqueous solubility of RES. The enhancement in the aqueous solubility of RES could be attributed to the encapsulation in the CD cavities and interstitial spaces of the NSs.

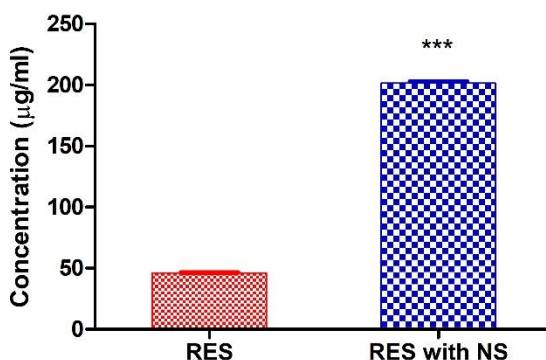


Figure 4. 41 Solubilization of the RES with GSHNSs. (***) $p < 0.0001$).

RES loaded GSHNSs were prepared by taking a different weight of drug into GSHNSs. Weight ratios of 1:2, 1:4, and 1:6 (w/w) were used. The drug loading of RES was 9.95 % at 1:2 w/w, 16.12 % at 1:4 w/w and 13.72 % at 1:6 w/w. A significant difference ($p < 0.05$) in the drug loading was observed between 1:2 w/w and 1:4 w/w for RES. However, no significant difference of drug loading between 1:4 w/w and 1:6 w/w was observed, probably it might be because of the achievement of the saturation solubility of RES.

As per the drug loading data, RES loaded GSHNSs (1:4 w/w) were selected for the further studies. The average particle size and zeta

Results and Discussion

potential of blank GSHNSs and RES loaded GSHNSs were determined as shown in Table 4.6.

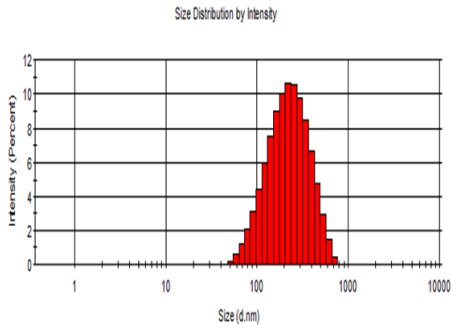
Table 4. 6 Physicochemical properties of GSHNSs and RES-GSHNSs.

| Properties | GSHNSs (Blank) | RES- GSHNSs | Fluorescent GSHNSs |
|---|---------------------------|------------------------|-------------------------------|
| Particle Size (nm) | 190.7 ± 0.60 | 206.3 ± 0.43 | 200 ± 0.80 |
| PDI | 0.20 ± 0.01 | 0.24 ± 0.005 | 0.20 ± 0.005 |
| Zeta Potential (mV) | -34.2 ± 1.40 | -29.2 ± 1.78 | -30.4 ± 0.64 |
| Encapsulation Efficiency (%) | - | 80.64 % | - |

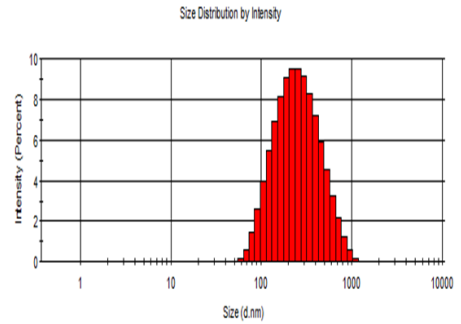
Results and Discussion

The particle size distributions of GSHNSs, RES loaded GSHNS, and Fluorescent GSHNSs (C-6) are shown below:

(A)



(B)



(C)

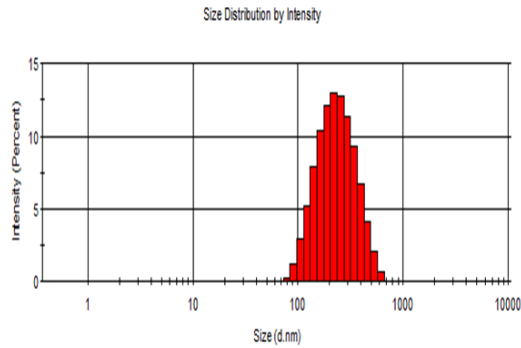


Figure 4. 42 Particle size distribution of GSHNSs (A), RES loaded GSHNS (B), and Fluorescent GSHNSs (C).

Results and Discussion

The characteristic peak of NS was observed at 1743 cm^{-1} because of the stretching vibrations of the carbonyl group. RES showed characteristic vibrations at 3209 cm^{-1} (O-H stretching), 3019 cm^{-1} (C-H stretching of phenyl ring), 1605 cm^{-1} (C=C stretching), 1322 cm^{-1} (O-H bending). Major characteristic peaks of RES were disappeared in the case of RES-GSHNS and a significant shift in O-H stretching was observed at 3450 cm^{-1} . It might be due to the encapsulation of RES within the GSHNSs (figure 4.43). Contrast to the inclusion complex, in physical mixture (PM-RES) FTIR peaks remains unchanged.

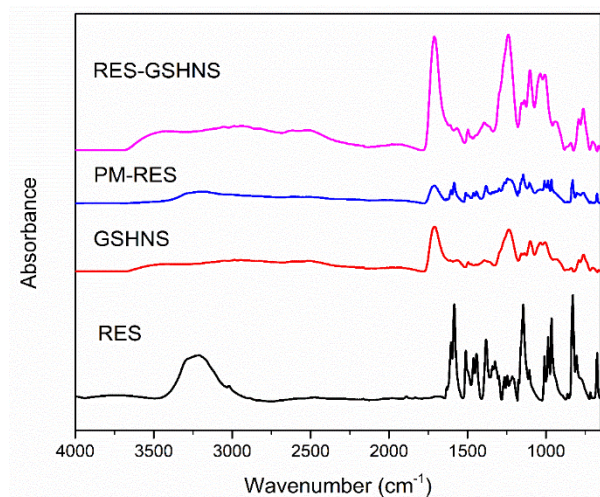


Figure 4. 43 FTIR spectra of RES, PM-RES, RES-GSHNS, and GSHNS.

DSC data suggested that Blank GSHNSs were stable and do not undergo any endothermic transition as shown in figure 4.44. RES alone showed an endothermic melting peak at $266.49\text{ }^{\circ}\text{C}$ which can also be seen in physical mixture (PM-RES). However, RES-GSHNS does not show any endothermic melting transitions because of possible encapsulation of RES within NSs.

Results and Discussion

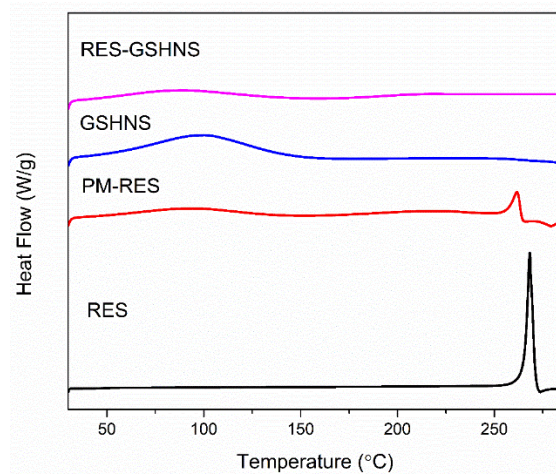


Figure 4. 44 DSC thermograms of RES, PM-RES, RES-GSHNS, and GSHNS.

The physical state of all the samples was determined by PXRD studies as shown in figure 4.45.

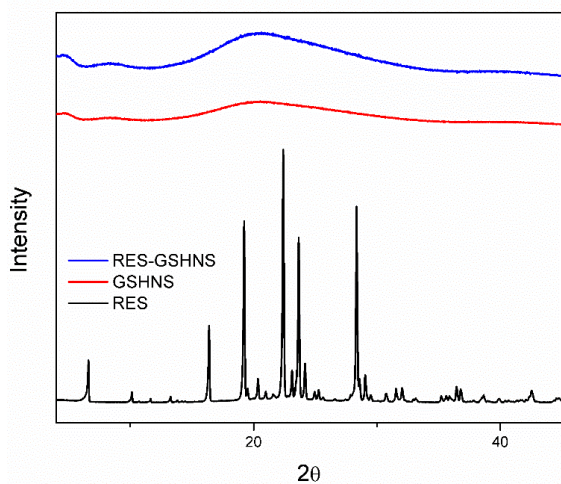


Figure 4. 45 PXRD pattern of RES, RES-GSHNS, and GSHNS.

The diffraction pattern of RES showed crystalline structure due to the presence of sharp and intense peaks at a 2θ angle of 6.61,

Results and Discussion

16.38, 19.24, 22.38, 23.10, and 28.33. However, the PXRD pattern of GSHNS alone demonstrated its amorphous nature. RES-GSHNS does not exhibit any intense peaks in their respective PXRD pattern which confirmed that the drug was molecularly dispersed in the amorphous state within the NSs.

Figure 4.46 represents TEM and FE-SEM images of RES-GSHNSs which confirms uniform size spherical particles. The particle size of RES-GSHNS obtained with TEM and FE-SEM is in agreement with the DLS data (180-200 nm).

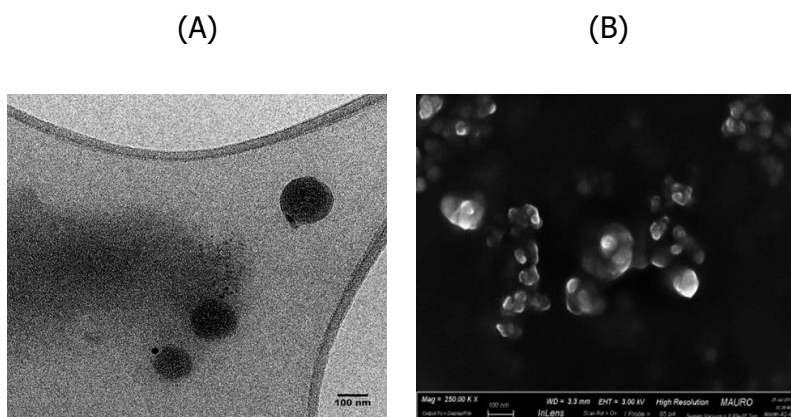


Figure 4. 46 Morphology of the RES-GSHNSs (A) TEM and (B) FE-SEM.

4.4.2 Release Profile of RES from GSHNSs

The in-vitro release profile of RES and RES-GSHNS is shown in the figure 4.47. A slow and consistent release profile was observed without an initial burst effect. From the dissolution profile, it was evident that RES-GSHNS showed higher release compared to RES alone. RES-GSHNS showed an almost 2-fold higher drug release

Results and Discussion

compared to RES alone after 24 hours. A higher release profile of RES might be due to enhanced solubilization potential of the GSHNSs. Moreover, more than 5-fold higher drug release was observed compared to free RES in the presence of 10 mM GSH that was further increased with 20 mM GSH. This behavior of the GSHNSs confirmed the GSH responsiveness of the nanocarrier. The presence of GSH in the release media causes rapid breakdown of the nanocarrier which allows the higher release of RES.

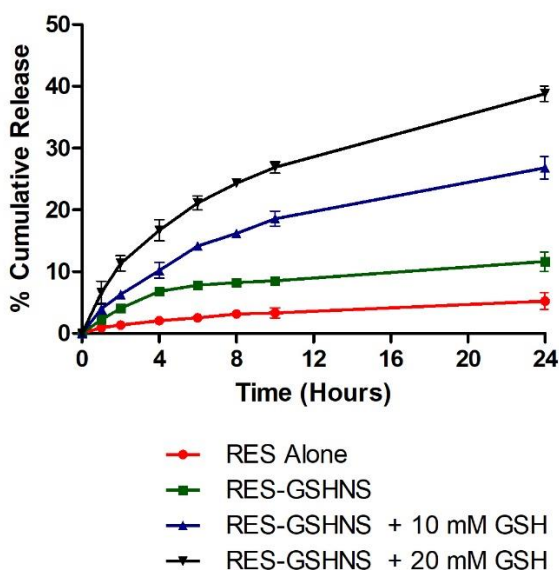


Figure 4. 47 Release profile of the RES and RES-GSHNSs.

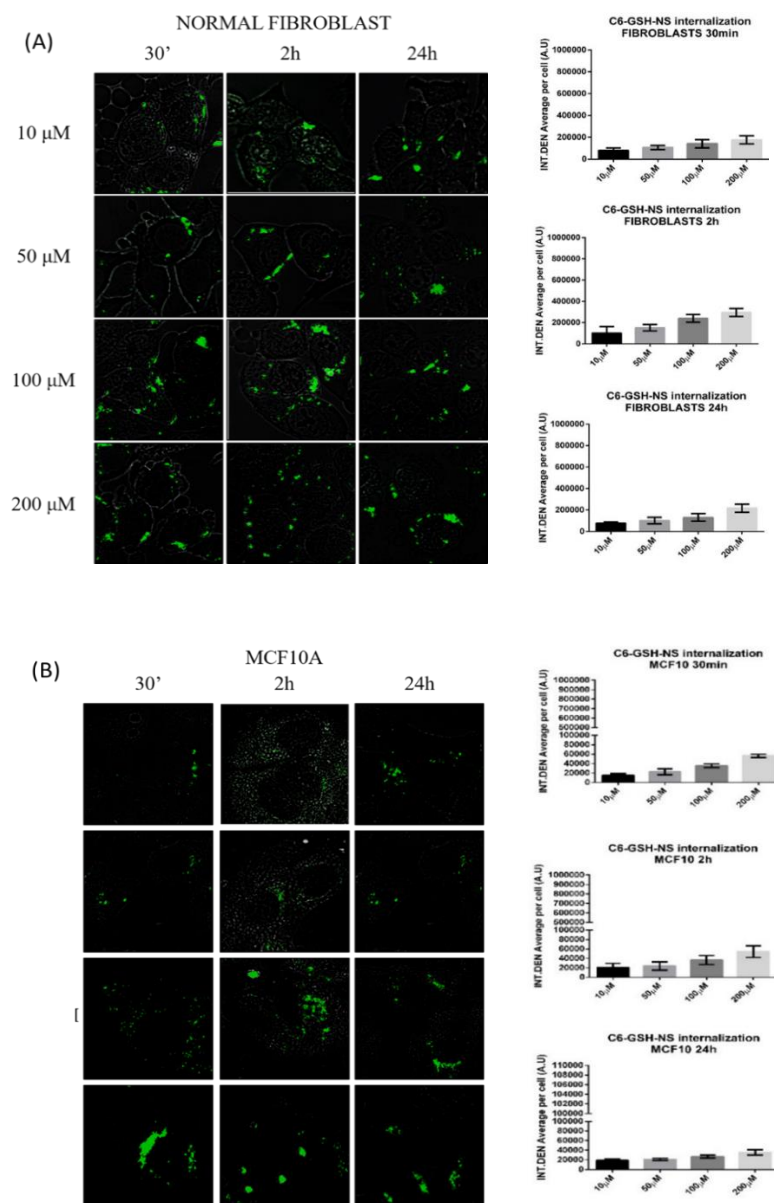
4.4.3 Biological Studies

4.4.3.1 Cell Internalization, Cell Viability and Necrosis Study

The data show that there is a difference between internalization in tumor cells compared to healthy cells. Cell internalization studies confirmed that fluorescent NSs were localized around the nucleus to

Results and Discussion

a greater extent confirming the internalization of the nanocarrier (figure 4.48).



Results and Discussion

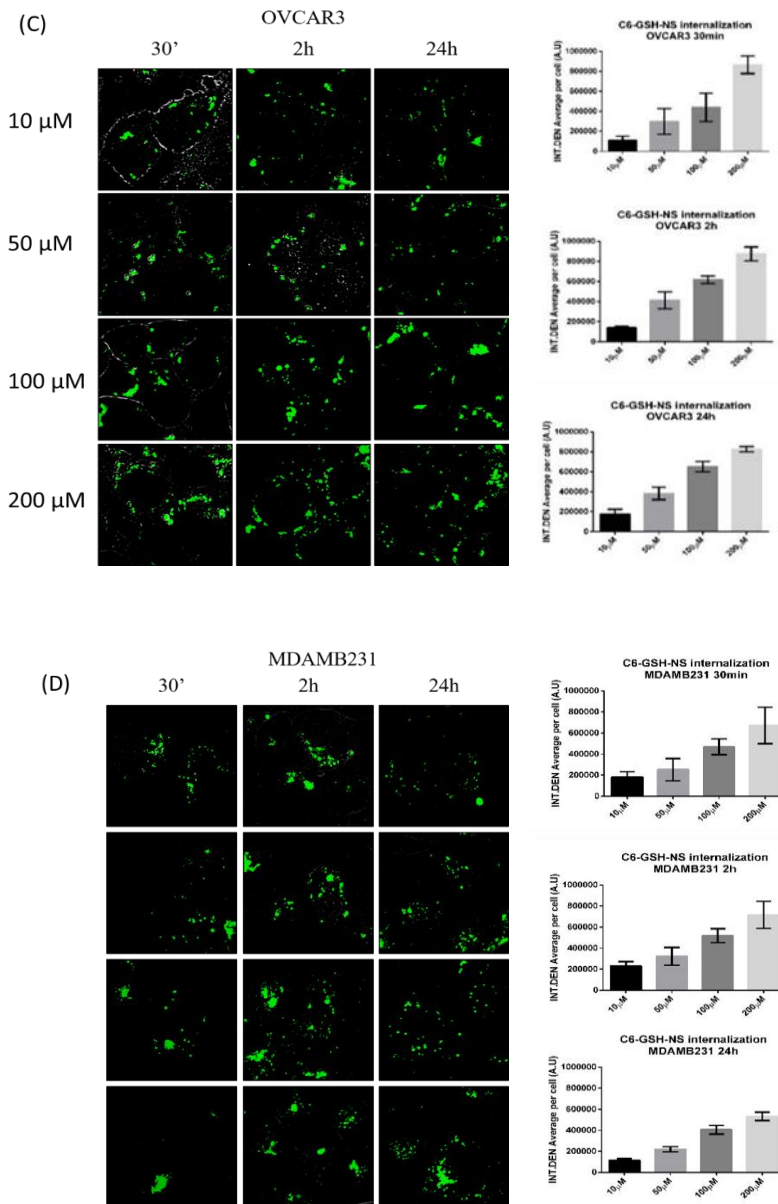


Figure 4. 48 Internalization of C-6 loaded GSHNSs in (A) Normal fibroblast cells, (B) MCF 10A cells (C) OVCAR3 cells, and (D) MDAMB231 cell lines.

Results and Discussion

Our data show that OVCAR3 cells record the highest internalization rate at each time point considered, followed by MDAMB231 cells. Indeed, from the comparison it can be observed that the ability of MDAMB231 cells to uptake NSs is about 25% less than OVCAR3 cells.

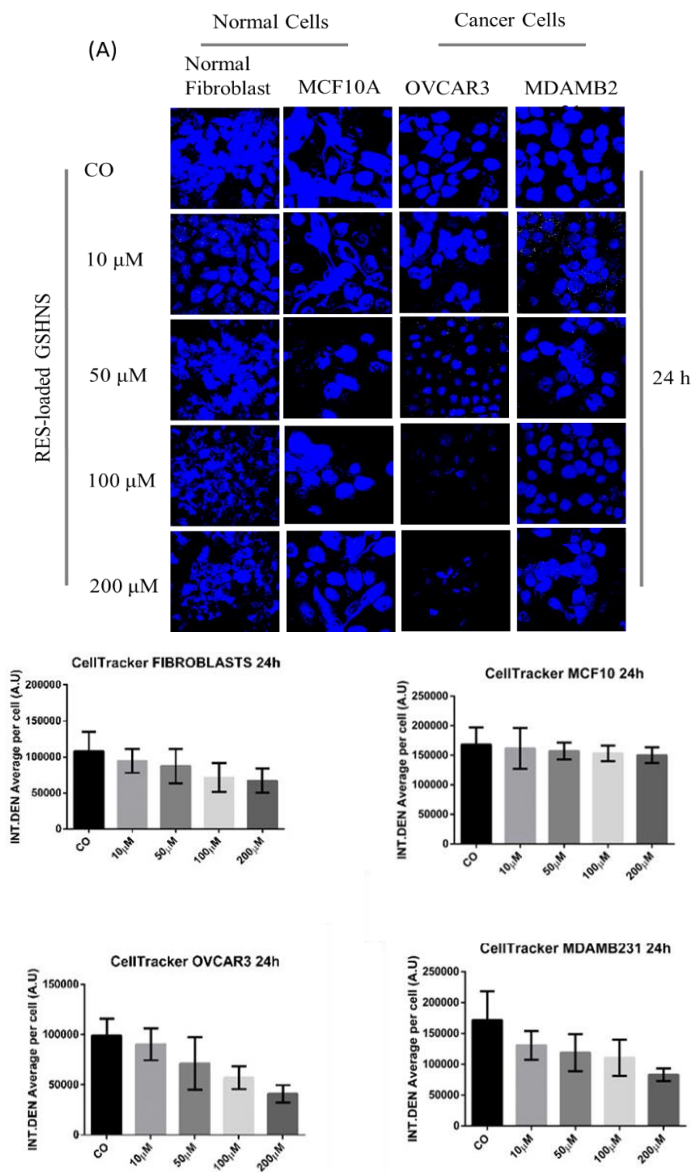
On the other hand, we found that fibroblasts internalize coumarin-6-GSHNSs about 4 times less than OVCAR3 cells and 3 times less than MDAMB231 cells. Likewise, MCF10A cells show about 10 times less uptake efficiency compared to their tumorigenic counterpart.

Our data indicate that RES-loaded GSH-NSs promote a great decrease in cell viability in the tumor cell lines compared to the healthy ones as shown by the decrease of fluorescence, that was dose and time-dependent.

Normal fibroblast cells and MCF10A were treated with RES-GSHNSs labeled with LysoTracker were taken by an endocytic pathway which was redistributed in the cytoplasm suggested that even at higher concentrations RES-GSHNSs were nontoxic to the normal cells up to 48 hours, confirming that the delivery occurs in a specific manner and GSHNSs were not toxic (figure 4.49).

These observations agree with the limited internalization rates of GSH-NSs previously observed in these cells.

Results and Discussion



Results and Discussion

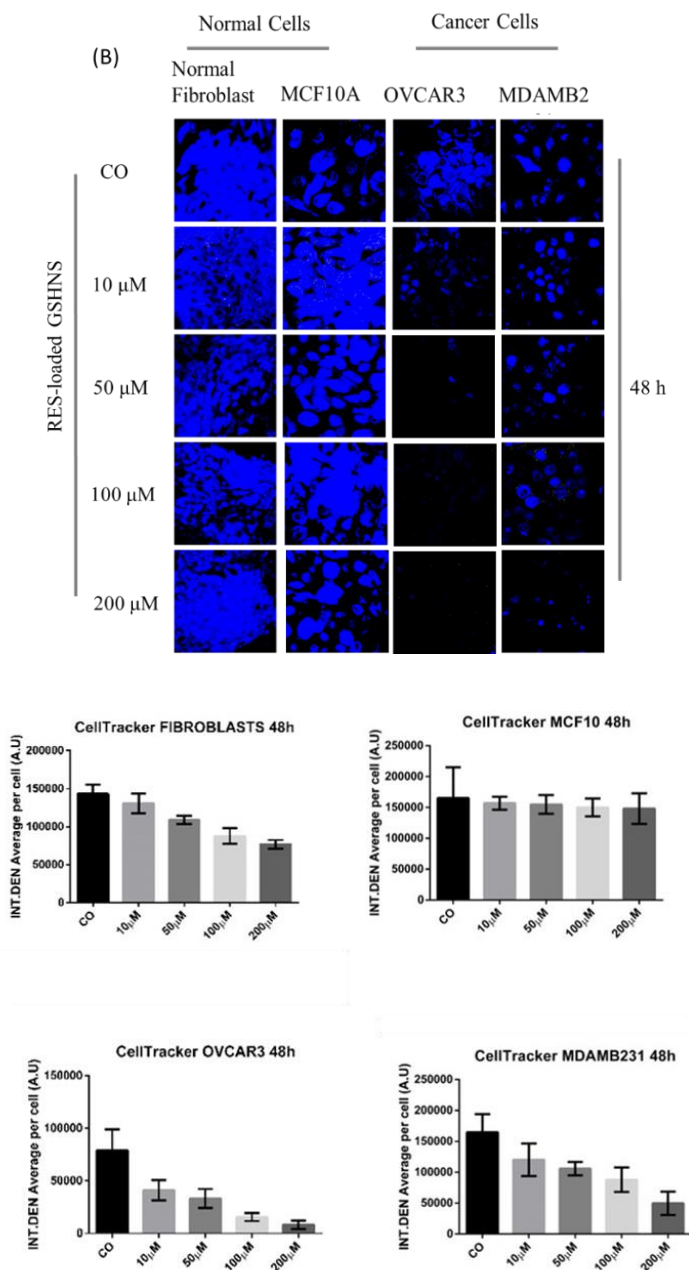


Figure 4. 49 Cell viability of different cell lines at increasing concentration of the RES loaded GSHNSs after 24 hours (A), and 48 hours (B).

Results and Discussion

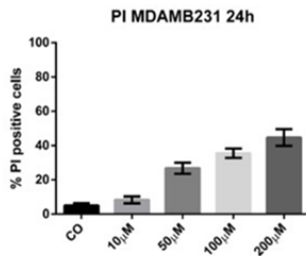
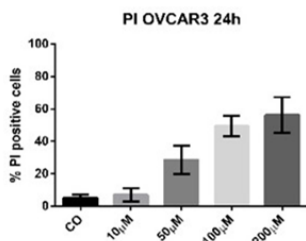
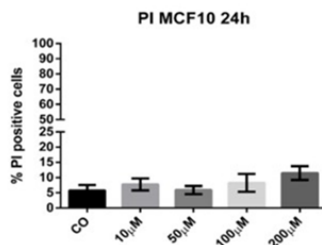
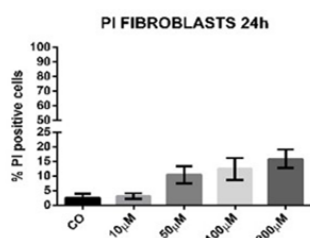
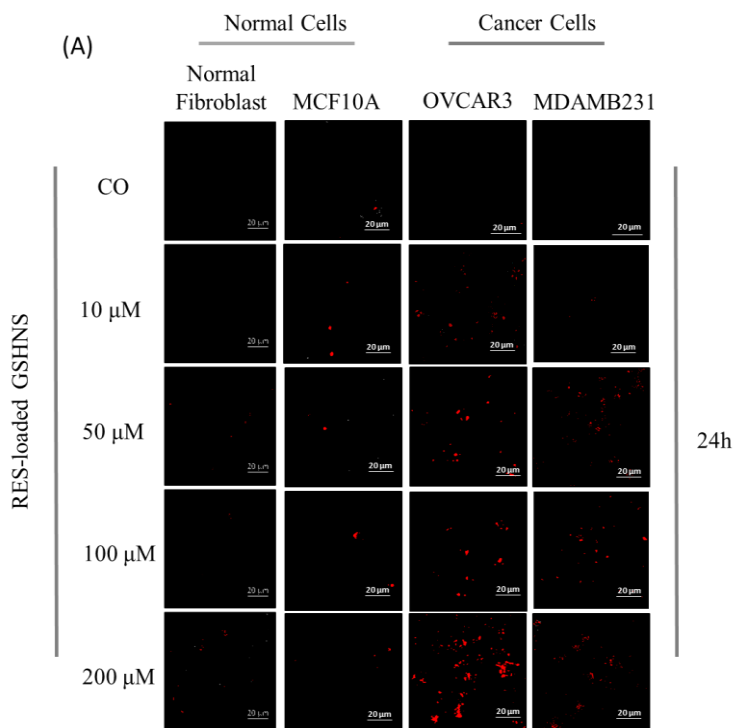
By contrast, in OVCAR3 and MDAMB231 cells we found a dose- and time-dependent reduction in cell viability, as shown by the decrease of fluorescence intensity. However, this trend was higher in OVCAR3 compared to MDAMB231 cells, accordingly to the uptake capability described above.

Another confirmation of selective targeting and increased toxicity of RES-loaded NS toward cancer cells has been given by propidium iodide staining. Figure 4.50 depicts fluorescence intensity and percentage of PI positive cells.

In this case, the increase of propidium iodide (PI) positive cells (red fluorescent signal) indicates the promotion of cellular necrosis. The data show a dose and time-dependent increase of necrotic mortality in cancer cells. By contrast, healthy cells do not exhibit necrosis, suggesting that the differential uptake observed before reflects in a differential toxic effect.

These studies confirmed that GSH responsive nanocarrier delivers the drug in a specific manner in the response to intracellular GSH of cancer cells without affecting the normal cells.

Results and Discussion



Results and Discussion

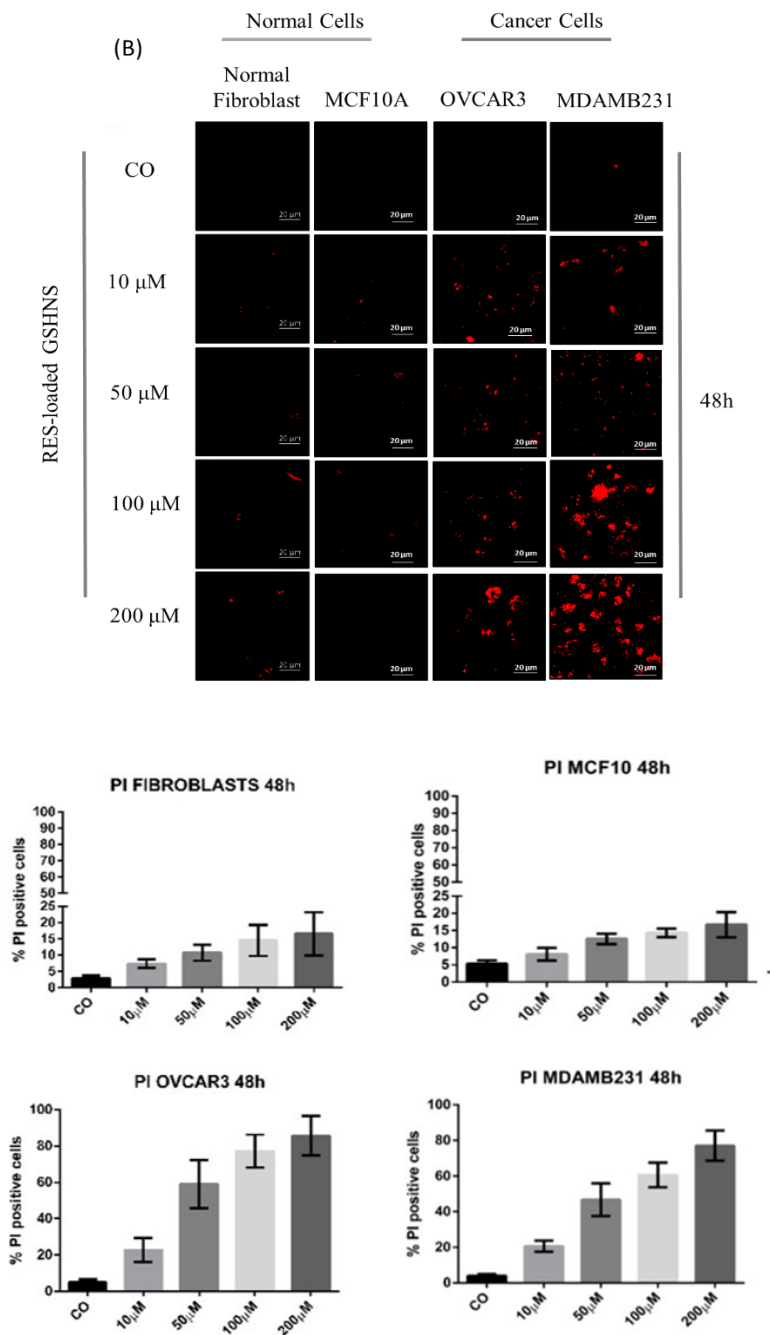


Figure 4. 50 Determination of the necrotic cells after treatment with RES loaded GSHNSs at 24 hours (A), and 48 hours (B).

Results and Discussion

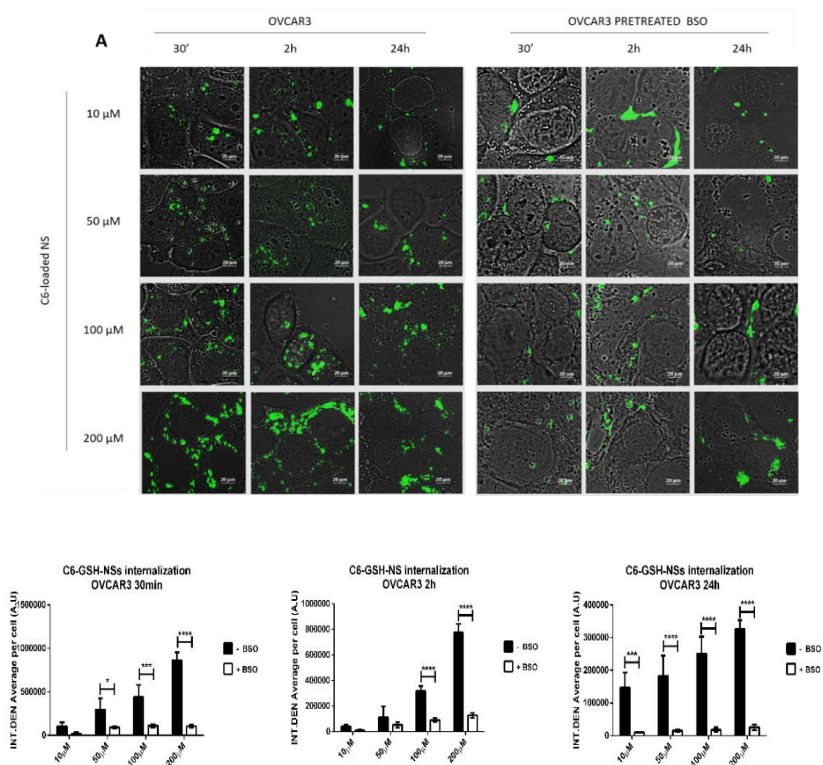
4.4.3.2 Effect of GSH depletion on Cell Internalization, Cell Viability and Necrosis Study

To prove that the targeting promoted by GSH-NS was guided by the intracellular concentration of GSH, we proceeded to treat the cancer cells with buthionine sulphoximine (BSO), an inhibitor of gamma-glutamylcysteine synthetase (GSH synthesis inhibitor) and comparing the internalization rates and the effects on the viability and toxicity of the NSs between the treated and untreated cells.

We chose to carry out such studies on the cell models that recorded the highest internalization rates: OVCAR3 and MDAMB231 cells. We found that both the cancer cells pretreated with BSO exhibited a significant decrease in the internalization profiles at each time point and concentration considered, indicating that GSH is crucial to guide the targeting of the NSs (figure 4.51).

Moreover, it is possible to appreciate that when adding BSO, there is no substantial differences in terms of internalization rate between the various concentrations tested in each time point for both cell models used, suggesting that GSH depletion strongly hampers the capability of cancer cells to uptake GSH-NSs.

Results and Discussion



Results and Discussion

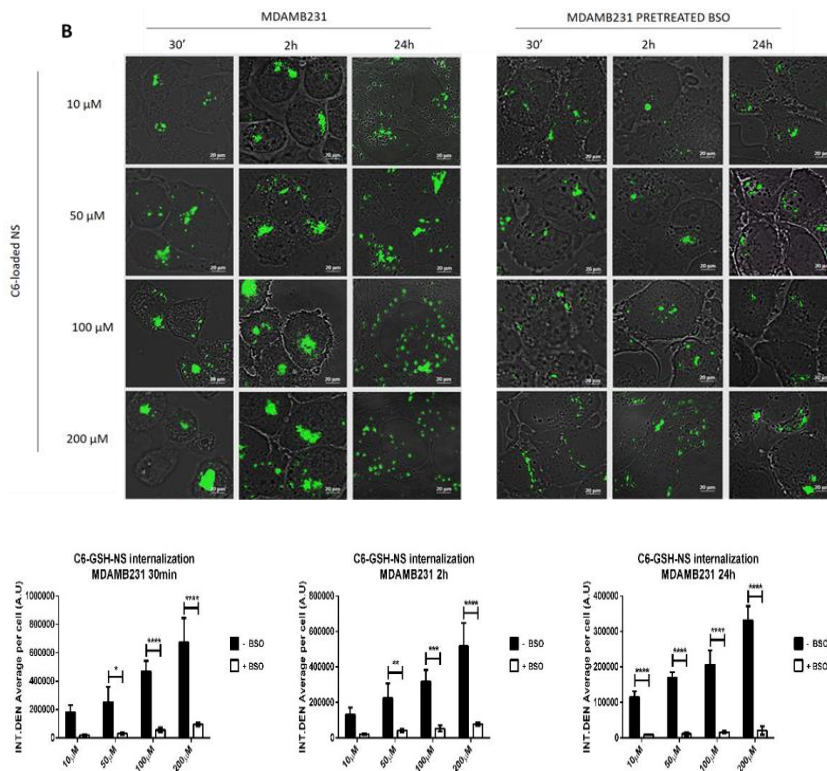
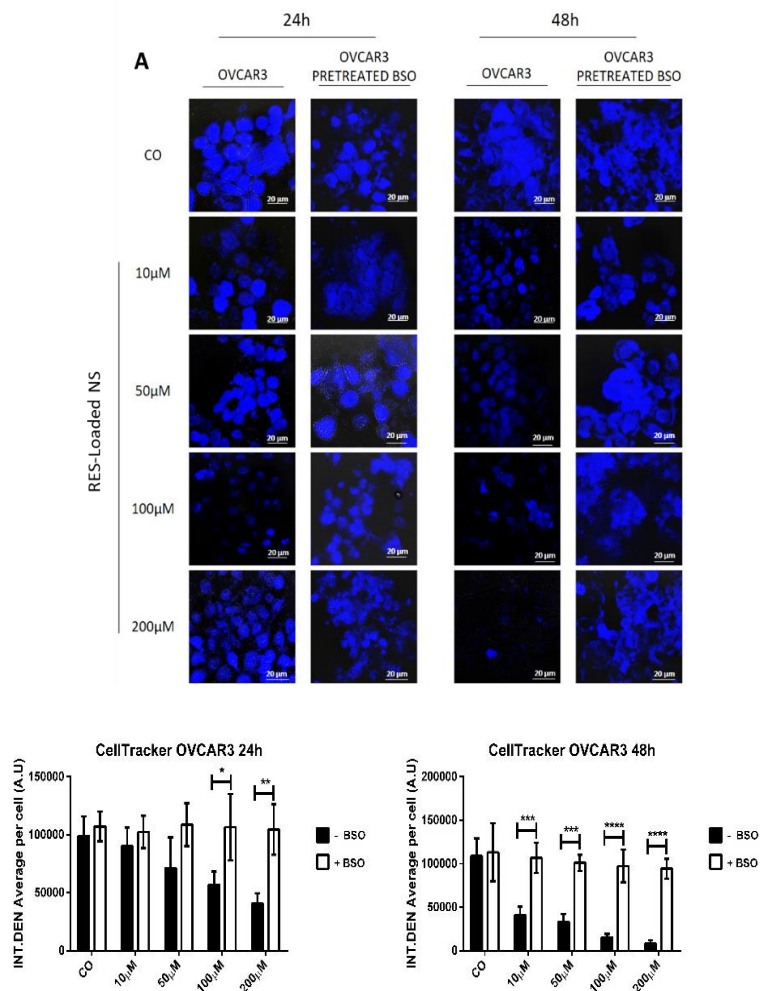


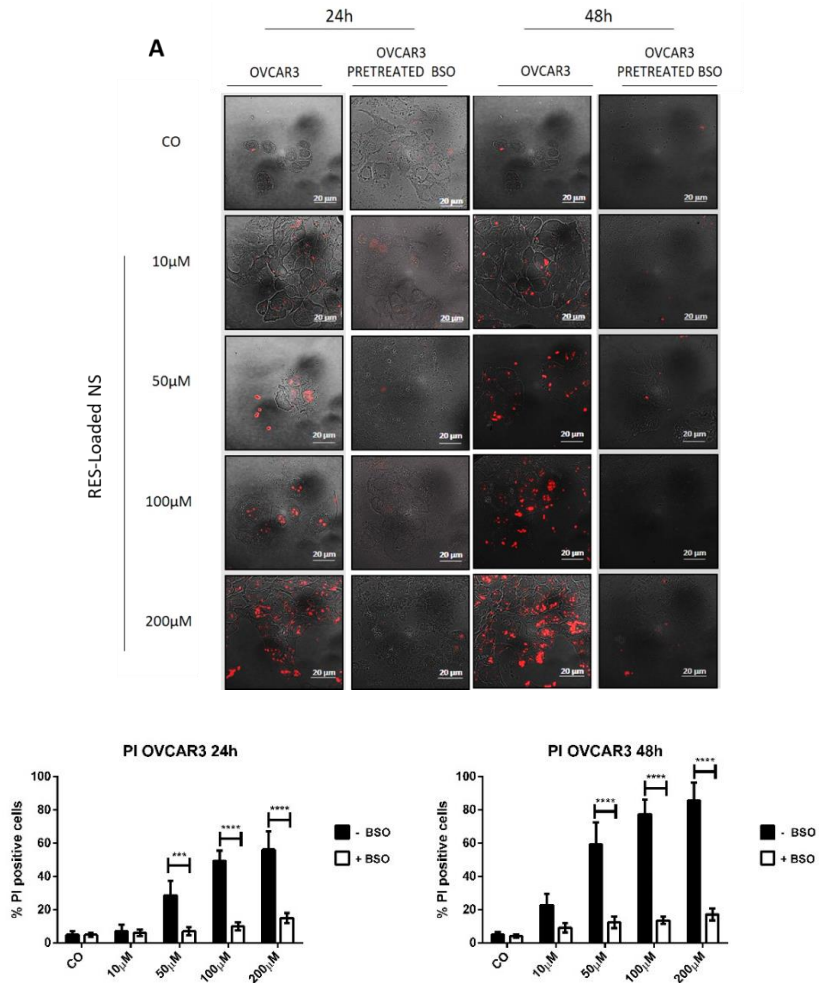
Figure 4.51 Comparison between internalization rate in (A) OVCAR3 and (B) MDAMB231 cancer cells exposed to C-6-GSH-NSs with/without BSO pre-treatment. **** $p < 0.0001$; *** $p < 0.001$; ** $p < 0.01$; * $p < 0.05$.

Finally, we aimed to demonstrate that our drug delivery system relies on GSH to release RES and promote the anti-cancer effects observed which was evaluated by cell tracker blue and iodide propidium staining.

Results and Discussion



Results and Discussion



In line with these findings, we observed a significant reduction of PI-positive cells in cells exposed to BSO compared to the untreated ones (Figure 4.53).

Results and Discussion

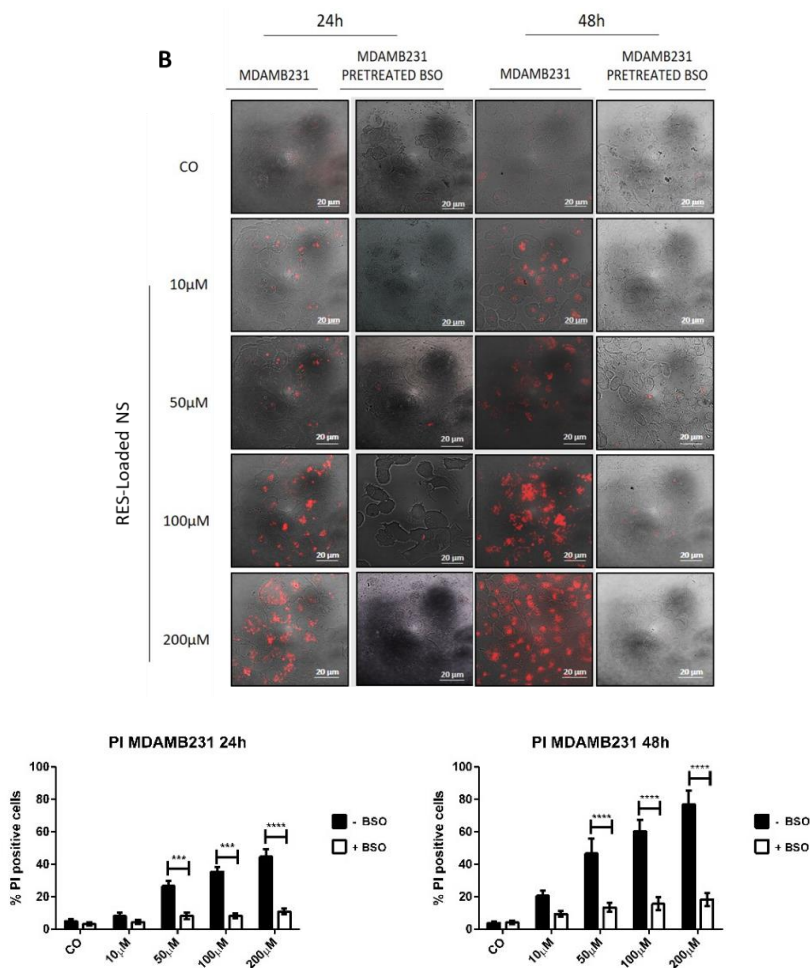


Figure 4. 53 Comparison of necrotic cell mortality in (A) OVCAR3 and (B) MDAMB231 cells exposed to RES-GSH-NSs for 24h and 48h with/without BSO pre-treatment. **** $p < 0.0001$; *** $p < 0.001$.

Taken together, our data clearly demonstrate that GSH depletion by BSO prevents NSs uptake and consequently resulted in a marked reduction (on average by at least 3 folds) in RES-mediated toxic effects in both cancer cell models.

Results and Discussion

4.5 Biotin-modified Nanosponges for Active Targeting of the Therapeutics

4.5.1 Characterization of the Biotin-modified Nanosponges

Ester-based NSs were prepared with PMDA as a crosslinker and biotin as a targeting ligand (figure 4.54). The post-synthetic modification of the PMDA-NSs was carried out by biotin with the help of EDC and DMAP.

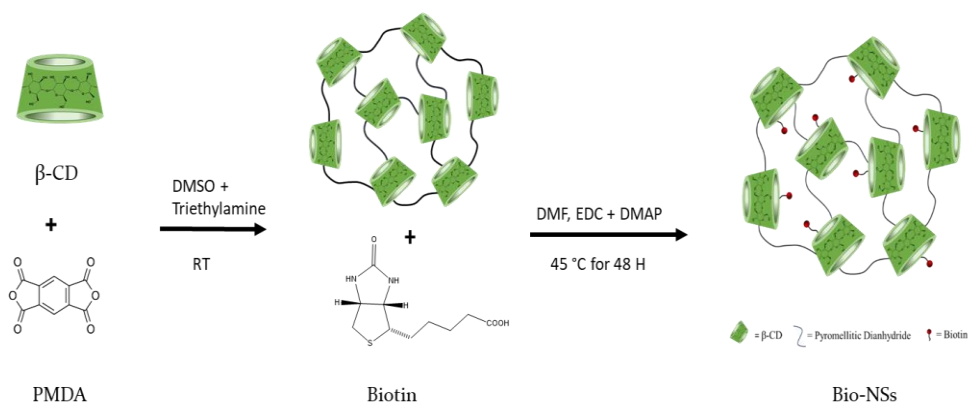


Figure 4. 54 A schematic of the biotinylated NSs.

The preliminary characterization of the biotin-functionalized nanosponges (Bio-NSs) was carried out by elemental analysis which showed the presence of sulfur content which was not available in the native NSs (table 4.7). It confirmed the presence of biotin with nanocarrier moreover, the exact amount of biotin on the surface of the NSs was confirmed by HABA-Avidin assay.

Results and Discussion

Table 4. 7 Elemental analysis of the NSs and Bio-NSs.

| Sample | % N | % C | % H | % S |
|----------------|------------|------------|------------|------------|
| NSs | 0.0 | 43.09 | 4.14 | 0.0 |
| Bio-NSs | 5.75 | 47.85 | 5.69 | 0.69 |

HABA/avidin binding assay is a spectrophotometric method for the determination of the biotin levels. HABA/Avidin complex shows an ultraviolet absorption maximum (λ_{\max}) at 500 nm. Moreover, the addition of biotin into the HABA/avidin complex leads to the displacement of HABA owing to the higher binding affinity of avidin with biotin. Figure 4.55 shows the UV-Vis spectra of HABA/avidin complex before and after the addition of biotinylated NSs. After the addition of the biotinylated NSs, the original reddish-pink HABA/avidin complex was destroyed and the yellowish complex was formed. As clearly seen in the figure, UV-Vis absorbance of HABA-Avidin complex was decreased significantly confirming the presence of biotin on the surface of the NSs. The concentration of biotin calculated on the surface of the NSs was 95 nmol/mL by HABA/avidin assay.

HABA/Avidin assay confirmed the presence of the biotin on the surface of the NSs which can be utilized for active targeting.

Results and Discussion

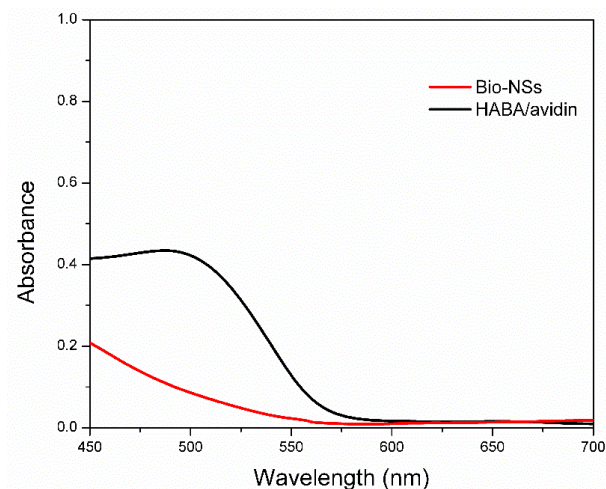


Figure 4. 55 UV-Vis absorbance of the HABA/avidin complex and Bio-NSs.

The solubilization of CUR alone and in the presence of β -CD or Bio-NSs is shown in figure 4.56. The aqueous solubility of CUR was 1 $\mu\text{g}/\text{mL}$ and it enhanced to ten-fold with β -CD.

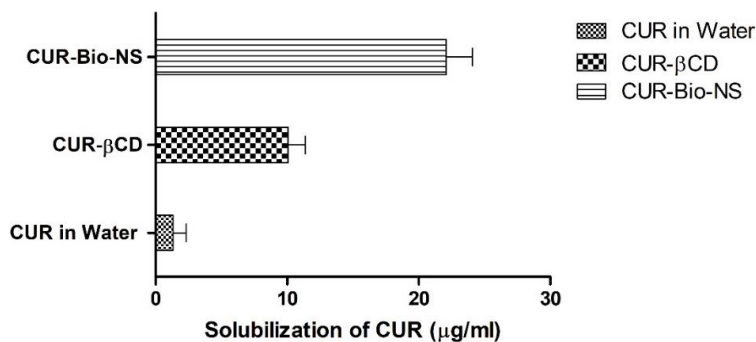


Figure 4. 56 Solubilization of the CUR alone, with β -CD, and Bio-NSs.

Moreover, Bio-NSs showed more than twenty-fold enhancement in the aqueous solubility of the CUR. The enhancement in the aqueous

Results and Discussion

solubility of CUR could be attributed to the encapsulation in the CD cavities and interstitial spaces of the Bio-NSs.

The FTIR spectrum of biotin functionalized NS showed a slight shift in the carbonyl peak from 1716 cm^{-1} to a higher value of 1724 cm^{-1} due to the formation of ester. Moreover, the emergence of two new peaks at 1648 cm^{-1} and 1532 cm^{-1} respectively, corresponds to amide-I and amide-II stretching vibration because of the presence of biotin functionalized on the NSs. The presence of these peaks confirmed the formation of biotin-functionalized NSs (figure 4.57).

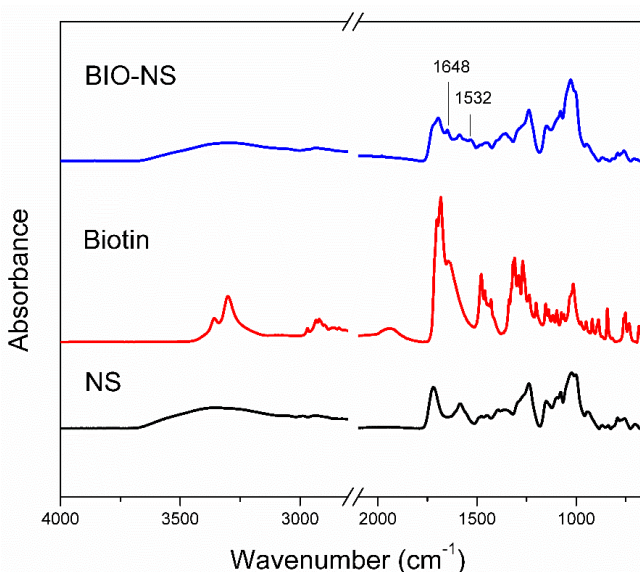


Figure 4. 57 FTIR spectra of biotinylated NSs.

The FTIR spectrum of CUR was characterized by the presence of peaks at 3510 cm^{-1} (Phenolic O-H stretching), 1615 cm^{-1} (Benzene ring vibrations), 1510 cm^{-1} (C=O stretching vibrations), 1250 cm^{-1} (C-O stretching) and 1030 cm^{-1} (C-O-C stretching). The FTIR of CUR and Bio-NS physical mixture (PM) showed an addition of the all the

Results and Discussion

peaks of the individual components. Moreover, CUR loaded Bio-NS showed significant shift in the phenolic O-H stretching vibration and carbonyl peak of the curcumin. However, other related peaks of CUR were masked which suggest successful inclusion of CUR within the NSs (figure 4.58).

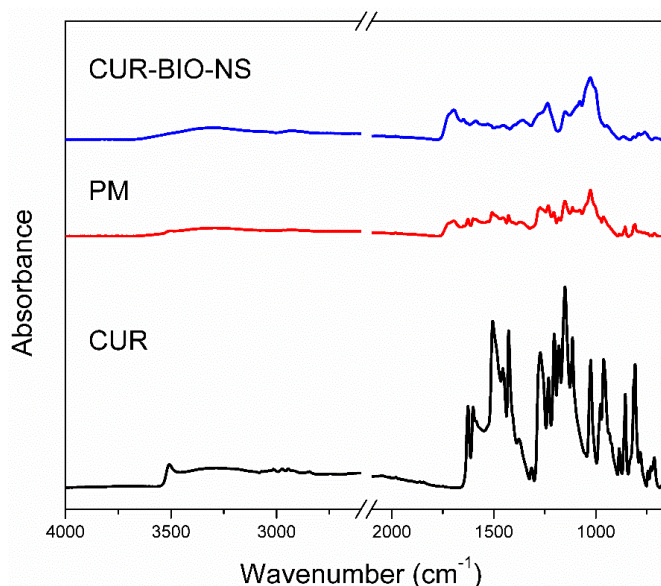


Figure 4. 58 FTIR spectra of CUR, PM and CUR-Bio-NS.

DSC thermograms of NS, biotin, and Bio-NS are shown in the figure 4.59. DSC thermograms of NS suggested the stability over a temperature range of 30 to 250 °C without any melting transition. Moreover, Biotin showed prominent melting transition at 232.13 °C. The biotin melting transition was masked in case of biotin-functionalized NS as no significant melting was observed.

Results and Discussion

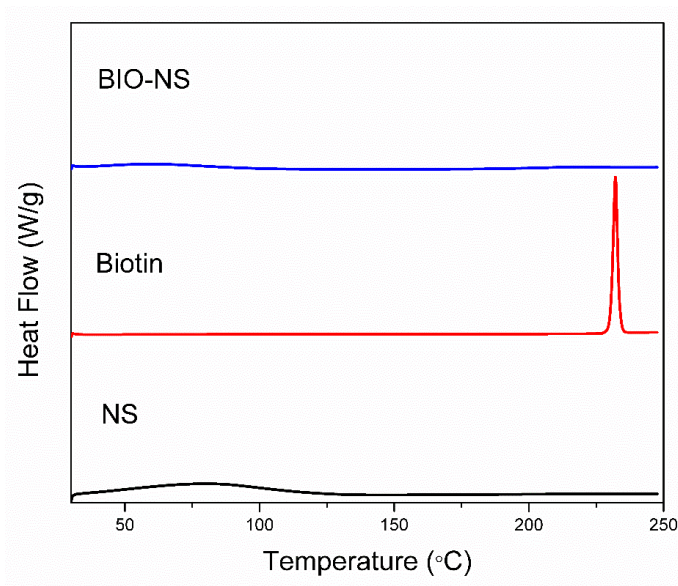


Figure 4. 59 DSC thermograms of biotinylated NSs.

The DSC thermogram of CUR showed a characteristic melting peak at 174.07 °C. Moreover, a physical mixture of CUR with Bio-NS also showed the melting peak which is related to the CUR confirmed the presence of non-inclusion complex. However, CUR loaded Bio-NSs do not show the characteristic melting peak of CUR. The absence of melting peaks of CUR could be attributed to the possible inclusion complex formation which leads to change in the physicochemical property of the CUR (figure 4.60).

It could be concluded that CUR was molecularly dispersed within the BIO-NSs thus it was easily distinguished from the non-inclusion complex (physical mixture).

Results and Discussion

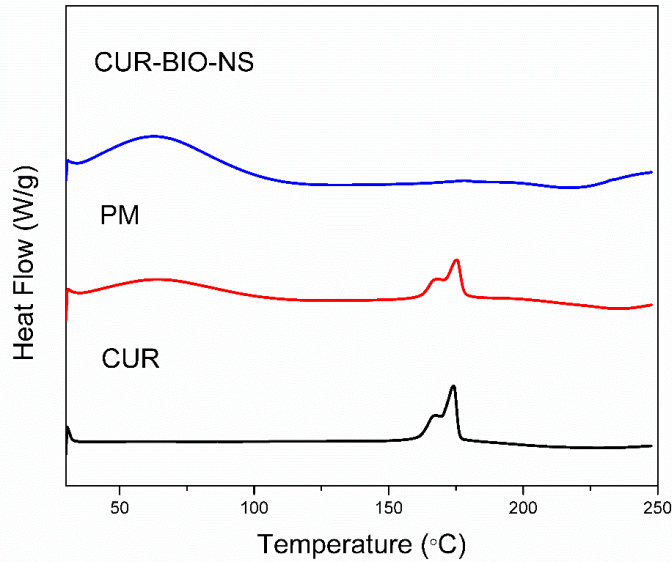


Figure 4. 60 DSC thermograms of CUR, PM and CUR-Bio-NS.

4.5.2 Release Profile of Curcumin from Bio-NSs.

The in-vitro release profile of CUR alone and CUR-Bio-NS was studied in phosphate buffer pH 7.4 as shown in figure 4.61.

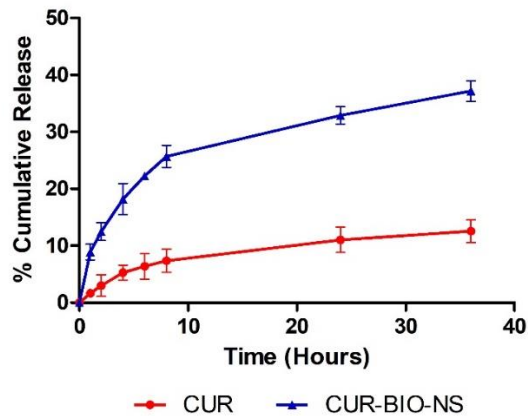


Figure 4. 61 Release profile of the CUR and CUR-Bio-NS.

Results and Discussion

CUR alone showed very low release and only 11 % of CUR was released after 24 hours. Indeed, the low solubility of the CUR alone is responsible for this behavior. However, CUR-Bio-NS showed more than three-fold higher drug release in the same time period. The higher CUR release could be attributed to the enhanced solubilization of the CUR within the NSs that led to the higher drug release.

Chapter 5

Conclusion

Conclusions

Conclusions

5. Conclusion

In the first project, we demonstrated the synthesis of KYNA loaded NSs and it was observed that high solubilization and drug loading of KYNA was achieved with β -CDNS2. The higher solubilization of KYNA was obtained because of the encapsulation of KYNA in the cyclodextrin cavities and porous matrix of NS. The KYNA loaded NS was characterized by FTIR, DSC, and PXRD which confirmed the formation of an inclusion complex of KYNA with NSs. The antioxidant potential of KYNA and KYNA loaded NSs was studied which further confirmed that KYNA loaded NSs show better antioxidant activity compared to free KYNA which can be attributed to the change in the physicochemical property and higher solubilization of KYNA with NSs. The cytotoxicity of KYNA and KYNA loaded NS was also evaluated on SHSY-5Y cell lines which demonstrated that KYNA alone and in the presence of NS does not produce any significant toxic effect. Moreover, nanosponges alone were found to be non-toxic. Thus, the above study demonstrated that cyclodextrin nanosponge acts as a promising carrier for the delivery of KYNA and can possibly be employed in biological systems for its antioxidant potential.

In the second project, we illustrated the synthesis of cyclodextrin nanosponges and the encapsulation of RES and OXY within the NSs was demonstrated. The inclusion complex formation between RES or OXY with NSs leads to higher solubilization compared to drugs used alone. The effect of different weight ratios of drug to nanosponges on drug loading was studied which confirmed that OXY and RES showed higher drug loading in 1:4 w/w ratio of drug to

Conclusions

nanosponge. The inclusion complex formation of RES and OXY was confirmed by FTIR, DSC, and PXRD. The drug release profile of RES and OXY suggested the capability of nanosponge to solubilize drug molecules and extended their drug release in a controlled manner. It was clearly evident that NSs protect both RES and OXY from the outer environment to prevent their degradation under UV light. Antioxidant activity of RES and OXY was further enhanced in the presence of NSs. Higher cytotoxicity was observed for both RES-NS and OXY-NS against DU-145 prostate cancer cells, induced by the change in the physicochemical property of OXY and RES. Moreover, nanosponges alone were biocompatible without any significant cytotoxicity. The above findings clearly suggest that nanosponges can be employed as a delivery vehicle for a variety of drug molecules to improve their solubilization, stability and to control their drug release profile.

In the third project, we studied and applied a new methodology to calculate, for the first time, the apparent inclusion complex constant (K_{Fapp}) between OXY and CD-NSs using UV-Vis measurement and the Benesi-Hildebrand method with modifications. The K_{Fapp} of OXY, with different CD-NSs, was evaluated showing that the K_{Fapp} is dependent on the type of cyclodextrin, bridges, and type of linker. The complex OXY/ β -CD-CDI 1:4 was studied in vitro with DSC, TGA and FTIR and its encapsulation efficiency and release behavior were also studied. An in-vitro digestion showed the capacity of CD-NS to protect OXY. Finally, in an anticancer study against colon (HT-29 and HCT-116) cell lines, the greater inhibition of cell viability was demonstrated. The findings as a whole represent the ability of the

Conclusions

complexation of drugs in CD-NSs and the use of OXY as an ingredient in nutraceutical products.

In the fourth project, we demonstrated the synthesis and characterization of RES loaded GSHNSs. It was observed that high solubilization and drug loading of RES (16.12 %) was obtained. The inclusion complex formation of RES with GSHNSs was confirmed by FTIR, DSC, and PXRD studies. In-vitro release profile suggested that higher solubilization of RES leads to high drug releases in a controlled manner. Moreover, the presence of GSH in the dissolution media further suggested that RES was released from the GSHNSs in the response to GSH. The biological studies were carried out to demonstrate the effect of RES loaded GSHNSs on different cell lines. Cell internalization studies suggested preferential uptake of C-6 to cancerous cells compared to normal cells. The cell viability studies confirmed that RES is effective against cancerous cells without affecting the viability of the normal cell lines. Moreover, the staining of cells with propidium iodide confirmed that the death of cancerous cells while no effect on the normal cells was observed. These studies supported the view that GSH responsive nanosponges can effective carriers for the delivery of RES.

In the fifth project, we developed novel biotin functionalized NSs for the delivery of the CUR. Solubilization studies confirmed that NSs provided better solubilization of CUR compared to native β -CD. The presence of biotin on the NSs was confirmed by elemental analysis. Moreover, the concentration of biotin on the NSs surface was evaluated by HABA/avidin assay. FTIR and DSC studies confirmed the inclusion complex of CUR with Bio-NSs. The release profile of

Conclusions

CUR further suggested the higher drug release compared to CUR alone due to the higher solubilizing potential of the Bio-NSs. These studies suggested that NSs can be functionalized with targeting moieties and can be used to deliver drugs for the desired applications.

References

References

References

References

1. Taniguchi, N. On the basic concept of nanotechnology. In Proceedings of the Proceedings of international conference on precision engineering (ICPE); Tokyo, Japan, 1974; pp. 18–23.
2. Vyas, S.P.; Khar, R.K. Targeted and Controlled Drug Delivery: Novel Carrier Systems. In *Targeted and Controlled Drug Delivery: Novel Carrier Systems*; CBS Publication, New Delhi, 2002; p. 331 ISBN 81-239-0799-0.
3. Allen, T.M.; Cullis, P.R. Liposomal drug delivery systems: From concept to clinical applications. *Adv. Drug Deliv. Rev.* **2013**, *65*, 36–48.
4. Desai, N.; Trieu, V.; Yao, Z.; Louie, L.; Ci, S.; Yang, A.; Tao, C.; De, T.; Beals, B.; Dykes, D.; et al. Increased antitumor activity, intratumor paclitaxel concentrations, and endothelial cell transport of cremophor-free, albumin-bound paclitaxel, ABI-007, compared with cremophor-based paclitaxel. *Clin. Cancer Res.* **2006**, *12*, 1317–1324.
5. Girek, T.; Ciesielski, W. Polymerization of β -cyclodextrin with maleic anhydride along with thermogravimetric study of polymers. *J. Incl. Phenom. Macrocycl. Chem.* **2011**, *69*, 445–451.
6. Harada, A.; Hashidzume, A.; Miyauchi, M. Polymers Involving Cyclodextrin Moieties. In *Cyclodextrins and Their Complexes*; John Wiley & Sons, Ltd, 2006; pp. 65–92 ISBN 9783527608980.
7. Jansook, P.; Ogawa, N.; Loftsson, T. Cyclodextrins: structure, physicochemical properties and pharmaceutical applications. *Int. J. Pharm.* **2018**, *535*, 272–284.
8. Muankaew, C.; Loftsson, T. Cyclodextrin-Based Formulations: A Non-Invasive Platform for Targeted Drug Delivery. *Basic Clin. Pharmacol. Toxicol.* **2018**, *122*, 46–55.
9. Loftsson, T.; Brewster, M.E. Pharmaceutical Applications of Cyclodextrins. 1. Drug Solubilization and Stabilization. *J. Pharm. Sci.* **1996**, *85*, 1017–1025.
10. Szejtli, J. Introduction and General Overview of Cyclodextrin

References

- Chemistry. *Chem. Rev.* **1998**, *98*, 1743–1754.
11. Stella, V.J.; Rao, V.M.; Zannou, E.A.; Zia, V. Mechanisms of drug release from cyclodextrin complexes. *Adv. Drug Deliv. Rev.* **1999**, *36*, 3–16.
 12. Saokham, P.; Muankaew, C.; Jansook, P.; Loftsson, T. Solubility of Cyclodextrins and Drug/Cyclodextrin Complexes. *Molecules* **2018**, *23*, 1161.
 13. Kurkov, S. V; Madden, D.E.; Carr, D.; Loftsson, T. The Effect of Parenterally Administered Cyclodextrins on the Pharmacokinetics of Coadministered Drugs. *J. Pharm. Sci.* **2012**, *101*, 4402–4408.
 14. Loftsson, T.; Moya-Ortega, M.D.; Alvarez-Lorenzo, C.; Concheiro, A. Pharmacokinetics of cyclodextrins and drugs after oral and parenteral administration of drug/cyclodextrin complexes. *J. Pharm. Pharmacol.* **2016**, *68*, 544–555.
 15. Brewster, M.E.; Loftsson, T. Cyclodextrins as pharmaceutical solubilizers. *Adv. Drug Deliv. Rev.* **2007**, *59*, 645–666.
 16. Conceição, J.; Adeoye, O.; Cabral-Marques, H.M.; Lobo, J.M.S. Cyclodextrins as excipients in tablet formulations. *Drug Discov. Today* **2018**, *23*, 1274–1284.
 17. Hincal, A.A.; Eroğlu, H.; Bilensoy, E. Regulatory Status of Cyclodextrins in Pharmaceutical Products. In *Cyclodextrins in Pharmaceuticals, Cosmetics, and Biomedicine*; John Wiley & Sons, Ltd, 2011; pp. 123–130 ISBN 9780470926819.
 18. Trotta, F.; Zanetti, M.; Cavalli, R. Cyclodextrin-based nanosponges as drug carriers. *Beilstein J. Org. Chem.* **2012**, *8*, 2091–2099.
 19. Trotta, F. Cyclodextrin Nanosponges and their Applications. In *Cyclodextrins in Pharmaceuticals, Cosmetics, and Biomedicine: Current and Future Industrial Applications*; John Wiley & Sons, Inc., 2011; pp. 323–342.
 20. Rossi, B.; Caponi, S.; Castiglione, F.; Corezzi, S.; Fontana, A.; Giarola, M.; Mariotto, G.; Mele, A.; Petrillo, C.; Trotta, F.; et al. Networking properties of cyclodextrin-based cross-linked polymers probed by inelastic light-scattering experiments. *J. Phys. Chem. B*

References

2012, *116*, 5323–5327.

21. Tejashri, G.; Amrita, B.; Darshana, J. Cyclodextrin based nanosponges for pharmaceutical use: A review. *Acta Pharm.* **2013**, *63*, 335–358.

22. Ma, M.; Li, D. Cyclodextrin polymer separation materials. 1998, Patent WO 9822197.

23. Mamba, B.B.; Krause, R.W.; Malefetse, T.J.; Gericke, G.; Sithole, S.P. Cyclodextrin nanosponges in the removal of organic matter to produce water for power generation. *Water* **2008**, *34*, 657–660.

24. Darandale, S.S.; Vavia, P.R. Cyclodextrin-based nanosponges of curcumin: formulation and physicochemical characterization. *J. Incl. Phenom. Macrocycl. Chem.* **2013**, *75*, 315–322.

25. Singh, V.; Xu, J.; Wu, L.; Liu, B.; Guo, T.; Guo, Z.; York, P.; Gref, R.; Zhang, J. Ordered and disordered cyclodextrin nanosponges with diverse physicochemical properties. *RSC Adv.* **2017**, *7*, 23759–23764.

26. Ansari, K.A.; Vavia, P.R.; Trotta, F.; Cavalli, R. Cyclodextrin-based nanosponges for delivery of resveratrol: in vitro characterisation, stability, cytotoxicity and permeation study. *AAPS PharmSciTech* **2011**, *12*, 279–286.

27. Kumar, S.; Pooja; Trotta, F.; Rao, R. Encapsulation of Babchi Oil in Cyclodextrin-Based Nanosponges: Physicochemical Characterization, Photodegradation, and In Vitro Cytotoxicity Studies. *Pharmaceutics* **2018**, *10*.

28. Wajs, E.; Caldera, F.; Trotta, F.; Fragoso, A. Peroxidase-encapsulated cyclodextrin nanosponge immunoconjugates as a signal enhancement tool in optical and electrochemical assays. *Analyst* **2014**, *139*, 375–380.

29. Ferro, M.; Castiglione, F.; Pastori, N.; Punta, C.; Melone, L.; Panzeri, W.; Rossi, B.; Trotta, F.; Mele, A. Dynamics and interactions of ibuprofen in cyclodextrin nanosponges by solid-state NMR spectroscopy. *Beilstein J. Org. Chem.* **2017**, *13*, 182–194.

References

30. Kono, H.; Nakamura, T. Polymerization of β -cyclodextrin with 1,2,3,4-butanetetracarboxylic dianhydride: Synthesis, structural characterization, and bisphenol A adsorption capacity. *React. Funct. Polym.* **2013**, *73*, 1096–1102.
31. Bednarz, S.; Lukasiewicz, M.; Mazela, W.; Pajda, M.; Kasprzyk, W. Chemical structure of poly(β -cyclodextrin-co-citric acid). *J. Appl. Polym. Sci.* **2011**, *119*, 3511–3520.
32. Castiglione, F.; Crupi, V.; Majolino, D.; Mele, A.; Rossi, B.; Trotta, F.; Venuti, V. Effect of Cross-Linking Properties on the Vibrational Dynamics of Cyclodextrins-Based Polymers: An Experimental–Numerical Study. *J. Phys. Chem. B* **2012**, *116*, 7952–7958.
33. Gidwani, B.; Vyas, A. Biointerfaces Synthesis , characterization and application of Epichlorohydrin- β -cyclodextrin polymer. *Colloids Surfaces B Biointerfaces* **2014**, *114*, 130–137.
34. Alvarez-Lorenzo, C.; RODRÍGUEZ-TENREIRO SÁNCHEZ, C.; TORRES LABANDEIRA, J.J.; CONCHEIRO NINE, A. Method of obtaining hydrogels of cyclodextrins with glycidyl ethers, compositions thus obtained and applications thereof. 2008, Patent EP1873167 A2.
35. Fenyvesi, É. Cyclodextrin polymers in the pharmaceutical industry. *J. Incl. Phenom.* **1988**, *6*, 537–545.
36. Machín, R.; Isasi, J.R.; Vélaz, I. β -Cyclodextrin hydrogels as potential drug delivery systems. *Carbohydr. Polym.* **2012**, *87*, 2024–2030.
37. SHAW, P.E.; WILSON, C.W. Debitting Citrus Juices with β -Cyclodextrin Polymer. *J. Food Sci.* **1983**, *48*, 646–647.
38. Hicks, K.B.; Haines, R.M.; Tong, C.B.S.; Sapers, G.M.; El-Atawy, Y.; Irwin, P.L.; Seib, P.A. Inhibition of Enzymatic Browning in Fresh Fruit and Vegetable Juices by Soluble and Insoluble Forms of β -Cyclodextrin Alone or in Combination with Phosphates. *J. Agric. Food Chem.* **1996**, *44*, 2591–2594.
39. Ferruti, P.; Manzoni, S.; Richardson, S.C.W.; Duncan, R.; Patrick, N.G.; Mendichi, R.; Casolaro, M. Amphoteric Linear Poly(amido-amine)s as Endosomolytic Polymers: Correlation

References

between Physicochemical and Biological Properties. *Macromolecules* **2000**, *33*, 7793–7800.

40. Swaminathan, S.; Cavalli, R.; Trotta, F.; Ferruti, P.; Ranucci, E.; Gerges, I.; Manfredi, A.; Marinotto, D.; Vavia, P.R. In vitro release modulation and conformational stabilization of a model protein using swellable polyamidoamine nanosponges of β -cyclodextrin. *J. Incl. Phenom. Macrocycl. Chem.* **2010**, *68*, 183–191.

41. Morales-Sanfrutos, J.; Lopez-Jaramillo, F.J.; Elremaily, M.A.A.; Hernández-Mateo, F.; Santoyo-Gonzalez, F. Divinyl Sulfone Cross-Linked Cyclodextrin-Based Polymeric Materials: Synthesis and Applications as Sorbents and Encapsulating Agents. *Molecules* **2015**, *20*, 3565–3581.

42. Malanga, M.; Bálint, M.; Puskás, I.; Tuza, K.; Sohajda, T.; Jicsinszky, L.; Szente, L.; Fenyvesi, É. Synthetic strategies for the fluorescent labeling of epichlorohydrin-branched cyclodextrin polymers. *Beilstein J. Org. Chem.* **2014**, *10*, 3007–3018.

43. Ncube, P.; Krause, R.W.M.; Mamba, B.B. Detection of chloroform in water using an azo dye-modified β -cyclodextrin – Epichlorohydrin copolymer as a fluorescent probe. *Phys. Chem. Earth, Parts A/B/C* **2014**, *67–69*, 79–85.

44. Lembo, D.; Swaminathan, S.; Donalisio, M.; Civra, A.; Pastero, L.; Aquilano, D.; Vavia, P.; Trotta, F.; Cavalli, R. Encapsulation of Acyclovir in new carboxylated cyclodextrin-based nanosponges improves the agent's antiviral efficacy. *Int. J. Pharm.* **2013**, *443*, 262–272.

45. Junthip, J.; Tabary, N.; Leclercq, L.; Martel, B. Cationic β -cyclodextrin polymer applied to a dual cyclodextrin polyelectrolyte multilayer system. *Carbohydr. Polym.* **2015**, *126*, 156–167.

46. Lo Meo, P.; Lazzara, G.; Liotta, L.; Riela, S.; Noto, R. Cyclodextrin–calixarene co-polymers as a new class of nanosponges. *Polym. Chem.* **2014**, *5*, 4499–4510.

47. Massaro, M.; Cinà, V.; Labbozzetta, M.; Lazzara, G.; Meo, P. Lo; Poma, P.; Riela, S.; Noto, R. Chemical and pharmaceutical evaluation of the relationship between triazole linkers and pore size on cyclodextrin–calixarene nanosponges used as carriers for natural

References

- drugs. *RSC Adv.* **2016**, *6*, 50858–50866.
48. Zhang, J.; Ma, P.X. Cyclodextrin-based supramolecular systems for drug delivery: Recent progress and future perspective. *Adv. Drug Deliv. Rev.* **2013**, *65*, 1215–1233.
49. Ganta, S.; Devalapally, H.; Shahiwala, A.; Amiji, M. A review of stimuli-responsive nanocarriers for drug and gene delivery. *J. Control. Release* **2008**, *126*, 187–204.
50. Trotta, F.; Caldera, F.; Dianzani, C.; Argenziano, M.; Barrera, G.; Cavalli, R. Glutathione Bioresponsive Cyclodextrin Nanosponges. *Chempluschem* **2016**, *81*, 439–443.
51. Jing, T.; Li, T.; Ruan, Z.; Yan, L. pH- and glutathione-stepwise-responsive polypeptide nanogel for smart and efficient drug delivery. *J. Mater. Sci.* **2018**, *53*, 14933–14943.
52. Russo, M.; Saladino, M.L.; Chillura Martino, D.; Lo Meo, P.; Noto, R. Polyaminocyclodextrin nanosponges: synthesis, characterization and pH-responsive sequestration abilities. *RSC Adv.* **2016**, *6*, 49941–49953.
53. Martin-Esteban, A. Molecular imprinting technology: a simple way of synthesizing biomimetic polymeric receptors. *Anal. Bioanal. Chem.* **2004**, *378*, 1875.
54. Turiel, E.; Martín-Esteban, A. Molecularly imprinted polymers for sample preparation: A review. *Anal. Chim. Acta* **2010**, *668*, 87–99.
55. Liu, J.; Wulff, G. Functional Mimicry of the Active Site of Carboxypeptidase A by a Molecular Imprinting Strategy: Cooperativity of an Amidinium and a Copper Ion in a Transition-State Imprinted Cavity Giving Rise to High Catalytic Activity. *J. Am. Chem. Soc.* **2004**, *126*, 7452–7453.
56. Deshmukh, K.; Tanwar, Y.S.; Shende, P.; Cavalli, R. Biomimetic estimation of glucose using non-molecular and molecular imprinted polymer nanosponges. *Int. J. Pharm.* **2015**, *494*, 244–248.
57. Ogoshi, T.; Harada, A. Chemical Sensors Based on Cyclodextrin Derivatives. *Sensors* **2008**, *8*, 4961–4982.

References

58. Trotta, F.; Caldera, F.; Cavalli, R.; Soster, M.; Riedo, C.; Biasizzo, M.; Barretta, G.U.; Balzano, F.; Brunella, V. Molecularly imprinted cyclodextrin nanosponges for the controlled delivery of L-DOPA: perspectives for the treatment of Parkinson's disease. *Expert Opin. Drug Deliv.* **2016**, *13*, 1671–1680.
59. Trotta, F.; Cavalli, R. Characterization and Applications of New Hyper-Cross-Linked Cyclodextrins. *Compos. Interfaces* **2009**, *16*, 39–48.
60. Momin, M.M.; Zaheer, Z.; Zainuddin, R.; Sangshetti, J.N. Extended release delivery of erlotinib glutathione nanosponge for targeting lung cancer. *Artif. Cells, Nanomedicine Biotechnol.* **2018**, *46*, 1064–1075.
61. Trotta, F.; Cavalli, R.; Tumiatti, W.; Zerbinati, O.; Roggero, C.; Vallero, R. Ultrasound-Assisted Synthesis of Cyclodextrin-Based Nanosponges. 2008, Patent US 2008/0213384 A1.
62. Anandam, S.; Selvamuthukumar, S. Optimization of microwave-assisted synthesis of cyclodextrin nanosponges using response surface methodology. *J. Porous Mater.* **2014**, *21*, 1015–1023.
63. Renard, E.; Deratani, A.; Volet, G.; Sebillé, B. Preparation and Characterization of Water Soluble High Molecular Weight β -Cyclodextrin-Epichlorohydrin Polymers. *Eur. Polym. J.* **1997**, *33*, 49–57.
64. Bastiancich, Chiara Scutera, S.; Alotto, Daniela Cambieri, Irene Fumagalli, Mara Casarin, S.; Rossi, S.; Trotta, Francesco Stella, M.; Cavalli, Roberta Musso, Tiziana Castagnoli, C. Cyclodextrin-Based Nanosponges as a Nanotechnology Strategy for Imiquimod Delivery in Pathological Scarring Prevention and Treatment. *J. Nanopharmaceutics Drug Deliv.* **2014**, *2*, 311–324.
65. Peila, R.; Scordino, P.; Shanko, D.B.; Caldera, F.; Trotta, F.; Ferri, A. Synthesis and characterization of β -cyclodextrin nanosponges for N,N-diethyl-meta-toluamide complexation and their application on polyester fabrics. *React. Funct. Polym.* **2017**, *119*, 87–94.
66. Shringirishi, M.; Prajapati, S.K.; Mahor, A.; Alok, S.; Yadav, P.; Verma, A. Nanosponges: a potential nanocarrier for novel drug

References

- delivery-a review. *Asian Pacific J. Trop. Dis.* **2014**, *4*, S519–S526.
67. Blanchard, J.; Proniuk, S. Some important considerations in the use of cyclodextrins. *Pharm. Res.* **1999**, *16*, 1796–1798.
68. Shende, P.; Kulkarni, Y.A.; Gaud, R.S.; Deshmukh, K.; Cavalli, R.; Trotta, F.; Caldera, F. Acute and repeated dose toxicity studies of different β -cyclodextrin-based nanosponge formulations. *J. Pharm. Sci.* **2015**, *104*, 1856–1863.
69. Shende, P.K.; Gaud, R.S.; Bakal, R.; Patil, D. Effect of inclusion complexation of meloxicam with β -cyclodextrin- and β -cyclodextrin-based nanosponges on solubility, in vitro release and stability studies. *Colloids Surfaces B Biointerfaces* **2015**, *136*, 105–110.
70. Shringirishi, M.; Mahor, A.; Gupta, R.; Prajapati, S.K.; Bansal, K.; Kesharwani, P. Fabrication and characterization of nifedipine loaded β -cyclodextrin nanosponges: An in vitro and in vivo evaluation. *J. Drug Deliv. Sci. Technol.* **2017**, *41*, 344–350.
71. Zainuddin, R.; Zaheer, Z.; Sangshetti, J.N.; Momin, M. Enhancement of oral bioavailability of anti-HIV drug rilpivirine HCl through nanosponge formulation. *Drug Dev. Ind. Pharm.* **2017**, *43*, 2076–2084.
72. Shende, P.; Deshmukh, K.; Trotta, F.; Caldera, F. Novel cyclodextrin nanosponges for delivery of calcium in hyperphosphatemia. *Int. J. Pharm.* **2013**, *456*, 95–100.
73. Osmani, R.A.M. Thirumaleshwar, S. Bhosale, R.R.; Kulkarni, P.K. Thirumaleshwar, S. Nanosponges: the spanking accession in drug delivery- an updated comprehensive review. *Der. Pharm. Sin.* **2014**, *5*, 7–21.
74. Jin, Y.; Liang, L.; Sun, X.; Yu, G.; Chen, S.; Shi, S.; Liu, H.; Li, Z.; Ge, K.; Liu, D.; et al. Deoxyribozyme-nanosponges for improved photothermal therapy by overcoming thermoresistance. *NPG Asia Mater.* **2018**, *10*, 373–384.
75. Anceschi, A.; Magnacca, G.; Trotta, F.; Zanetti, M. Preparation and characterization of microporous carbon spheres from high amylose pea maltodextrin. *RSC Adv.* **2017**, *7*, 36117–36123.

References

76. Anceschi, A.; Guerretta, F.; Magnacca, G.; Zanetti, M.; Benzi, P.; Trotta, F.; Caldera, F.; Nisticò, R. Sustainable N-containing biochars obtained at low temperatures as sorbing materials for environmental application: Municipal biowaste-derived substances and nanosponges case studies. *J. Anal. Appl. Pyrolysis* **2018**, *134*, 606–613.
77. Panda, S.; Vijayalakshmi, S.; Pattnaik, S.; Swain, R.P. Nanosponges: A novel carrier for targeted drug delivery. *Int. J. PharmTech Res.* **2015**, *8*, 213–224.
78. Shivani, S.; Poladi, K.K. Nanosponges-novel emerging drug delivery system: A review. *Int J Pharm Sci Res* **2015**, *6*, 529–540.
79. Trotta, F.; Tumiatti, V.; Cavalli, R.; Roggero, C.; Mognetti, B.; Berta, G. Cyclodextrin-based Nanosponges as a Vehicle for Antitumoral Drugs. 2009, Patent WO 2009/003656.
80. Avgoustakis, K.; Beletsi, A.; Panagi, Z.; Klepetsanis, P.; Karydas, A.G.; Ithakissios, D.S. PLGA–mPEG nanoparticles of cisplatin: in vitro nanoparticle degradation, in vitro drug release and in vivo drug residence in blood properties. *J. Control. Release* **2002**, *79*, 123–135.
81. Crupi, V.; Fontana, A.; Majolino, D.; Mele, A.; Melone, L.; Punta, C.; Rossi, B.; Rossi, F.; Trotta, F.; Venuti, V. Hydrogen-bond dynamics of water confined in cyclodextrin nanosponges hydrogel. *J. Incl. Phenom. Macrocycl. Chem.* **2014**, *80*, 69–75.
82. Berto, S.; Bruzzoniti, M.C.; Cavalli, R.; Perrachon, D.; Prenesti, E.; Sarzanini, C.; Trotta, F.; Tumiatti, W. Synthesis of new ionic β -cyclodextrin polymers and characterization of their heavy metals retention. *J. Incl. Phenom. Macrocycl. Chem.* **2007**, *57*, 631–636.
83. Jadhav, N. V.; Vavia, P.R. Supercritical processed starch nanosponge as a carrier for enhancement of dissolution and pharmacological efficacy of fenofibrate. *Int. J. Biol. Macromol.* **2017**, *99*, 713–720.
84. Trotta, F.; Zanetti, M.; Camino, G. Thermal degradation of cyclodextrins. *Polym. Degrad. Stab.* **2000**, *69*, 373–379.
85. Mihailiasa, M.; Caldera, F.; Li, J.; Peila, R.; Ferri, A.; Trotta,

References

- F. Preparation of functionalized cotton fabrics by means of melatonin loaded β -cyclodextrin nanosponges. *Carbohydr. Polym.* **2016**, *142*, 24–30.
86. Swaminathan, S.; Vavia, P.R.; Trotta, F.; Torne, S. Formulation of betacyclodextrin based nanosponges of itraconazole. *J. Incl. Phenom. Macrocycl. Chem.* **2007**, *57*, 89–94.
87. Bachir, Y.N.; Bachir, R.N.; Hadj-Ziane-Zafour, A. Nanodispersions stabilized by β -cyclodextrin nanosponges: application for simultaneous enhancement of bioactivity and stability of sage essential oil. *Drug Dev. Ind. Pharm.* **2019**, *45*, 333–347.
88. Alongi, J.; Poskovic, M.; Frache, A.; Trotta, F. Role of β -cyclodextrin nanosponges in polypropylene photooxidation. *Carbohydr. Polym.* **2011**, *86*, 127–135.
89. Vyas, A.; Saraf, S.; Saraf, S. Cyclodextrin based novel drug delivery systems. *J. Incl. Phenom. Macrocycl. Chem.* **2008**, *62*, 23–42.
90. Conte, C.; Caldera, F.; Catanzano, O.; D'Angelo, I.; Ungaro, F.; Miro, A.; Pellosi, D.S.; Trotta, F.; Quaglia, F. β -Cyclodextrin Nanosponges as Multifunctional Ingredient in Water-Containing Semisolid Formulations for Skin Delivery. *J. Pharm. Sci.* **2014**, *103*, 3941–3949.
91. Rao, M.; Bajaj, A.; Khole, I.; Munjapara, G.; Trotta, F. In vitro and in vivo evaluation of β -cyclodextrin-based nanosponges of telmisartan. *J. Incl. Phenom. Macrocycl. Chem.* **2013**, *77*, 135–145.
92. Swaminathan, Shankar Vavia, P.R.; Trotta, F.; Cavalli, R. Nanosponges Encapsulating Dexamethasone for Ocular Delivery: Formulation Design, Physicochemical Characterization, Safety and Corneal Permeability Assessment. *J. Biomed. Nanotechnol.* **2013**, *9*, 998–1007.
93. Rao, M.R.P.; Bhingole, R.C. Nanosponge-based pediatric-controlled release dry suspension of Gabapentin for reconstitution. *Drug Dev. Ind. Pharm.* **2015**, *41*, 2029–2036.
94. Deshmukh, K.; Tanwar, Y.S.; Sharma, S.; Shende, P.; Cavalli, R. Functionalized nanosponges for controlled antibacterial and antihypocalcemic actions. *Biomed. Pharmacother.* **2016**, *84*,

References

485–494.

95. Swaminathan, S.; Pastero, L.; Serpe, L.; Trotta, F.; Vavia, P.; Aquilano, D.; Trotta, M.; Zara, G.; Cavalli, R. Cyclodextrin-based nanosponges encapsulating camptothecin: Physicochemical characterization, stability and cytotoxicity. *Eur. J. Pharm. Biopharm.* **2010**, *74*, 193–201.

96. Pushpalatha, R.; Selvamuthukumar, S.; Kilimozhi, D. Carbonyl and carboxylate crosslinked cyclodextrin as a nanocarrier for resveratrol: in silico, in vitro and in vivo evaluation. *J. Incl. Phenom. Macrocycl. Chem.* **2018**, *92*, 261–272.

97. Cavalli, R.; Akhter, A.K.; Bisazza, A.; Giustetto, P.; Trotta, F.; Vavia, P. Nanosponge formulations as oxygen delivery systems. *Int. J. Pharm.* **2010**, *402*, 254–257.

98. Femminò, S.; Penna, C.; Bessone, F.; Caldera, F.; Dhakar, N.; Cau, D.; Pagliaro, P.; Cavalli, R.; Trotta, F. α -Cyclodextrin and α -Cyclodextrin Polymers as Oxygen Nanocarriers to Limit Hypoxia/Reoxygenation Injury: Implications from an In Vitro Model. *Polymers (Basel)*. **2018**, *10*.

99. Morin-Crini, N.; Crini, G.; Ronzoni, G. Environmental applications of water-insoluble β -cyclodextrin–epichlorohydrin polymers. *Prog. Polym. Sci.* **2013**, *38*, 344–368.

100. Euvrard, É.; Morin-Crini, N.; Druart, C.; Bugnet, J.; Martel, B.; Cosentino, C.; Moutarlier, V.; Crini, G. Cross-linked cyclodextrin-based material for treatment of metals and organic substances present in industrial discharge waters. *Beilstein J. Org. Chem.* **2016**, *12*, 1826–1838.

101. Pushpalatha, R.; Selvamuthukumar, S.; Kilimozhi, D. Cross-linked, cyclodextrin-based nanosponges for curcumin delivery - Physicochemical characterization, drug release, stability and cytotoxicity. *J. Drug Deliv. Sci. Technol.* **2018**, *45*, 45–53.

102. Mendes, C.; Meirelles, G.C.; Barp, C.G.; Assreuy, J.; Silva, M.A.S.; Ponchel, G. Cyclodextrin based nanosponge of norfloxacin: Intestinal permeation enhancement and improved antibacterial activity. *Carbohydr. Polym.* **2018**, *195*, 586–592.

103. Caldera, F.; Argenziano, M.; Trotta, F.; Dianzani, C.; Gigliotti,

References

- L.; Tannous, M.; Pastero, L.; Aquilano, D.; Nishimoto, T.; Higashiyama, T.; et al. Cyclic nigerosyl-1,6-nigerose-based nanosponges: An innovative pH and time-controlled nanocarrier for improving cancer treatment. *Carbohydr. Polym.* **2018**, *194*, 111–121.
104. Gangadharappa, H. V.; Prasad, S.M.C.; Singh, R.P. Formulation, in vitro and in vivo evaluation of celecoxib nanosponge hydrogels for topical application. *J. Drug Deliv. Sci. Technol.* **2017**, *41*, 488–501.
105. Torne, S.J.; Ansari, K.A.; Vavia, P.R.; Trotta, F.; Cavalli, R. Enhanced oral paclitaxel bioavailability after administration of paclitaxel-loaded nanosponges. *Drug Deliv.* **2010**, *17*, 419–425.
106. Torne, S.; Darandale, S.; Vavia, P.; Trotta, F.; Cavalli, R. Cyclodextrin-based nanosponges: effective nanocarrier for tamoxifen delivery. *Pharm. Dev. Technol.* **2013**, *18*, 619–625.
107. Anandam, S.; Selvamuthukumar, S. Fabrication of cyclodextrin nanosponges for quercetin delivery: physicochemical characterization, photostability, and antioxidant effects. *J. Mater. Sci.* **2014**, *49*, 8140–8153.
108. Argenziano, M.; Haimhoffer, A.; Bastiancich, C.; Jicsinszky, L.; Caldera, F.; Trotta, F.; Scutera, S.; Alotto, D.; Fumagalli, M.; Musso, T.; et al. In Vitro Enhanced Skin Permeation and Retention of Imiquimod Loaded in β -Cyclodextrin Nanosponge Hydrogel. *Pharmaceutics* **2019**, *11*, 138.
109. Sapino, S.; Carlotti, M.E.; Cavalli, R.; Ugazio, E.; Berlier, G.; Gastaldi, L.; Morel, S. Photochemical and antioxidant properties of gamma-oryzanol in beta-cyclodextrin-based nanosponges. *J. Incl. Phenom. Macrocycl. Chem.* **2013**, *75*, 69–76.
110. Dora, C.P.; Trotta, F.; Kushwah, V.; Devasari, N.; Singh, C.; Suresh, S.; Jain, S. Potential of erlotinib cyclodextrin nanosponge complex to enhance solubility, dissolution rate, in vitro cytotoxicity and oral bioavailability. *Carbohydr. Polym.* **2016**, *137*, 339–349.
111. Ramírez-Ambrosi, M.; Caldera, F.; Trotta, F.; Berrueta, L.A.; Gallo, B. Encapsulation of apple polyphenols in β -CD nanosponges. *J. Incl. Phenom. Macrocycl. Chem.* **2014**, *80*, 85–92.

References

112. Swaminathan, S.; Vavia, P.R.; Trotta, F.; Cavalli, R.; Tumbiolo, S.; Bertinetti, L.; Coluccia, S. Structural evidence of differential forms of nanosponges of beta-cyclodextrin and its effect on solubilization of a model drug. *J. Incl. Phenom. Macrocycl. Chem.* **2013**, *76*, 201–211.
113. Cavalli, R.; Trotta, F.; Tumiatti, W. Cyclodextrin-based Nanosponges for Drug Delivery. *J. Incl. Phenom. Macrocycl. Chem.* **2006**, *56*, 209–213.
114. Shende, P.K.; Trotta, F.; Gaud, R.S.; Deshmukh, K.; Cavalli, R.; Biasizzo, M. Influence of different techniques on formulation and comparative characterization of inclusion complexes of ASA with β -cyclodextrin and inclusion complexes of ASA with PMDA cross-linked β -cyclodextrin nanosponges. *J. Incl. Phenom. Macrocycl. Chem.* **2012**, *74*, 447–454.
115. Rao, M.R.P.; Chaudhari, J.; Trotta, F.; Caldera, F. Investigation of Cyclodextrin-Based Nanosponges for Solubility and Bioavailability Enhancement of Rilpivirine. *AAPS PharmSciTech* **2018**, *19*, 2358–2369.
116. Rao, M.R.P.; Shirsath, C. Enhancement of Bioavailability of Non-nucleoside Reverse Transcriptase Inhibitor Using Nanosponges. *AAPS PharmSciTech* **2017**, *18*, 1728–1738.
117. Turski, M.P.; Turska, M.; Kocki, T.; Turski, W.A.; Paluszkiwicz, P. Kynurenic Acid Content in Selected Culinary Herbs and Spices. *J. Chem.* **2015**, *2015*, 1–6.
118. Turski, M.P.; Turska, M.; Zgrajka, W.; Kuc, D.; Turski, W.A. Presence of kynurenic acid in food and honeybee products. *Amino Acids* **2009**, *36*, 75–80.
119. László, V.; Beal, M.F. Comparative behavioral and pharmacological studies with centrally administered kynurenine and kynurenic acid in rats. *Eur. J. Pharmacol.* **1991**, *196*, 239–246.
120. Carpenedo, R.; Pittaluga, A.; Cozzi, A.; Attucci, S.; Galli, A.; Raiteri, M.; Moroni, F. Presynaptic kynurenate-sensitive receptors inhibit glutamate release. *Eur. J. Neurosci.* **2001**, *13*, 2141–2147.
121. Stone, T.W.; Connick, J.H. Quinolinic acid and other kynurenines in the central nervous system. *Neuroscience* **1985**, *15*,

References

597–617.

122. Schwarcz, R.; Bruno, J.P.; Muchowski, P.J.; Wu, H.-Q. Kynurenines in the Mammalian Brain: When Physiology Meets Pathology. *Nat. Rev. Neurosci.* **2012**, *13*, 465–477.

123. Hornok, V.; Bujdosó, T.; Toldi, J.; Nagy, K.; Demeter, I.; Fazakas, C.; Krizbai, I.; Vécsei, L.; Dékány, I. Preparation and properties of nanoscale containers for biomedical application in drug delivery: preliminary studies with kynurenic acid. *J Neural Transm* **2012**, *119*, 115–121.

124. Stone, T.W. Endogenous neurotoxins from tryptophan. *Toxicol* **2001**, *39*, 61–73.

125. Moroni, F.; Russi, P.; Lombardi, G.; Beni, M.; Carlh, V. Presence of Kynurenic Acid in the Mammalian Brain. *J. Neurochem.* **1988**, *51*, 177–180.

126. Varga, N.; Csapó, E.; Majláth, Z.; Ilisz, I.; Krizbai, I.A.; Wilhelm, I.; Knapp, L.; Toldi, J.; Vécsei, L.; Dékány, I. Targeting of the kynurenic acid across the blood-brain barrier by core-shell nanoparticles. *Eur. J. Pharm. Sci.* **2016**, *86*, 67–74.

127. López, T.; Ortiz, E.; Gómez, E.; la Cruz, Verónica Pérez-de Carrillo-Mora, P.; Novaro, O. Preparation and Characterization of Kynurenic Acid Occluded in Sol-Gel Silica and SBA-15 Silica as Release Reservoirs. *J. Nanomater.* **2014**, *2014*, 1–9.

128. Dalpiaz, A.; Pavan, B.; Vertuani, S.; Vitali, F.; Scaglianti, M.; Bortolotti, F.; Biondi, C.; Scatturin, A.; Tanganelli, S.; Ferraro, L.; et al. Ascorbic and 6-Br-ascorbic acid conjugates as a tool to increase the therapeutic effects of potentially central active drugs. *Eur. J. Pharm. Sci.* **2005**, *24*, 259–269.

129. Vécsei, L.; Szalárdy, L.; Fülöp, F.; Toldi, J. Kynurenines in the CNS: recent advances and new questions. *Nat. Rev. Drug Discov.* **2013**, *12*, 64–82.

130. Wirthgen, E.; Hoeflich, A.; Rebl, A.; Gunther, J. Kynurenic Acid: The Janus-Faced Role of an Immunomodulatory Tryptophan Metabolite and Its Link to Pathological Conditions. *Front. Immunol.* **2017**, *8*, 1957.

References

131. Kim, J.; Stewart, B.; Weiss, R.H. Extraction and Quantification of Tryptophan and Kynurenine from Cultured Cells and Media Using a High Performance Liquid Chromatography (HPLC) System Equipped with an Ultra-Sensitive Diode Array Detector. *Bio-protocol* **2016**, *6*, e1781.
132. Badawy, A.A.-B.; Morgan, C.J. Rapid Isocratic Liquid Chromatographic Separation and Quantification of Tryptophan and Six kynurenine Metabolites in Biological Samples with Ultraviolet and Fluorimetric Detection. *Int. J. Tryptophan Res.* **2010**, *3*, 175–186.
133. Lesniak, W.G.; Jyoti, A.; Mishra, M.K.; Louissaint, N.; Romero, R.; Chugani, D.C.; Kannan, S.; Kannan, R.M. Concurrent quantification of tryptophan and its major metabolites. *Anal Biochem* **2013**, *443*, 222–231.
134. Singh, A.P.; Singh, R.; Verma, S.S.; Rai, V.; Kaschula, C.H.; Maiti, P.; Gupta, S.C. Health benefits of resveratrol: Evidence from clinical studies. *Med. Res. Rev.* **2019**, 1–41.
135. Brown, L.; Kroon, P.A.; Das, D.K.; Das, S.; Tosaki, A.; Chan, V.; Singer, M. V; Feick, P. The Biological Responses to Resveratrol and Other Polyphenols From Alcoholic Beverages. *Alcohol. Clin. Exp. Res.* **2009**, *33*, 1513–1523.
136. Gresele, P.; Cerletti, C.; Guglielmini, G.; Pignatelli, P.; de Gaetano, G.; Violi, F. Effects of resveratrol and other wine polyphenols on vascular function: an update. *J. Nutr. Biochem.* **2011**, *22*, 201–211.
137. Villaflores, O.B.; Chen, Y.-J.; Chen, C.-P.; Yeh, J.-M.; Wu, T.-Y. Curcuminoids and resveratrol as anti-Alzheimer agents. *Taiwan. J. Obstet. Gynecol.* **2012**, *51*, 515–525.
138. Murtaza, G.; Saqib, M.; Ghafoor, A.; Javed, W.; Murtaza, B.; Ali, M.K.; Abbas, G. Climate Change and Water Security in Dry Areas Dry areasClimate changeWater security. In *Handbook of Climate Change Adaptation*; Leal Filho, W., Ed.; Springer Berlin Heidelberg: Berlin, Heidelberg, 2021; pp. 1–25 ISBN 978-3-642-40455-9.
139. Catalgol, B.; Batirel, S.; Taga, Y.; Ozer, N. Resveratrol: French Paradox Revisited. *Front. Pharmacol.* **2012**, *3*, 141.
140. Amidon, G.L.; Lennernäs, H.; Shah, V.P.; Crison, J.R. A

References

Theoretical Basis for a Biopharmaceutical Drug Classification: The Correlation of in Vitro Drug Product Dissolution and in Vivo Bioavailability. *Pharm Res* **1995**, *12*, 413.

141. Trela, B.C.; Waterhouse, A.L. Resveratrol: Isomeric Molar Absorptivities and Stability. *J. Agric. Food Chem.* **1996**, *44*, 1253–1257.

142. Andlauer, W.; Kolb, J.; Siebert, K.; Fürst, P. Assessment of resveratrol bioavailability in the perfused small intestine of the rat. *Drugs Exp. Clin. Res.* **2000**, *26*, 47–55.

143. Bertelli, A.A.; Giovannini, L.; Stradi, R.; Bertelli, A.; Tillement, J.P. Plasma, urine and tissue levels of trans- and cis-resveratrol (3,4',5-trihydroxystilbene) after short-term or prolonged administration of red wine to rats. *Int. J. Tissue React.* **1996**, *18*, 67–71.

144. Soleas, G.J.; Yan, J.; Goldberg, D.M.B.T.-M. in E. Measurement of trans-resveratrol, (+)-catechin, and quercetin in rat and human blood and urine by gas chromatography with mass selective detection. In *Flavonoids and Other Polyphenols*, Academic Press, 2001; Vol. 335, pp. 130–145 ISBN 0076-6879.

145. Goldberg, D.M.; Yan, J.; Soleas, G.J. Absorption of three wine-related polyphenols in three different matrices by healthy subjects. *Clin. Biochem.* **2003**, *36*, 79–87.

146. Lançon, A.; Delma, D.; Osman, H.; Thénot, J.-P.; Latruffe N, B.J. Human hepatic cell uptake of resveratrol: involvement of both passive diffusion and carrier-mediated process. *Biochem. Biophys. Res. Commun.* **2004**, *316*, 1132–1137.

147. Burkon, A.; Somoza, V. Quantification of free and protein-bound trans-resveratrol metabolites and identification of trans-resveratrol-C/O-conjugated diglucuronides – Two novel resveratrol metabolites in human plasma. *Mol. Nutr. Food Res.* **2008**, *52*, 549–557.

148. Walle, T.; Hsieh, F.; DeLegge, M.H.; Oatis, J.E.; Walle, U.K. HIGH ABSORPTION BUT VERY LOW BIOAVAILABILITY OF ORAL RESVERATROL IN HUMANS. *Drug Metab. Dispos.* **2004**, *32*, 1377 LP – 1382.

References

149. Belguendouz, L.; Frémont, L.; Gozzelino, M.-T. Interaction of Transresveratrol with Plasma Lipoproteins. *Biochem. Pharmacol.* **1998**, *55*, 811–816.
150. Chen, X.; He, H.; Wang, G.; Yang, B.; Ren, W.; Ma, L.; Yu, Q. Stereospecific determination of cis- and trans-resveratrol in rat plasma by HPLC: application to pharmacokinetic studies. *Biomed. Chromatogr.* **2007**, *21*, 257–265.
151. Katsagonis, A.; Atta-Politou, J.; Koupparis, M.A. HPLC Method with UV Detection for the Determination of trans-Resveratrol in Plasma. *J. Liq. Chromatogr. Relat. Technol.* **2005**, *28*, 1393–1405.
152. Vijayakumar, M.R.; Kosuru, R.; Vuddanda, P.R.; Singh, S.K.; Singh, S. Trans resveratrol loaded DSPE PEG 2000 coated liposomes: An evidence for prolonged systemic circulation and passive brain targeting. *J. Drug Deliv. Sci. Technol.* **2016**, *33*, 125–135.
153. Lorenz, P.; Roychowdhury, S.; Engelmann, M.; Wolf, G.; Horn, T.F.W. Oxyresveratrol and resveratrol are potent antioxidants and free radical scavengers: Effect on nitrosative and oxidative stress derived from microglial cells. *Nitric Oxide* **2003**, *9*, 64–76.
154. Likhitwitayawuid, K.; Sritularak, B.; Benchanak, K.; Lipipun, V.; Mathew, J.; Schinazi, R.F. Phenolics with antiviral activity from *Millettia erythrocalyx* and *Artocarpus lakoocha*. *Nat. Prod. Res.* **2005**, *19*, 177–182.
155. Kim, S.; Ko, H.; Park, J.E.; Jung, S.; Lee, S.K.; Chun, Y.-J. Design, Synthesis, and Discovery of Novel trans-Stilbene Analogues as Potent and Selective Human Cytochrome P450 1B1 Inhibitors. *J. Med. Chem.* **2002**, *45*, 160–164.
156. Andrabi, S.A.; Spina, M.G.; Lorenz, P.; Ebmeyer, U.; Wolf, G.; Horn, T.F.W. Oxyresveratrol (trans-2,3',4,5'-tetrahydroxystilbene) is neuroprotective and inhibits the apoptotic cell death in transient cerebral ischemia. *Brain Res.* **2004**, *1017*, 98–107.
157. Chao, J.; Yu, M.-S.; Ho, Y.-S.; Wang, M.; Chang, R.C.-C. Dietary oxyresveratrol prevents parkinsonian mimetic 6-hydroxydopamine neurotoxicity. *Free Radic. Biol. Med.* **2008**, *45*,

References

1019–1026.

158. Simon, H.-U.; Haj-Yehia, A.; Levi-Schaffer, F. Role of reactive oxygen species (ROS) in apoptosis induction. *Apoptosis* **2000**, *5*, 415–418.

159. Wen, P.; Hu, T.-G.; Linhardt, R.J.; Liao, S.-T.; Wu, H.; Zou, Y.-X. Mulberry: A review of bioactive compounds and advanced processing technology. *Trends Food Sci. Technol.* **2019**, *83*, 138–158.

160. Matencio, A.; García-Carmona, F.; José Manuel, L.-N. The inclusion complex of oxyresveratrol in modified cyclodextrins: A thermodynamic, structural, physicochemical, fluorescent and computational study. *Food Chem.* **2017**, *232*, 177–184.

161. Mei, M.; Ruan, J.-Q.; Wu, W.-J.; Zhou, R.-N.; Lei, J.P.-C.; Zhao, H.-Y.; Yan, R.; Wang, Y.-T. In Vitro Pharmacokinetic Characterization of Mulberroside A, the Main Polyhydroxylated Stilbene in Mulberry (*Morus alba* L.), and Its Bacterial Metabolite Oxyresveratrol in Traditional Oral Use. *J. Agric. Food Chem.* **2012**, *60*, 2299–2308.

162. Bertram, R.M.; Davies, N.M. Elucidating the pharmacodynamics and disposition of oxyresveratrol. In Proceedings of the Summer Undergraduate Research Poster Symposium; Washington State University, Washington State, USA, 2009.

163. Huang, H.; Chen, G.; Lu, Z.; Zhang, J.; Guo, D.-A. Identification of seven metabolites of oxyresveratrol in rat urine and bile using liquid chromatography/tandem mass spectrometry. *Biomed. Chromatogr.* **2010**, *24*, 426–432.

164. Huang, H.; Zhang, J.; Chen, G.; Lu, Z.; Sha, N.; Guo, D. Simultaneous Determination of Oxyresveratrol and Resveratrol in Rat Bile and Urine by HPLC after Oral Administration of Smilax china Extract. *Nat. Prod. Commun.* **2009**, *4*, 1934578X0900400617.

165. Sangsen, Y.; Likhitwitayawuid, K.; Sritularak, B.; Wiwattanawongsa, K.; Wiwattanapatapee, R. Novel Solid Lipid Nanoparticles for Oral Delivery of Oxyresveratrol: Effect of the Formulation Parameters on the Physicochemical Properties and in vitro Release. *Int. J. Medical, Heal. Biomed. Bioeng. Pharm. Eng.*

References

2013, *7*, 877–884.

166. Huang, H.; Zhang, J.; Chen, G.; Lu, Z.; Wang, X.; Sha, N.; Shao, B.; Li, P.; Guo, D. High performance liquid chromatographic method for the determination and pharmacokinetic studies of oxyresveratrol and resveratrol in rat plasma after oral administration of Smilax china extract. *Biomed. Chromatogr.* **2008**, *22*, 421–427.

167. Lin, H.-S.; Choo, Q.-Y.; Ho, P.C. Quantification of oxyresveratrol analog trans-2,4,3',5'-tetramethoxystilbene in rat plasma by a rapid HPLC method: application in a pre-clinical pharmacokinetic study. *Biomed. Chromatogr.* **2010**, *24*, 1373–1378.

168. Bertram, R.M.; Takemoto, J.K.; Remsberg, C.M.; Vega-Villa, K.R.; Sablani, S.; Davies, N.M. High-performance liquid chromatographic analysis: applications to nutraceutical content and urinary disposition of oxyresveratrol in rats. *Biomed. Chromatogr.* **2010**, *24*, 516–521.

169. Aggarwal, B.B.; Sundaram, C.; Malani, N.; Ichikawa, H. CURCUMIN: THE INDIAN SOLID GOLD-The Molecular Targets and Therapeutic Uses of Curcumin in Health and Disease. In *ADVANCES IN EXPERIMENTAL MEDICINE AND BIOLOGY*; Aggarwal, B.B., Surh, Y.-J., Shishodia, S., Eds.; Springer US: Boston, MA, 2007; pp. 1–75.

170. Hoehle, S.I.; Pfeiffer, E.; Sólyom, A.M.; Metzler, M. Metabolism of Curcuminoids in Tissue Slices and Subcellular Fractions from Rat Liver. *J. Agric. Food Chem.* **2006**, *54*, 756–764.

171. Wang, Y.-J.; Pan, M.-H.; Cheng, A.-L.; Lin, L.-I.; Ho, Y.-S.; Hsieh, C.-Y.; Lin, J.-K. Stability of curcumin in buffer solutions and characterization of its degradation products. *J. Pharm. Biomed. Anal.* **1997**, *15*, 1867–1876.

172. SREEJAYAN; RAO, M.N.A. Nitric Oxide Scavenging by Curcuminoids. *J. Pharm. Pharmacol.* **1997**, *49*, 105–107.

173. Sreejayan, N.; Rao, M.N. Free radical scavenging activity of curcuminoids. *Arzneimittelforschung.* **1996**, *46*, 169–171.

174. SRIMAL, R.C.; DHAWAN, B.N. Pharmacology of diferuloyl methane (curcumin), a non-steroidal anti-inflammatory agent*. *J. Pharm. Pharmacol.* **1973**, *25*, 447–452.

References

175. Huang, M.-T.; Lysz, T.; Ferraro, T.; Abidi, T.F.; Laskin, J.D.; Conney, A.H. Inhibitory Effects of Curcumin on in Vitro Lipoxygenase and Cyclooxygenase Activities in Mouse Epidermis. *Cancer Res.* **1991**, *51*, 813 LP – 819.
176. Girish, C.; Pradhan, S. Hepatoprotective activities of picroliv, curcumin, and ellagic acid compared to silymarin on carbon-tetrachloride-induced liver toxicity in mice. *J. Pharmacol. Pharmacother.* **2012**, *3*, 149–155.
177. Negi, P.S.; Jayaprakasha, G.K.; Jagan Mohan Rao, L.; Sakariah, K.K. Antibacterial Activity of Turmeric Oil: A Byproduct from Curcumin Manufacture. *J. Agric. Food Chem.* **1999**, *47*, 4297–4300.
178. Anand, P.; Kunnumakkara, A.B.; Newman, R.A.; Aggarwal, B.B. Bioavailability of Curcumin: Problems and Promises. *Mol. Pharm.* **2007**, *4*, 807–818.
179. Sharma, R.A.; Steward, W.P.; Gescher, A.J. PHARMACOKINETICS AND PHARMACODYNAMICS OF CURCUMIN BT - The Molecular Targets and Therapeutic Uses of Curcumin in Health and Disease. In; Aggarwal, B.B., Surh, Y.-J., Shishodia, S., Eds.; Springer US: Boston, MA, 2007; pp. 453–470.
180. Ravindranath, V.; Chandrasekhara, N. Absorption and tissue distribution of curcumin in rats. *Toxicology* **1980**, *16*, 259–265.
181. Ireson, C.; Orr, S.; Jones, D.J.L.; Verschoyle, R.; Lim, C.-K.; Luo, J.-L.; Howells, L.; Plummer, S.; Jukes, R.; Williams, M.; et al. Characterization of Metabolites of the Chemopreventive Agent Curcumin in Human and Rat Hepatocytes and in the Rat in Vivo, and Evaluation of Their Ability to Inhibit Phorbol Ester-induced Prostaglandin E2 Production. *Cancer Res.* **2001**, *61*, 1058 LP – 1064.
182. Li, J.; Jiang, Y.; Wen, J.; Fan, G.; Wu, Y.; Zhang, C. A rapid and simple HPLC method for the determination of curcumin in rat plasma: assay development, validation and application to a pharmacokinetic study of curcumin liposome. *Biomed. Chromatogr.* **2009**, *23*, 1201–1207.
183. Wichitnithad, W.; Jongaroonngamsang, N.; Pummangura, S.; Rojsitthisak, P. A simple isocratic HPLC method for the

References

simultaneous determination of curcuminoids in commercial turmeric extracts. *Phytochem. Anal.* **2009**, *20*, 314–319.

184. Chao, I.-C.; Wang, C.-M.; Li, S.-P.; Lin, L.-G.; Ye, W.-C.; Zhang, Q.-W. Simultaneous Quantification of Three Curcuminoids and Three Volatile Components of *Curcuma longa* Using Pressurized Liquid Extraction and High-Performance Liquid Chromatography. *Molecules* 2018, *23*.

185. Jadhav, B.-K.; Mahadik, K.-R.; Paradkar, A.-R. Development and Validation of Improved Reversed Phase-HPLC Method for Simultaneous Determination of Curcumin, Demethoxycurcumin and Bis-Demethoxycurcumin. *Chromatographia* **2007**, *65*, 483–488.

186. Benesi, H.A.; Hildebrand, J.H. A Spectrophotometric Investigation of the Interaction of Iodine with Aromatic Hydrocarbons. *J. Am. Chem. Soc.* **1949**, *71*, 2703–2707.